

SHEAR INVESTIGATION OF POLYPROPYLENE
FIBER-REINFORCED CONCRETE BEAMS

by

EHSAN NAVADEH

Presented to the Faculty of the Graduate School of
The University of Texas at Arlington in Partial Fulfillment
of the Requirements
for the Degree of

MASTER OF SCIENCE IN CIVIL ENGINEERING

THE UNIVERSITY OF TEXAS AT ARLINGTON

December 2016

Copyright © by Ehsan Navadeh 2016

All Rights Reserved



Acknowledgements

I would like to offer my sincere appreciation to Dr. Ali Abolmaali for his guidance and support throughout my graduate academic career. Dr. Abolmaali has been a wonderful mentor to me, providing invaluable technical and academic guidance over the course of this research. His knowledge and advice has always provided me with great inspiration and motivation in dealing with academic and personal challenges. I would also like to thank Michael Daniels who provided me with invaluable support and assistance throughout the course of this project. Michael dedicated his unconditional support and encouragement during my graduate studies. Appreciations are also extended to Dr. Kermanshachi and Dr. Azzawi for their valuable advice and feedback with this research project. I would also like to appreciate BASF for providing the macro-synthetic polypropylene fibers to make this research possible. I would like to thank my parents, who have always provided great encouragement and support helping me overcome some of the greatest challenges.

December 16, 2016

Abstract

SHEAR INVESTIGATION OF POLYPROPYLENE
FIBER-REINFORCED CONCRETE BEAMS

Ehsan Navadeh, M.S.

The University of Texas at Arlington, 2016

Supervising Professor: Dr. Ali Abolmaali

This study investigates the effect of macro-synthetic Polypropylene fibers on the shear strength and failure behavior of longitudinally reinforced concrete beams with and/or without transverse reinforcement. Eight large-scale were constructed, cured and tested at Civil Engineering Laboratory Building (CELB). This includes flexural reinforced concrete beams without transverse reinforcement (RC), reinforced concrete beam with minimum transverse reinforcement (RCS), 0.5% volume macro-synthetic polypropylene fiber-reinforced concrete beams without stirrups (SNFRC 0.5%), and 0.75% macro-synthetic polypropylene-fiber reinforced concrete beams without stirrups (SNFRC 0.75%). During production of large-scale beams, 19 Cylinders and 9 small-scale beams were produced from the same mix-design and cured for testing. Cylinders of 4 inch diameter and 8 inch height, were tested after 28 days curing using ASTM C496 and ASTM C39 standards. Likewise, small-scale beams of 6 inch by 6 inch by 20 inch were produced and tested using ASTM C1609. This study reports on the increased shear strength performance of large-scale beams due to the application of 0.5% and 0.75% macro-synthetic polypropylene fibers into the concrete matrix.

Table of Contents

Acknowledgements	iii
Abstract	iv
Table of Contents	v
List of Illustrations	vii
List of Tables	x
1 INTRODUCTION	1
1.1 Objectives	2
1.2 Research Contribution	2
1.3 Outline for Thesis	3
2 LITERATURE REVIEW	5
3 EXPERIMENTAL PROGRAM	11
3.1 General	11
3.2 Material Properties of Polypropylene fibers	12
3.3 Fabrication of Test Specimens	13
3.3.1 Design of Beam Specimens	13
3.3.2 Test Specimens	15
3.3.2.1 Steel Strain Gauges	17
3.3.2.2 Concrete Strain Gages	26
3.3.2.3 Concrete Pouring	29
3.4 Test Set-Up and Procedure	35
3.4.1 Testing of Large-Scale Beams	35
3.4.2 Testing of Small-Scale Beams	38
3.4.3 Tensile Strength Testing of Cylinders	40
3.4.4 Compressive Strength Testing of Cylinders	41

4	EXPERIMENTAL RESULTS AND ANALYSIS.....	43
4.1	Large-Scale Beams	43
4.1.1	Failure Mechanism	44
4.1.2	Strain Measurements	48
4.1.2.1	Principal Strains in Concrete	48
4.2	Tensile Cylinder Specimens	50
4.3	Compressive Cylinder Specimens.....	51
4.4	Flexural Beam Specimens.....	54
5	SUMMARY AND CONCLUSIONS	57
	Appendix A Crack Patterns and Propagation	60
	Appendix B Principal Strain Values	69
	Appendix C Principal Strain Orientations.....	72
	Appendix D Failure Crack Patterns.....	75
	Appendix E Load-Deflection curves for large-scale specimens.....	78
	Appendix F Steel Strain-Gauges	87
	Appendix G Concrete Strain-Gauges	96
	Appendix H Design of Large-Scale Beams.....	105
	Appendix I Project Planning.....	108
	REFERENCES.....	110
	BIOGRAPHICAL INFORMATION.....	114

List of Illustrations

Figure 1 Typical photo of shear span to depth ratio (Wight, 2015).....	11
Figure 2 Moment at cracking and failure (Wight, 2015).....	11
Figure 3 Shear at cracking and failure (Wight, 2015)	12
Figure 4 Details of large-scale beam without transverse reinforcement.....	14
Figure 5 Details of large-scale beam with transverse reinforcement.....	14
Figure 6 Cross section of large-scale beam with transverse reinforcement.....	14
Figure 7 Typical Formwork for large-scale specimens	15
Figure 8 Formwork for Small-Scale Flexure Beams	15
Figure 9 Grinding Steel Reinforcement for Strain Gage Application	17
Figure 10 Neutralizing a smooth glass surface.....	18
Figure 11 Abrading of steel surface	19
Figure 12 Steel strain gage installation kit	20
Figure 13: Catalyst applied to bonding side of strain gage.....	20
Figure 14 Removing the tape from the gage assembly	21
Figure 15 Inspection of an installed steel strain gage.....	22
Figure 16 M-Coat C coated steel strain gage	22
Figure 17 M-Coat B coated strain gage	22
Figure 18: waterproof and UV-resistant sealed strain gage assembly	23
Figure 19 Tubed strain gage wires installed on steel reinforcement	24
Figure 20 Steel Strain Gauge Pattern.....	25
Figure 21 Layout of strain gauges on reinforcement of typical RC & SNFRC beams.....	26
Figure 22 Layout of strain gauges on reinforcement of typical RCS beam	26
Figure 23 Tee, Rectangular and Delta Rosettes, respectively	27
Figure 24 Stacked rectangular rosette gauges used in this study	28

Figure 25 Type and location of concrete strain gauges.....	29
Figure 26 Formworks for large-scale beams	30
Figure 27 Concrete Pouring and vibrating	31
Figure 28 Slump test performed on-site.....	32
Figure 29 Typical images of (i) plain concrete, (ii) 0.5% SNFRC (iii) 0.75% SNFRC.....	33
Figure 30 Small-scale specimens in curing room	33
Figure 31 Poured large-scale concrete beams.....	34
Figure 32 400 Kip compression machine.....	35
Figure 33 Typical test setup for large-scale beams	37
Figure 34 Data acquisition network.....	37
Figure 35 Material Test System (MTS).....	38
Figure 36 Tensile-Splitting Test	40
Figure 37 60-kip compression machine	41
Figure 38 500-Kip Compression machine.....	42
Figure 39 Testing jig mounted to cylinder for compression test	42
Figure 40 Typical compression test setup	42
Figure 41 Compression test data acquisition network	42
Figure 42 Comparison of Shear strength for Large-Scale Beams.....	43
Figure 43 Typical shear crack on a large-scale Beam.....	44
Figure 44 Failure crack widening and pullout resistance of fibers	45
Figure 45 Pullout resistance and rupture of fibers in SNFRC beams.....	46
Figure 46 Mohr-circle for rosette concrete strain gauge in RC BM#1 on gridline F5	49
Figure 47 Average tensile strength of cylinders.....	50
Figure 48 Average compressive strength for cylinders.....	51
Figure 49 Compressive stress-strain curves for Plain-Concrete cylinders	52

Figure 50 Compressive stress-strain curves for SNFRC 0.5% cylinders	52
Figure 51 Compressive stress-strain curves for SNFRC 0.75% cylinders	53
Figure 52 Average tensile strength for flexural beams	54
Figure 53 Load-deflection curves for Plain Concrete beams.....	55
Figure 54 Load-deflection curves for SNFRC 0.5% beams.....	55
Figure 55 Load-deflection curves for SNFRC 0.75% beams.....	56

List of Tables

Table 1: Framework of Research Study	4
Table 2 Properties of Fibers used in this study (BASF Corporation).....	12
Table 3 Details of large-scale beams.....	16
Table 4 Dimensions of Steel Strain Gauges	25
Table 5 Rosette Strain Gauge Dimensions.....	28
Table 6 Mix-design of delivered concrete mix.....	34
Table 7 Compression test setup and instrumentation for cylindrical specimens	42
Table 8 Large-Scale Beam Test Result.....	43
Table 9 Tensile strength of cylinder specimens.....	50
Table 10 Compressive strength of cylinder specimens	51
Table 11 Flexural strength of small-scale beam specimens.....	54
Table 12 Energy dissipation values for small-scale beams.....	56

1 INTRODUCTION

Reinforced concrete (RC) used in a variety of forms and shapes is one of the major building blocks of the nation's infrastructure. Reinforcing concrete using structural steel is a fundamental part of the design and construction process. Although being a well-studied and successfully implemented method, certain disadvantages of this conventional method have prompted further research and investigation into alternative methods of reinforcing concrete. In this regard, fiber-reinforced concrete (FRC) has attracted a considerable amount of research in the past few decades and has demonstrated promising potential in being a major element for refining future structural design methods and practices. In particular, macro-synthetic polypropylene fibers present an advantageous choice for concrete reinforcement. Results obtained from previous investigations led to application of fibers in different concrete infrastructures. FRC provides easier construction application and gives architects/structural designers the capability to explore complex shapes. In addition, application of polypropylene synthetic fibers which have corrosion resistance properties as an alternative to conventional steel reinforcement dismisses concerns of dealing with various deterioration challenges which conventional RC is notoriously known for. This study capitalizes on experimental methods to research the shear strength and performance of fiber-reinforced concrete beams (SNFRC). The obtained results are compared to conventional longitudinally reinforced concrete beams without transverse reinforcement (RC) and longitudinally reinforced concrete beams with minimum transverse reinforcement (RCS). The outcomes include the assessment of the shear performance of 8 large-scale beams and its 28 small-scale accompanying specimens subjected to 28 days of standard curing.

1.1 Objectives

The main objective of this study is to compare the shear strength performance of macro-synthetic polypropylene reinforced concrete beams with conventionally reinforced concrete beams. This includes investigating whether SNFRC beams have the capability to outperform RC beams and whether SNFRC beams can be used as an alternative to RCS beams. To meet this objective, corrosion-free macro-synthetic polypropylene fibers are introduced with two volume fractions to concrete's matrix during production. Large-scale specimens are cured and tested under monotonic loading. The obtained results are used for studying the shear performance of SNFRC beams with respect to RC and RCS beams.

1.2 Research Contribution

Adoption of new structural material into standard codes require long-term investigation and research by various scientists from credible institutions. Although Macro-synthetic polypropylene-fiber have been a subject of experimental research since their debut, further research is required to provide comprehensive understanding of the material's behavior. Therefore, this research contributes to the growing literature laying a solid foundation for standard code adoption (ACI, ASCE, AASHTO, etc.). The benefits include optimizing construction costs by saving labor work with safer structure service life due to better ductility. In addition, exclusion transverse reinforcement in structural members which would benefit industry professionals in design and construction. Moreover, reducing the amount of steel reinforcement helps in preventing deterioration and failure of concrete due to corrosion. It is noteworthy to mention that the publications resulting from this research will propagate the obtained knowledge through academic institutes and design firms.

1.3 Outline for Thesis

This thesis is organized into the five following chapters respectively:

Chapter 1 – Introduction: This chapter explains the nature of concrete in tension and why fibers have been introduced to the concrete mixture.

Chapter 2 – Literature Review: This chapter presents the background of fiber-reinforcement concrete. Moreover, this chapter includes summaries of research studies performed on previous fiber-reinforced structural members.

Chapter 3 – Experimental Program: This chapter presents design and fabrication of large-scale beam specimens, test set-up and procedure, curing of all the specimens in this study.

Chapter 4 – Experimental Results and Analysis: This chapter presents the failure mode and mechanism of large-scale beams, load-deflection response of large-scale and small flexural beams, load-strain response, displacement-strain response, compressive and tensile strength of cylinder specimens.

Chapter 5 – Summary and Conclusions: The findings of this research are summarized and the conclusions are presented.

Table 1: Framework of Research Study

SHEAR INVESTIGATION OF POLYPROPYLENE FIBER-REINFORCED CONCRETE BEAMS			
Specimen Types			
Large-Scale Specimens	8 Beams $p = 2.4\%$ $p' = 0.3\%$ Large Scale Testing	2 Reinforced Concrete Beams without transverse reinforcement	(RC)
		2 Reinforced Concrete Beams with transverse reinforcement	(RCS)
		2 Synthetic Fiber-Reinforced Concrete Beams with $V_f = 0.5\%$	(SNFRC 0.5%)
		2 Synthetic Fiber-Reinforced Concrete Beams with $V_f = 0.75\%$	(SNFRC 0.75%)
Small-Scale Specimens	9 Flexure Beams ASTM C1609	3 Plain Concrete Cylinders	(Plain Conc.)
		3 Synthetic Fiber-Reinforced Concrete Cylinders with $V_f = 0.5\%$	(SNFRC 0.5 %)
		3 Synthetic Fiber-Reinforced Concrete Cylinders with $V_f = 0.75\%$	(SNFRC 0.75 %)
	10 Cylinders Compressive Strength Test ASTM C39	4 Plain Concrete Cylinders	(Plain Conc.)
		3 Synthetic Fiber-Reinforced Concrete Cylinders with $V_f = 0.5\%$	(SNFRC 0.5 %)
		3 Synthetic Fiber-Reinforced Concrete Cylinders with $V_f = 0.75\%$	(SNFRC 0.75 %)
	10 Cylinders Tensile Strength Test ASTM C469	3 Plain Concrete Beams	(Plain Conc.)
		3 Synthetic Fiber-Reinforced Concrete Beams with $V_f = 0.5\%$	(SNFRC 0.5 %)
		3 Synthetic Fiber-Reinforced Concrete Beams with $V_f = 0.75\%$	(SNFRC 0.75 %)

2 LITERATURE REVIEW

Brittle shear failure of concrete structures because of their rapid and unpredictable nature is an unfavorable mode of failure (ACI 318-14, 2014). The design of reinforced concrete elements accounts for this limitation and ensures that unpredictable brittle shear failure does not occur in any case. Therefore, it is more favorable for flexural failure to control the design (Wight and MacGregor, 2012). Shear failure occurs when an inclined diagonal crack starts to develop on the beam's surface from loading point to the support. These cracks are often due to extreme principal tensile stress pulling the specimen apart rapidly with very little warning. Therefore, it is critical to prevent this unfavorable mode of failure by resisting the principal stress in the critical section. Concrete is known for its low strain capacity and its low tensile strength during failure. Introduction of synthetic fibers into concrete's matrix improves the material's ductility and mechanical behavior. ACI recognizes the introduction of fibrous content into concrete to potentially improve the structural element's capability in preserving its strength and reliability over its designed service life (Daniel, et. Al, 2002). Previous research studies show fibers can prevent large cracks from occurring and improve the structure's serviceability. Improved crack control means lower chance of liquids probing through cracks causing deterioration of the material through corrosion of steel reinforcement. In addition, reinforcement congestion in structural elements has been known to create poor quality concrete leading to honeycombing which in turn affects concrete's strength and durability. Application of fibers into the mix can potentially enhance the tensile strength of the structural member (Balaguru and Shah, 1992). Tensile stresses play a major part in the shear failure mechanism and application of fibers leads to the improvement of the material's tensile strength in resisting shear cracks. These conclusions are based on previously conducted research studies on fiber-reinforced concrete. Initial studies date back to the early 1900s when metal chips, nails,

and wire segments were randomly introduced into the matrix to enhance its general strength (Naaman, 1985). Since then, significant resources have been utilized in assessing the possibility of reinforcing concrete using steel fibers (Romualdi and Batson, 1963). Extensive research performed on the application of steel fibers in concrete as a different method of reinforcing concrete for shear strength ultimately led to the adoption of steel fibers for ACI's 2008 building code requirements (ACI 318-08, 2008). The material has since been utilized in construction of slab on grade, slope stabilization, tunnel linings, etc. It is understood that application of fibers into the concrete mix negatively affects its workability and this negative effect is exacerbated when the fibers are used at relatively higher volume fractions. Hence, structural designers must account for the resultant slump loss and take adequate steps to ensure proper field practices are conducted during construction. However, other fibrous material has shown improved fracture performance by counteracting the pullout effect from the concrete matrix. Increased tensile and compressive strength, shear and torsion capacity, flexural strength has also been reported in previous research studies (Daniel, et. Al, 2002). ACI's 2002 report on fiber reinforced concrete addresses this fact and mentions how steel fibers with rough surfaces and hooked ends have improved post-fracture performance (Daniel, et. Al, 2002). The advantage of introducing this new material is that no special alterations are made to current construction material. Moreover, utilizing this method can significantly reduce overall construction cost by ultimately eliminating the use of steel. Although steel fibers improve the mechanical properties of the mix but its disadvantages cannot be overlooked. Steel fibers do not provide a solution to the problem of corrosion—one that plays a main role in concrete's structural failure and deterioration. For instance, corrosion in steel bridges, an integral part of transportation infrastructure, has a direct annual cost of greater than 13.6 billion dollars (NACE, 2012). Rectifying the damaging effect of corrosion on steel bridges would cost

taxpayers 20.5 billion dollars annually. Seeing as steel fibers reinforced by concrete do not solve this problem, an alternative fibrous material which can simultaneously improve the structural properties of concrete but preclude its corrosion is needed. One such material is macro-synthetic polypropylene fibers which has performed favorably in recent studies by enhancing concrete's structural ability. The shear performance behavior of these fibers, however, has hardly been reviewed because of the lack of availability of quality polypropylene fibers in the past. Nevertheless, these fibers and its likes were manufactured to enhance the structural abilities of concrete and such products materialized the possibility of low-cost fiber-reinforced concrete. Bettering the properties of concrete namely extended service life, elastic modulus, durability, crack resistance, tensile strength and compressive strength can lead the way advancement in structural material knowledge.

A 1992 study by V. Li, et al. investigating synthetic fiber-reinforced concrete behavior demonstrated improved ultimate strength because of an increased resistance to tensile forces in the way of diagonal cracks. This study sought to explore the outcome fiber-reinforcement would have on the strength and failure mode of longitudinally reinforced beams without stirrups in the plane of shear and bending forces. Results showed greater efficiency of these fibers as shear reinforcement when the ratio of shear to span increased. This was owed to their negligible effect on arch action in contrast to their noticeable effect on beam action. The high percentage increase in initial shear crack stress and shear strength were also worthy of notice. This can all be attributed to the heightened resistance to propagation of dowel cracks as a byproduct of greater volume of synthetic fibers. Furthermore, a study conducted by Noghabai in 2000 reported the improvement of the web and tension zone in resisting tensile cracks. This resistance leads to stress redistribution contributing to the increased overall toughness and stiffness of beams (Noghabai, 2000). Likewise, Kwak et al. performed experiments on twelve reinforced-concrete beams with

variable shear span to depth ratios. Beams reinforced with 0.5% and 0.75% fiber dosage demonstrated enhanced higher nominal stress during shear crack occurrence along with higher ultimate shear strength and compressive strength values as fiber volume increased (Kwak, et. Al, 2002). Similarly, a study performed on 1% and 1.5% steel-fiber reinforced concrete beams reported up to 50% improvement in shear performance (Hwang, et al, 2013). Likewise, a study utilized 12 steel fiber-reinforced lightweight concrete beams tested without web reinforcement under four-point loading to conclude 30% increased shear capacity and higher ductile behavior (Kang, et. Al, 2011). A major experimental study conducted by Cho and Kim tested thirty steel fiber-reinforced concrete beams in 2003. The results show improved crack resistance, ultimate load capacity, stiffness, shear resistance while the fiber-reinforced beams resisted higher deflections (Cho and Kim, 2003). Similarly, a study tested 49 simply supported beams under concentrated loading of which a number of beams utilized transverse reinforcement whereas some beams used steel fibers instead. This comparative experimental analysis which used various fiber dosage volumes, shear-span to depth ratios not only showed improved initial shear cracking strength, but also concluded that beams reinforced with 1% volume fraction of fibers improved shear performance as much as the conventional shear-reinforcement (Narayanan and Darwish, 1987). Compiling research done on steel-fibers led to the adoption of these fibers by the ACI-318 building requirement design code. Consequently, a research study performed on synthetic-fiber reinforced concrete beams demonstrated a linear strength improvement as fiber dosage in the mix was increased, enhancing ductility and shear load resistance (Majzadeh, et. Al, 2006). Likewise, Greenough conducted an experimental research study on self-consolidating concrete reinforced with 1% synthetic fibers which showed significant improvement in shear capacity of the tested specimens (Greenough, 2008). Similarly, a comprehensive experimental research study performed on 88 notched small beams

studying the effect of polypropylene fibers on fracture behavior of concrete beams with various strengths was performed by Cifuentes and his colleagues. Results of three-point bending tests on the beams showed enhanced mechanical properties, improved failure behavior and ductility. Polypropylene fibers positively affected the elastic modulus of the concrete, enhanced compressive strength and demonstrated high resistance mechanism versus pullout of fibers (Cifuentes, et. Al, 2013). Furthermore, other various studies show that specimens reinforced with polypropylene fibers require relatively more energy for extraction while failure crack propagates which in turn affects the pullout mechanism yielding higher ductility and increased load bearing capacity (Di Maida, et. Al, 2015). Furthermore, Furlan and Hanai reported increased tensile strength, modulus of elasticity, ductility and improved shear strength in a study which used polypropylene synthetic fibers to reinforce the concrete matrix (Furlan and Hanai, 1997). A recent research study on flexural performance of polypropylene fiber-reinforced concrete beams reported increased tensile strength, ductility, increased ultimate flexural resistance along with enhanced post-cracking residual strength response due to extensive multiple cracks resulting from redistribution of stresses and fiber-bridge action (Sahoo, et. Al, 2014).

Research and implementation of macro-synthetic fibers shows considerable improvement in overall performance of concrete structures (Roesler, et. Al, 2004). The scientific research data on this material show promising benefits of implementing high modulus synthetic fibers in structural concrete members. Recent studies show enhanced bonding of fibers and concrete due to high elastic modulus, which means higher tensile strength capacity of the member. A recent study used macro-synthetic fibers in large-scale beams without transverse reinforcement to test the shear strength and behavior of the beams. The study involved using short and slender beams with 0.5%, 0.75% and 1.0% fiber-reinforcement volumes and reported initial shear crack strength improvement by up

to 30% along with ultimate shear strength improvement by 28% (Altoubat, et. Al, 2009). The study reported variation in crack pattern and considerable change in mode of failure. Beams reinforced with macro-synthetic fibers are known to alter mode of failure from abrupt brittle shear failure to a more gradual failure, where shear cracks develop to the supports showing ductile behavior and altering mode of failure from web-shear to flexural-shear cracking. This change in failure behavior is a result of improved arch-action in concrete beams reinforced with macro-synthetic fibers. The study reported higher strain capacity as a result of effective distribution of stresses along the cracks and higher ductility with increased deflection capacity. Fiber-reinforced beams resisted higher loads after initial diagonal shear crack was formed and ultimately resisted higher deflection. This was evident in short beams, which showed 138% increase in deflection capacity.

Reinforcing beams with macro-synthetic fibers resulted in improved ultimate shear strength and enhanced ductile behavior. Consequently, the load-deflection response reported in this research study show potential enhancement to global structural response due to addition of polypropylene fibers into the concrete matrix. The failure crack in conventionally reinforced beams occurred with an initial diagonal crack which resulted in total failure of the structural element. The main diagonal crack did not mark the failure of fiber-reinforced beams, since the beams were able to resist higher loads and develop multiple shear cracks as a result of improved arch-action. While shear strength improved, mode of failure changed from web-shear cracking to flexure-shear cracking. The strain-deflection response shows that the specimen resisted higher shear forces after the initial shear crack leading to stress redistribution and resistance to higher loads. The results of this research study contribute to the growing volume of literature arising from experiments in this field. This study includes comprehensive details of the tests and analysis on large-scale concrete beams and their associated small-scale beams and cylinders.

3 EXPERIMENTAL PROGRAM

3.1 General

Influence of effective shear span to depth ratio (a/d) on shear strength of beams without transverse reinforcement according to James Wight's reinforced concrete design 2015 are illustrated in figure 1, figure 2 and figure 3

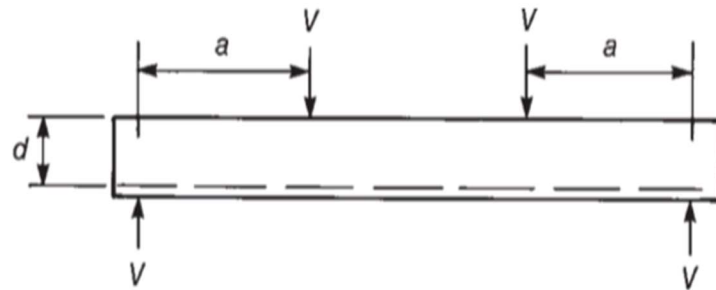


Figure 1 Typical photo of shear span to depth ratio (Wight, 2015)

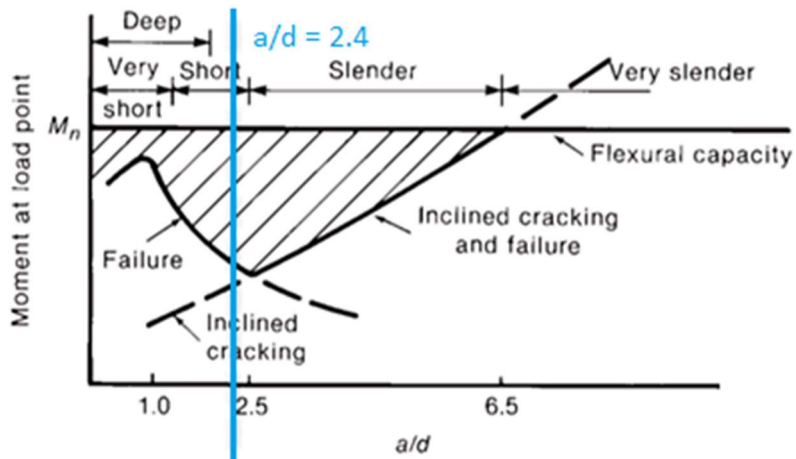


Figure 2 Moment at cracking and failure (Wight, 2015)

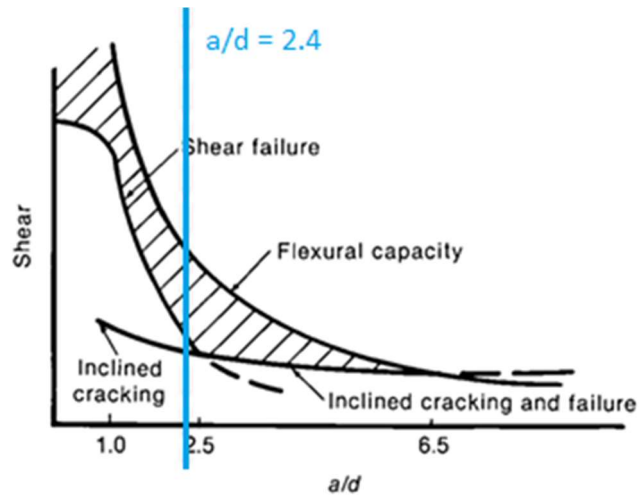


Figure 3 Shear at cracking and failure (Wight, 2015)

3.2 Material Properties of Polypropylene fibers

The macro-synthetic polypropylene synthetic fibers used in this research are rust proof and alkali resistant MasterFiber MAC Matrix fibers. The properties of the fibers used are briefly described in Table 2.

Table 2 Properties of Fibers used in this study (BASF Corporation)

Manufacturer	<i>BASF</i>
Type	<i>Macro-Synthetic Polypropylene</i>
Specific Gravity	<i>0.91</i>
Aspect Ratio	<i>67</i>
Fiber Type	<i>Embossed</i>
Material	<i>100% Virgin Polypropylene</i>
Length	<i>2.1 in. (54 mm)</i>
Tensile Strength	<i>85 ksi (585 Mpa)</i>
Alkali Resistance	<i>Excellent</i>
Chemical Resistance	<i>Excellent</i>
Absorption	<i>Nil</i>
Ignition Point	<i>1094 °F (590 °C)</i>
Melting Point	<i>320 °F (160 °C)</i>

The application of the aforementioned fibers brings about various advantages such as providing a cost-effective means of reducing project duration and labor costs as a result of excluding transverse reinforcement from design and construction. In addition, it provides a better long-term service life and helps in reducing future maintenance cost by eliminating challenges arising from corrosion and deterioration of steel reinforcement. Moreover, it aids in the crack resistance improvement of concrete as it makes the structural element behave with improved ductility. On the other hand, its high thermal expansion coefficient along with its poor UV and thermal stability makes it challenging for application at high temperatures. It is noteworthy to mention that application of fibers during casting brings about workability considerations which should be accounted for and addressed accordingly.

3.3 Fabrication of Test Specimens

3.3.1 *Design of Beam Specimens*

The beams are designed to fracture and fail in shear. As previously mentioned, they have a shear span to depth ratio of 2.4 ($a/d = 2.4$) being 6ft long and 1.25ft deep with a 2.4% reinforcement ratio. All the beams have a height of 15in. with a shear span to effective depth ratio of 2.4 and reinforcement ratio of 2.4% ($\rho=2.4\%$). Moreover, the beams are designed such that shear failure would occur on one side of the beam. This not only helped in better monitoring and tracking the failure during testing, but also reduced the number of steel reinforcement and strain gauge sensors required for performing each test.

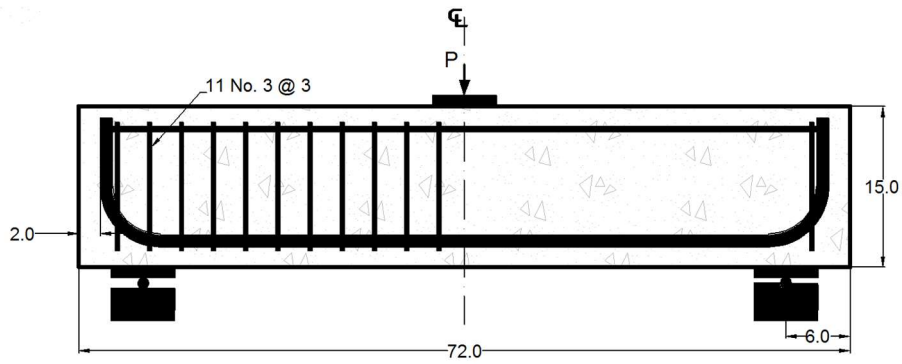


Figure 4 Details of large-scale beam without transverse reinforcement

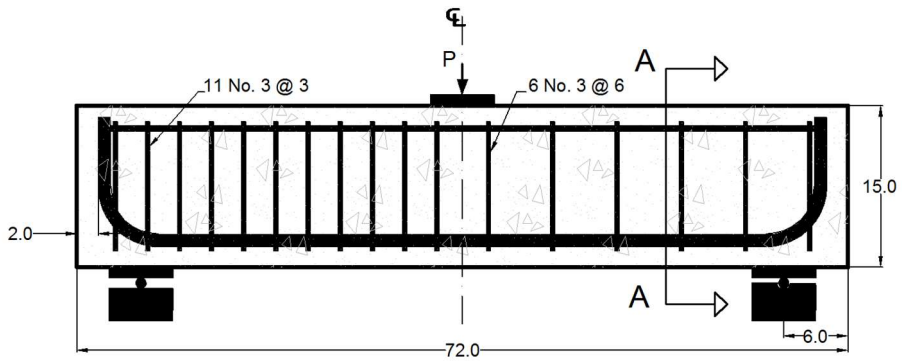
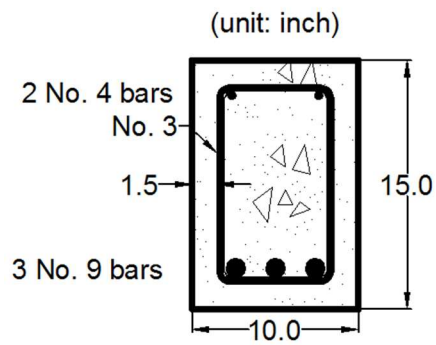


Figure 5 Details of large-scale beam with transverse reinforcement



Section A-A

Figure 6 Cross section of large-scale beam with transverse reinforcement

3.3.2 Test Specimens

Timber formworks are constructed for 8 for large-scale beams and 9 small flexural beams as illustrated in Figure 7 and Figure 8. To avoid any bonding between the timber formworks and poured concrete, the interior panels of all formworks are oiled up. Furthermore, this significantly helped in demolding of casted specimens from the formworks in the next stage.

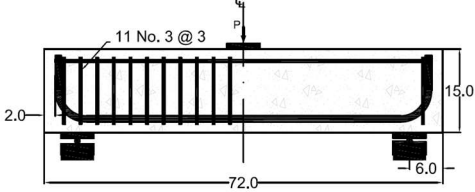
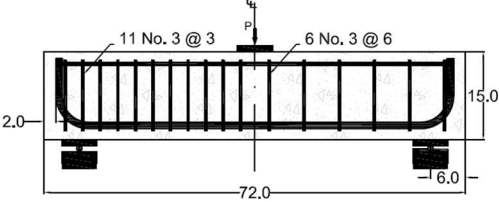
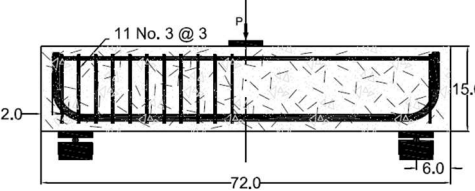
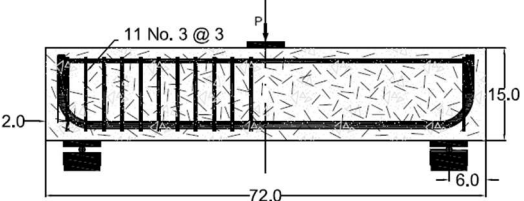


Figure 7 Typical Formwork for large-scale specimens



Figure 8 Formwork for Small-Scale Flexure Beams

Table 3 Details of large-scale beams

Specimen Name	Reinforcement and Dimension Details
<p>Reinforced Concrete Beam without Transverse Reinforcement (RC)</p>	
<p>Reinforced Concrete Beam with Minimum Transverse Reinforcement (RCS)</p>	
<p>Synthetic Fiber-Reinforced Concrete Beams with $V_f = 0.5\%$ (SNFRC 0.5%)</p>	
<p>Synthetic Fiber-Reinforced Concrete Beams with $V_f = 0.75\%$ (SNFRC 0.75%)</p>	

3.3.2.1 Steel Strain Gauges

The steel-reinforcement are prepared for application of strain gages. They are initially grinded using an *AirDie* grinder producing a smooth and flat surface (Figure 9). The threading on steel reinforcement is complimentary to bonding between steel and concrete and therefore extensive grinding of the threads can be detrimental to the required bonding. As a result, an insignificant amount of the thread is grinded just to provide a smooth available surface. Strain gage manufacturer's (Micro-Measurements precision group) instruction bulletin B-137 and B-129 of manufacturer are followed in preparing the steel surface and installation of strain gauges.

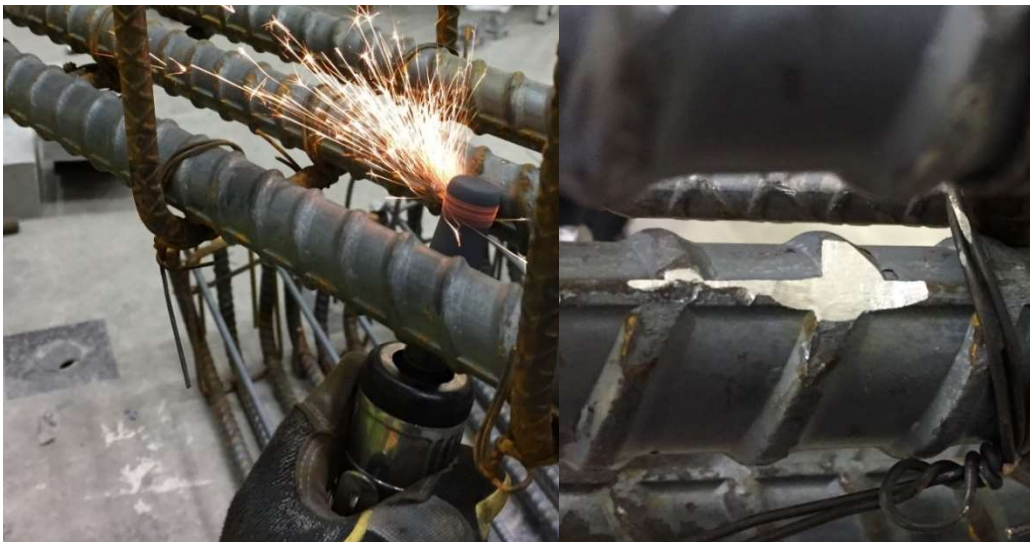


Figure 9 Grinding Steel Reinforcement for Strain Gage Application

Developing a strong bond between an installed strain gauge and the steel rebar is crucial to obtaining an accurate strain measurement. Therefore, the physical and chemical properties of the strain gauges in-use are studied and considered. The challenge here is to initially assure a complete healthy bond between the strain gauge and the steel for transmission of surface strains. Next, to assure that all components of the installed strain

gauge are completely protected during casting, demolding, curing and is fit for testing. Project conditions and demands are discussed with the strain gage manufacturer, recommended settings and necessary measures are taken to satisfy study goals and objectives. From this point, strain gauges installed on steel reinforcement embedded in concrete are referred to as “*steel strain gauges*” and strain gauges installed on the surface of concrete a few hours before testing are referred to as “*concrete strain gauges*”. Initially, the surface where the strain gauge is to be installed must be prepared for using the surface preparation procedure instructed by the manufacturer (Micro-Measurements, 2009). The surface preparation step includes degreasing, abrading, burnishing, conditioning and finally neutralizing. The surface preparations step is common for installing steel or concrete strain gauges. However, the steps following the surface preparation are not the same. Initially, the steel strain gauge installation process shall be discussed in detail. It is noteworthy to mention that the strain gauge should not encounter non-neutral surfaces.



Figure 10 Neutralizing a smooth glass surface

Therefore, a smooth neutralized glass surface is used to place a C2A strain gage on with a PTC tape covering the gauge prior to placement on steel surface. Furthermore, a degreaser is used to on the steel surface and wiped with a gauze sponge. Abrading of the surface includes two parts, an initial dry abrasion stage using a rough silicon carbide

paper and then a wet abrasion part done by applying liberal amounts of conditioner and scrubbing with a softer grit paper. Only the manufacturer specified gauze sponge is used to clean steel surface after each step. Figure 11 shows a typical grinded steel surface subjected to dry abrading and cleaning using a gauze sponge.

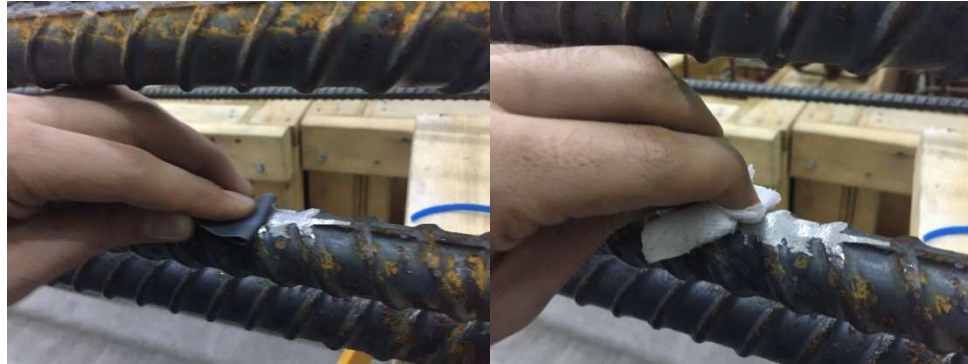


Figure 11 Abrading of steel surface

Note that at this point the strain gauge is on a neutralized glass surface aligned using a PCT tape. To ensure proper alignment of the gauge assembly on the steel surface, a 4H pencil is utilized to burnish layout lines onto the steel rebar. Furthermore, the surface is conditioned using the M-Prep Conditioner-A and a cotton applicator and then wiped clean. An M-Prep Neutralizer 5A is then used to neutralize the steel surface which helps in sufficient bonding. Cotton tip applicators are used with neutralizing agent to scrub the area and then the surface is wiped clean making it ready for strain gauge application. The prepared surface, being exposed to laboratory environmental conditions, may lose the developed bonding qualities after 30 minutes. Therefore, the strain gauge is installed quickly after the surface preparation step. This makes it challenging when installing multiple gauges since the procedure is repeated for every strain gauge which needs to be installed.



Figure 12 Steel strain gage installation kit



Figure 13: Catalyst applied to bonding side of strain gage

The steel strain gage is installed using a M-Bond 200 adhesive and a M-Bond 200 catalyst as seen on image 12 along with other material used for this step. A neutralized tweezer is used to pick the corners of the PCT tape overlaying the strain gage which is then placed on top of the steel surface considering the alignment lines burnished previously. Then the tweezer is used to pick the tape at a shallow angle and rotate the

gage to place it back on itself as seen in image 13, exposing the bonding side of the gage along with the wiring terminal.



Figure 14 Removing the tape from the gauge assembly

Extra attention must be paid to the wiring terminal connection on the strain gauge, the connection is known to be very sensitive and any unnecessary rapid strong action affecting the terminals will lead to a damaged connection and erroneous strain readings during testing phase. A thin layer of catalyst is applied on the bonding side of the strain gauge, as seen in figure 13. This layer prevents moisture absorption by uncured adhesive. The catalyst takes approximately a minute to dry out. A drop of adhesive is then placed onto the steel surface at the intersection of the steel surface and the flipped over gauge assembly. Then the gauge assembly is turned back onto the steel surface spreading the adhesive under the assembly obtaining a homogenous adhesive distribution under the gauge. Firm thumb pressure is applied onto the gauge for over two minutes. The tape is then carefully removed at a shallow angle paying extra attention to the connection terminals. At this point, the well being of an installed strain gauge is inspected using an ohm meter. Different types strain gages have different resistance, which is specified by the manufacturer. The resistance of the steel strain gauge used in this study is 350 ohms. Figure 15 shows the inspection performed on a successfully installed typical steel strain gauge.



Figure 15 Inspection of an installed steel strain gauge

The strain gauges are then coated with 0.02 inch thick transparent non-corrosive silicone rubber film called M-Coat C (as seen in figure 16). This coat has good electrical properties offering chemical, water and corrosion protection. Once applied, 24 hours of curing is required at 75°F before other layers of coating are applied.



Figure 16 M-Coat C coated steel strain gauge

Furthermore, the solvent-thinned flexible nitrile rubber M-Coat B is used as the next coating layer (as seen in figure 17).



Figure 17 M-Coat B coated strain gauge

Precautionary steps are taken to ensure protection of vinyl wires connected to the strain gauge. Parts of the wire will be embedded in concrete, considering the challenging sporadic dynamic load applied on the wire during casting of beams, polyethylene tubes are used to protect the wires. Moreover, the 0.17-inch-thick polyethylene tubes protect the wires from liquid penetrating through its microscopic pores which can lead to shorting out the strain gauge circuit. In addition, since the two ends of the polyethylene tube are open, there is a chance of unwanted material penetrating into the wire. The end which leads to the strain gauge assembly is coated and sealed with a 3M electrical tape covering the front end of the tube along with the whole gauging assembly (as seen on the left side of figure 18). Finally, a GB electric liquid tape is utilized to coat the setup ensuring optimum physical and chemical protection of the whole assembly (as seen on the right side of figure 18).



Figure 18: waterproof and UV-resistant sealed strain gage assembly

In summary, coating the strain gauges with M-Coat C, M-Coat B, 3M electric tape and GB liquid tape gives significant protection to the gauge setup. The polyethylene tubes exit the beam at the far most end so that the shear behavior of the beam is not influence by the setup. Figure 19 shows a steel cage with applied strain gauges tubed and ready for placement into formwork.

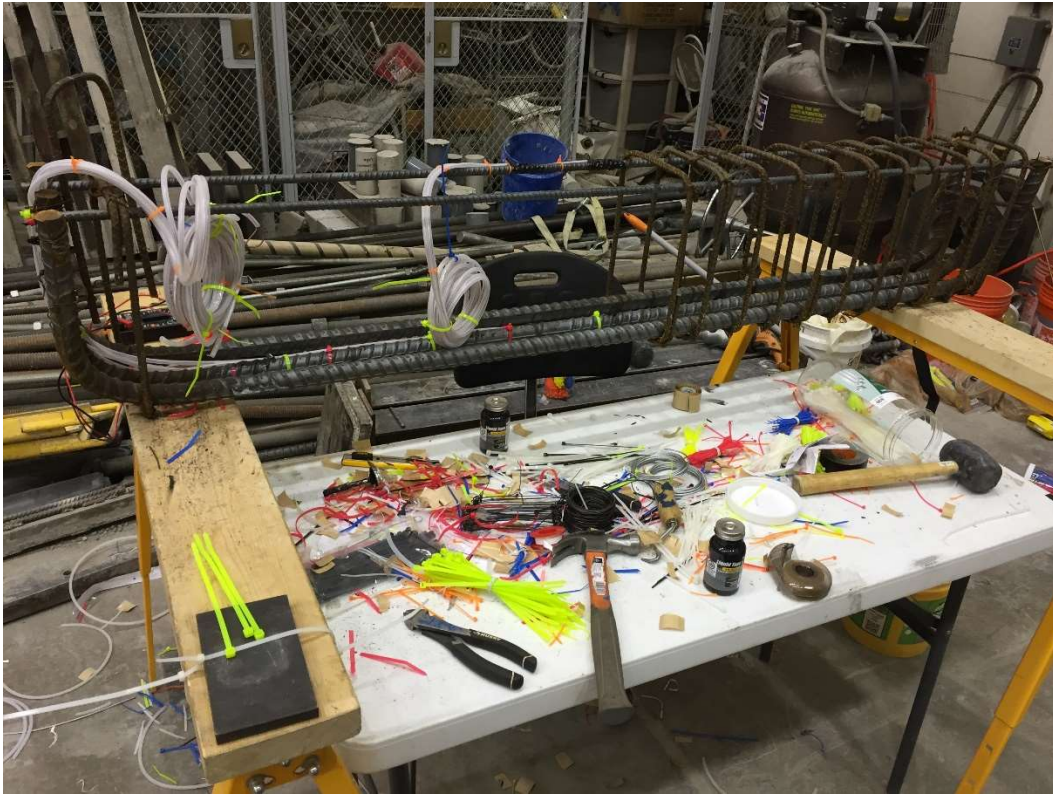


Figure 19 Tubed strain gage wires installed on steel reinforcement

Table 4 gives the dimensions of the steel strain gauges utilized in this study. Figure 21 shows the gauge pattern of a wired-strain gage. 64 of the illustrated gauges are used in this study with 7 gauges installed on each RC, SNFRC 0.5%, SNFRC 0.75% beams and 11 gages installed on each RCS beam.

Table 4 Dimensions of Steel Strain Gauges

C2A-06-125LW-350					
Gage Length	Overall Length	Grid Width	Overall Width	Matrix Length	Matrix Width
0.125 in	6.05 in	1.78 in	2.03 in	8.00 in	4.32 in

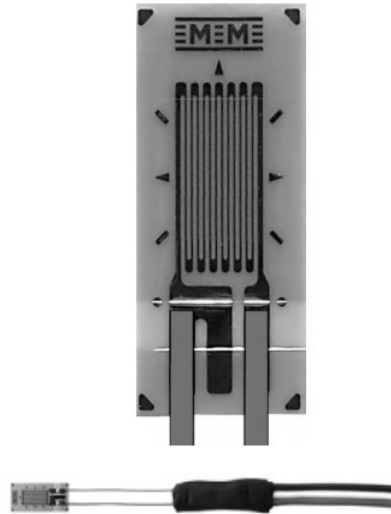


Figure 20 Steel Strain Gauge Pattern

RC and SNFRC beams do not have stirrups on the monitored half of the beam. Therefore, strain gauges are installed on the bottom reinforcement at the middle of the beam. This region is of particular interest since flexure in that area is a dominating mechanism. Similarly, since shear cracks develop from face of support to the face of the steel load plate placed on middle top of the beam, other strain gauges are placed on the anticipated shear fracture line. The location and orientation of the installed strain gages on beams without transverse reinforcement is illustrated in figure 21. Similarly, steel strain gauges utilized on RCS beams are placed considering the shear fracture path and flexure fracture location. The location of the installed strain gauges on beams with transverse steel reinforcement is see in figure 22. It is noteworthy to mention that steel strain gauges are

tagged considering their girder location. For instance, strain gauge E5 is located on vertical grid line E and horizontal grid line 5.

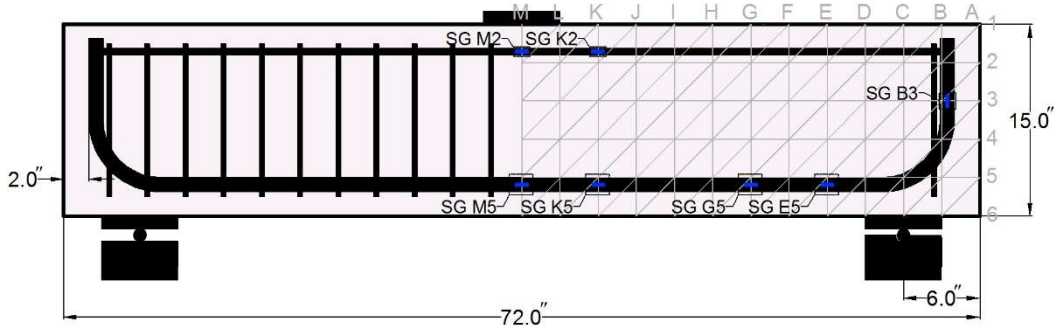


Figure 21 Layout of strain gauges on reinforcement of typical RC & SNFRC beams

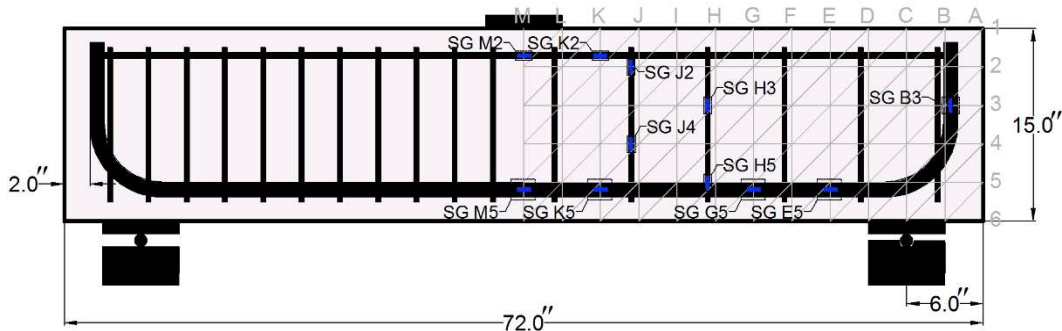


Figure 22 Layout of strain gauges on reinforcement of typical RCS beam

3.3.2.2 Concrete Strain Gages

In addition to the 64 strain gauge sensors installed on steel reinforcement embedded in the concrete beams, 56 strain gauges are installed on surface of concrete beams, referred to as "*concrete strain gauges*" in this study. Concrete strain gauges used are either rosette strain gauges or ordinary C2A gauges used previously on steel, utilized based on the failure mechanism dominating the area on the which the gauge is to be installed. Therefore, a total of 32 rosette gauges along with 24 C2A strain gauges are installed on concrete surface of the 8 beams.

Rosette strain gauge consists of two or more closely located gage grids, each oriented with regards to measuring normal strains in different directions. These are specific

purposes strain gauges used to obtain principal strains and stresses when structural element is subject to biaxial stresses. There are three common rosette gauges as seen in figure 23: Tee rosette with two perpendicular grids, Rectangular rosette gauges with 45° angular displacements between second and first grid and 90° angular displacements between third and first grids. The third type, known as delta rosettes, have a 60° angular displacement between each grid. Each rosette comes in different gauge lengths and therefore selection of rosette for experimental purposes should take the dimension of the gauges into account.

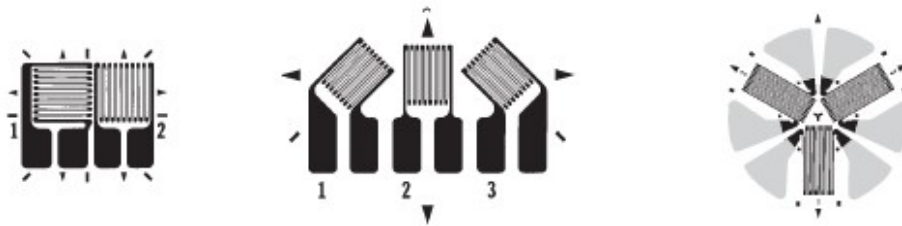


Figure 23 Tee, Rectangular and Delta Rosettes, respectively

In addition, these gauges are either single-plane or stacked. In the event that principal strains directions are known, the most suitable rosette would be the tee. In case other stresses such as axial or bending influence the direction of principal axes, utilization of rectangular or delta rosettes is recommended. Apart from this consideration, the selection criteria is governed by practicality of installation and testing. Planar rosettes, require a larger installation area versus stacked rosettes. The three grids on the stacked rosette gauges measure the strain at the same point. The C2A-06-125WW-350 stacked rosette strain gauges with a $\pm 3\%$ strain capacity are selected for measuring surface strains in this study, as seen in figure 24. (Micro-measurements, 2008). Moreover, the dimensions of the the gauges used in this study are summarized in table 5.

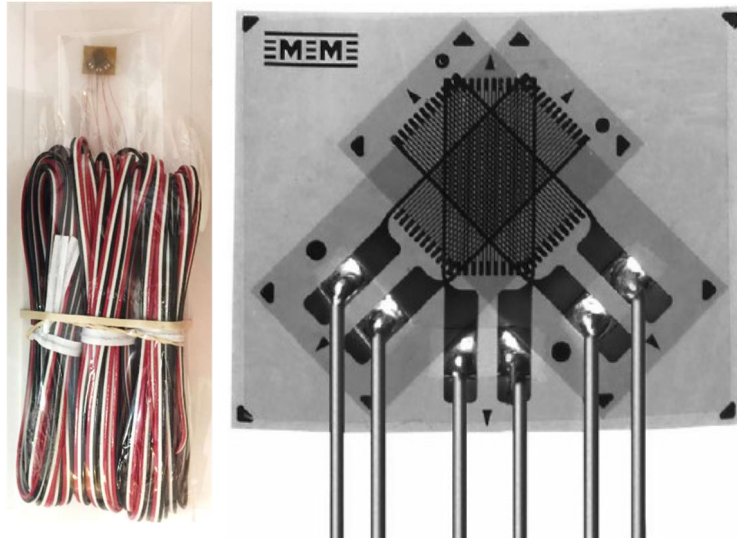


Figure 24 Stacked rectangular rosette gauges used in this study

Table 5 Rosette Strain Gauge Dimensions

C2A-06-125WW-350 (inch)					
Gage Length	Overall Length	Grid Width	Overall Width	Matrix Length	Matrix Width
0.125 ES	0.241 CP	0.07 ES	0.280 CP	0.309	0.375

It is noteworthy to mention that labelling of each individual grid has to follow a particular sequence designated by the manufacturer. Failure to follow prescribe labelling methods leads to erroneous results. For example, an H2-3 label means that the gauge is located on vertical gridline H, horizontal gridline 2 and is oriented in direction 3, as seen on figure 25. Strain transformation formulas are utilized for determination of principal strain measurements obtained testing. Concrete specimens fracture when maximum tensile stress supersedes the tensile stress capacity of the specimen. The tensile stress capacity of a large-scale beam is determined from material testing of small specimens according to

ASTM standard test method for flexural performance of fiber-reinforced concrete (ASTM, 2005). Normal strains are expressed in terms of angular distance from the principal axis.

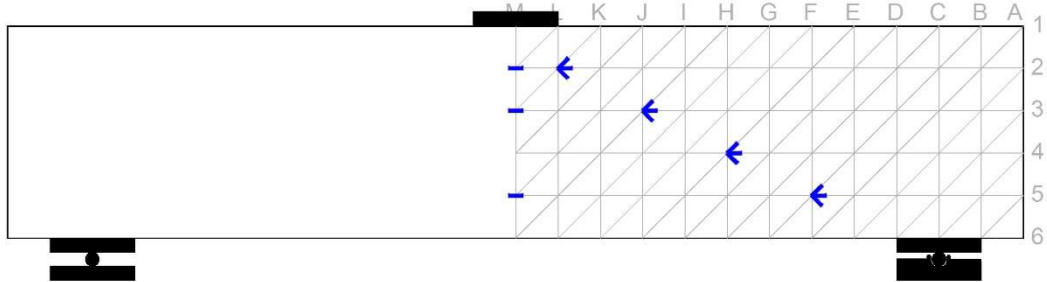


Figure 25 Type and location of concrete strain gauges

3.3.2.3 Concrete Pouring

Formworks are fabricated for 8 large-scale beams along with 9 small-scale beams and 19 cylinders. Initially, the 4 RC and RCS beams which had no fibers are casted. Then the 4 SNFRC beams with different fiber volume fractions are casted. Each large-scale beam's accompanying small-scale beams and cylinders are casted using their equivalent batch. In summary, after the steel skeleton of the beams with installed strain gauge sensors were ready, they were placed into the formworks and ready for concrete pouring, as seen in figure 26.



Figure 26 Formworks for large-scale beams

Concrete was delivered by a volumetric mixer which carried necessary mix-design ingredients on the truck. The volumetric mixer has the ability of measuring the volume of raw materials and using an auger to blend the mix blends with water. A batch metering system performs these volumetric measurements before the raw ingredients enter the mixing chamber. The mixer then starts mixing the raw ingredients per the required concrete specified, on-site, a few minutes before pouring starts. The result is a fresh on-site concrete mix which is poured into the formworks. An internal vibrating device is used to vibrate the poured concrete to achieve proper consolidation of the concrete mix, as seen on figure 27.



Figure 27 Concrete Pouring and vibrating

Two cubic yards 5 ksi strength concrete with a slump of 7.0 to 9.0 inches was delivered to Civil Engineering Building Laboratory (CELB) in University of Texas at Arlington (UTA). An on-site slump test is performed according to ASTM C143, which involves utilizing an 8 inch bottom diameter and 4-inch top diameter 12-inch high slump cone (ASTM, 2003). Fresh concrete is poured into the cone up to one-thirds of the cone's height, the next one-third is poured after tamping the concrete 25 times. The procedure is repeated until the cone is complete filled with concrete and then struck flush from the top with a rod. The concrete subsides after carefully removing the cone vertically. The measured subsidence gives the slump of the concrete mix, as seen in figure 28.



Figure 28 Slump test performed on-site

Figure 29 shows fresh concrete pours, the first one being a plain concrete mix which is used for 2 RC beams and 2 RCS beams. The second image shows the 0.5% volume fraction concrete mix used for the two 0.5% SNFRC beams and the third image shows the 0.75% volume fraction concrete mix used for the two 0.75% SNFRC beams. Moisture loss of the casted specimens was prevented by covering the specimens with polyethylene tarps after the pour. Finally, the specimens were demolded and placed into the curing room, as seen in figure 30.

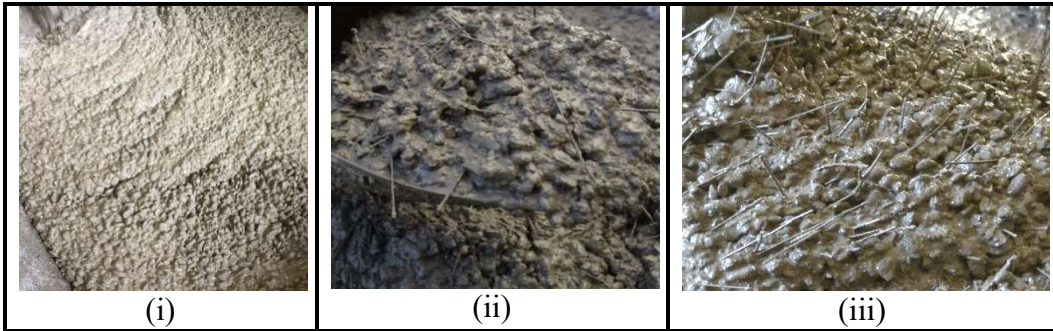


Figure 29 Typical images of (i) plain concrete, (ii) 0.5% SNFRC (iii) 0.75% SNFRC



Figure 30 Small-scale specimens in curing room

Table 6 Mix-design of delivered concrete mix

<i>Source</i>	<i>Description</i>	<i>ASTM</i>	<i>SG</i>	<i>Abs.Vol. (CF)</i>	<i>Admix. Oz.</i>	<i>SSD Wt. (lbs)</i>
CCI	Type I/II/Pozzoslavag Blend	C-1157	2.85	3.7		658
Trinity Materials	Pea Gravel	C-33	2.65	11		1819
Trinity Materials	Concrete Sand	C-33	2.66	6.71		1114
Dallas	City Water	C-1602	1	3.93		245
Sika	6100	C-494	1.02	0.04	39	3
Euclid	Air 30	C-260	1		7.92	1
	Air			1.62		
f'_c	5000 psi @ 28d			27		
Slump	7.00 to 8.00 inch	Designed Unit Weight		142.22		
Specified Air	0.00 to 0.00	Designed W/C Ratio		0.37		
Designed Air	6.00%	Designed Volume		27	TOTAL	3840



Figure 31 Poured large-scale concrete beams

3.4 Test Set-Up and Procedure

3.4.1 Testing of Large-Scale Beams

The 8 large-scale beams are tested using a 400-Kip load-controlled compression machine. In addition, the 9 small-scale beams are tested using the 50-kip Materials Test System (MTS) machine. Furthermore, the cylinders were tested in compression machine using a 500-kip compression testing machine. Splitting-tensile testing of cylinders are performed using a 60-Kip compression machine. This section elaborates the testing equipment and procedure utilized for performing each of the aforementioned tests.

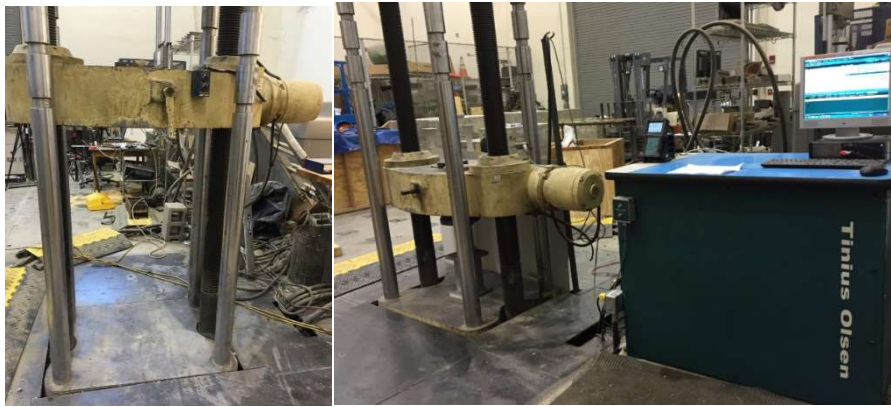


Figure 32 400 Kip compression machine

A simply supported setup is used for testing of the 8 large-scale testing using the 400-kip compression machine. The machine has two cross-heads, one on the top and one on the bottom, as seen in figure 32. The top cross-head stays fixed in place after initial adjustments are made to accommodate the supports, the beam, the load plates and the load cell. The lower cross-head moves upward in a steady manner and the machines load cell monitors the loading rate. Two 10 feet long wide-flange steel girders are aligned on the lower plate. The roller and pin support on the two ends are placed on the steel girder. A rollers support permitting lateral translation is used on the left end of the beam and a pin

support with no allowable lateral translation is setup on the right end of the beam. Aligning and centering the girders, the supports and specimen under the loading plate is fundamental to obtaining accurate results. The objective here is to make sure that the point load is applied exactly at the mid-span of the beam and that the supports are at their designated location in accordance to the beam design criteria of the study. Moreover, the top surface of the beams is grouted. The load cell is placed on top of 3 plates that are placed on top of the beam. Once the setup is ready for testing, a monotonic load 2.2 kip/minute constant point load is applied. Simultaneously, the load cell records the instantaneous load applied and the two-linear variable differential transformers (LVDT) records the mid-span and quarter-span deflection of the beams. The LVDT's are connected to the steel girders under the concrete beam and vertically intersect a thin aluminum plate attached under the concrete beam to take deflection measurements, as seen in figure 33. It is noteworthy to mention that all the measuring devices used for testing were calibrated by their respective manufacturers before any test was carried out. All the recordings were transmitted to a network of data acquisition scanners. The scanner network comprised of 3 Micro-Measurements VPG scanners connected to each other using relay cables, this provided 60 available channels. Data is obtained at a 0.02 second time intervals. Furthermore, each strain gauge sensor is connected to the scanner network using wiring adaptors acquired from strain gauge manufacturing firm. The main scanner within the network is the connected to a windows based StrainSmart equipped computer using PC5101B PCMCIA interface adapter (as seen in figure 34). Thus, the assembly produces accurate and reliable test data which lays a concrete foundation for performing an accurate stress analysis study.

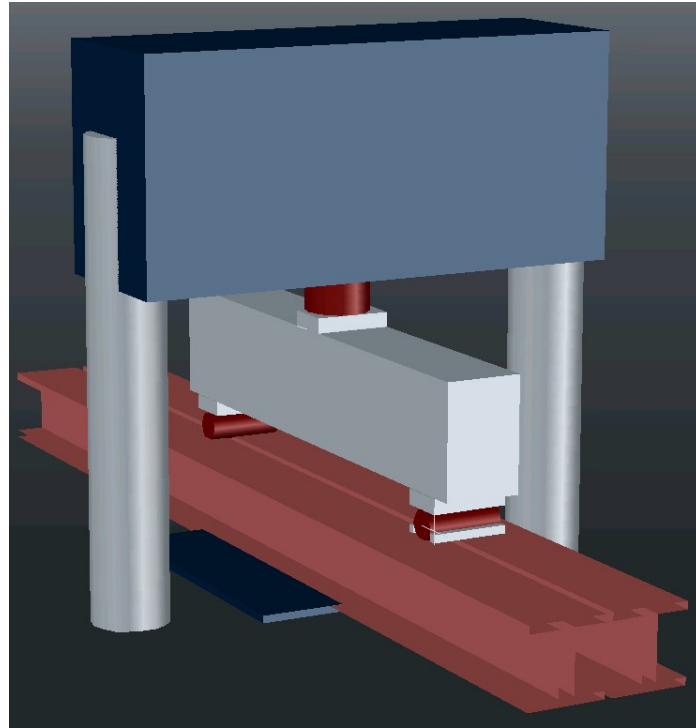


Figure 33 Typical test setup for large-scale beams

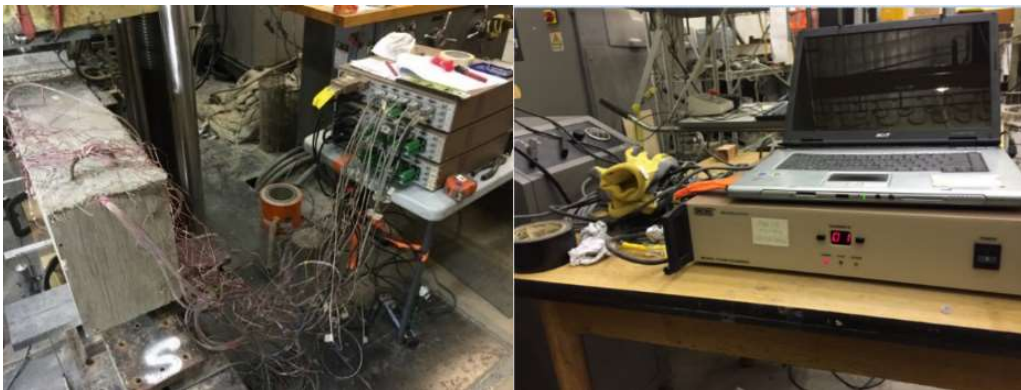


Figure 34 Data acquisition network

3.4.2 Testing of Small-Scale Beams

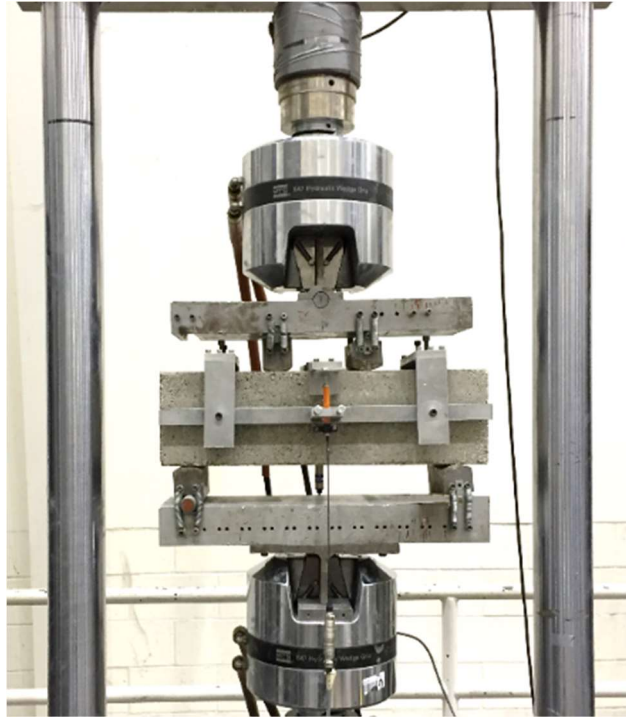


Figure 35 Material Test System (MTS)

Similarly, the MTS machine used for testing of small-scale beams in accordance with ASTM C1609 standards has two hydraulic wedges which compress the specimen. The produced 20-inch long beams have a 6-inch by 6-inch cross section, in compliance with the 1609 standard. Furthermore, the setup included utilizing a standard fixture mounted to the beam providing a specially designated holding place for two LVDTs on either side of the beam. This leads to obtaining the mid-span deflection on the front face and the back face of the beam. Calculating the average of the two readings results in the net mid-span deflection in the center of the beam. A roller support and a pin support make up the boundary conditions for this test. Deflection is recorded up to 1/150th of the span using a constant loading rate of 0.004 inch/minute. The linear displacement sensors transmit the data to a windows based laptop equipped with StrainSmart software via a VPG

scanner. In the meantime, the MTS machine which is operated by a separate computer and a flex-test scanner, is recording the displacement and load applied by the machine. This data is transmitted to StrainSmart by connecting the flex-test scanner to the VPG scanner using high-level adapters. The MTS machine along with a typical test setup used for determining the tensile strength of the produced material is seen in Figure 35. Formula (1) is used for determining the modulus of rupture of the tested specimens.

$$f_r = \frac{P \times L}{b \times d^2} \dots\dots\dots (1)$$

Where:

f_r = the strength, psi (MPa),

P= the load, lbf (N),

L= the span length, in. (mm),

b= the average width of the specimen, in. (mm),

d= the average depth of the specimen, in. (mm).

The area under the load-deflection curve, up to a deflection of 1/150th of the span (0.12in.), is called toughness and can measure the ductility of the beams. The peak load, modulus of rupture (f_r), and the area under the load-deflection (toughness) are calculated for each tested specimen, and results are presented in the forthcoming sections.

3.4.3 Tensile Strength Testing of Cylinders

9 cylinders accompanying their respective large-scale beams are used for performing split-cylinder test according to ASTM C496 using the 60-kip compression machine seen in figure 37 (ASTM, 1984). The results are valuable for assessing the shear strength of concrete. To perform this test, a cylindrical specimen is placed flat on its long-axis, as seen on Figure 36, allowing a compressive diametric force to be applied its length. The test is performed using a constant rate of 100 to 200 lb/in² per minute until the specimen develops a tension crack along its diameter. The maximum sustained load due to the triaxial compression force is used in calculating the splitting tensile strength of the specimen.



Figure 36 Tensile-Splitting Test



Figure 37 60-kip compression machine

3.4.4 Compressive Strength Testing of Cylinders

Similarly, a 500-kip compression machine is used to perform the ASTM C39 test on 10 cylindrical specimens (ASTM, 2001). However, since the study's scope involved obtaining stress-strain curves of cylindrical specimens tested in compression, a special alignment-jig with the capability of accommodating two linear displacement sensors is used. The LVDT measures the displacement in the middle 5.5 inch of the 4-inch diameter by 8-inch cylinder. The test results are highly dependent on a proper setup. The jig is tightly screwed onto the specimen, holding two LVDTs. The test involves connecting the load cell and the LVDTs to a scanner which transmits the recorded data to a *StrainSmart* equipped laptop. The maximum sustained load under a constant loading rate of 400 lb/sec (35 psi/sec) is recorded and used for determining the compressive strength of a tested specimen. Furthermore, the load-deflection data acquired by *StrainSmart* is used in plotting strain-stress curves used for stress analysis in this study. Table 7 contains images of test setup and instrumentation.

Table 7 Compression test setup and instrumentation for cylindrical specimens



Figure 38 500-Kip Compression machine



Figure 39 Testing jig mounted to cylinder for compression test



Figure 40 Typical compression test setup



Figure 41 Compression test data acquisition network

4 EXPERIMENTAL RESULTS AND ANALYSIS

4.1 Large-Scale Beams

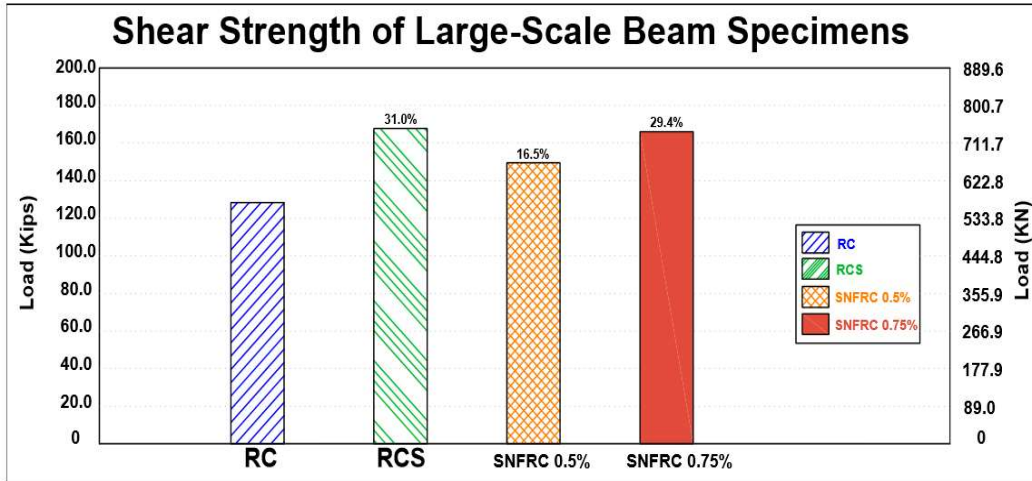


Figure 42 Comparison of Shear strength for Large-Scale Beams

Table 8 Large-Scale Beam Test Result

LARGE-SCALE BEAM TEST RESULTS				
Beam #	Beam Type	Failure Load (Kips)	Avg. Failure Load (Kips)	Avg. Shear Capacity (kips)
1	RC	123.80	128.28	64.1
2	RC	132.77		
3	RCS	166.85	167.69	83.8
4	RCS	168.53		
5	SNFRC 0.5%	147.06	149.50	74.7
6	SNFRC 0.5%	151.93		
7	SNFRC 0.75%	164.25	166.03	83.0
8	SNFRC 0.75%	167.80		

4.1.1 Failure Mechanism



Figure 43 Typical shear crack on a large-scale Beam

Cracking and failure in tested beams mainly occur within the mid-15 inches from the beam centerline. Appendix-A of this study presents a detailed documentation of the failure crack patterns in large-scale beams. The initiation, development and propagation of these cracks were closely monitored during testing. An inclined crack extending upward from the face of the support reaching the compression zone where the point load is being applied. The critical section, being “d” distance from the face of the support, located at 12.5 inches is the location where shear failure becomes prominent and critical. The first crack usually occurred at the mid-span and then propagated to the shear span. After the initial vertical crack, as the applied load kept increasing, cracks started to incline as they moved away from the mid-span and closer to the support. These cracks are a result of both flexure and shear forces and are popularly referred to as diagonal cracks. SNFRC beams resisted higher loads and did not fail after the first crack, whereas RC beam’s failure occurred rapidly after the initial crack. SNFRC beams resisted higher deflection and showing higher ductility, this behavior was clearly evident during testing especially with SNFRC 0.75%

beams. Moreover, the diagonal cracks in RC beams were steeper in comparison to diagonal cracks observed in RCS and SNFRC beams. This observation shows a cracking similarity between RCS and SNFRC beams. Moreover, another noteworthy observation was the failure mechanism of fibers which are subject to tension while attempting to resist the crack width widening. Fibers resisted crack widening until they failed due to rupture, rather than pullout.



Figure 44 Failure crack widening and pullout resistance of fibers

Failure crack widths formed on SNFRC beams were relatively smaller in comparison to RC and RCS beams, mainly due to a phenomenon known as “fiber bridging”. This occurs when fibers create a bridge at the location of the crack and resist the two splitting surfaces from separating. Figure 44 illustrates the bridging of fibers during the testing of a SNFRC beam as diagonal shear crack widens. The resistance continues as induced load increases while fibers resist increasing principal stresses while the inclined crack continues to widen. Testing observations show that the fibers in tension usually fail due to rupture rather than pullout from concrete matrix, although pullout of fibers have also

been observed in some cases. Figure 45 shows the failure mode of synthetic polypropylene fibers in an SNFRC beam at the location of the failure shear crack.



Figure 45 Pullout resistance and rupture of fibers in SNFRC beams

RC beams failed due an sudden brittle shear crack resulting from a web-shear crack due to the maximum induced shear stress exceeded the tensile strength of concrete causing a sudden failure crack. However, this undesirable mode of failure did not occur in SNFRC beams. Reinforcing the concrete matrix with macro-synthetic fibers changed the failure mode to more of a flexure-shear crack rather than a web-shear crack. These cracks often began initiated the mid region of the shear span, steadily inclining towards the support and loading point, separating the concrete surface into two planes. At this moment, the specimen acts as two rigid bodies, while fibers resist the widening of these cracks and surface concrete strain gauges show a constant strain measurement. Constant strain measurement at this point shows that principal strain on the surface of the concrete have a maximum value exceeding the materials tensile capacity. Furthermore, enhancing the beams with macro-synthetic polypropylene fibers improved arch-action in beams leading

to increased shear strength. Other previous studies on effect of fibers in concrete matrices have reported increases shear strength as a result of improved arch-action as well (Fenwick and Paulay, 1968). The effect of macro-synthetic polypropylene fibers after the formation of the main diagonal crack cannot be overemphasized. With pronounced effect on increasing shear strength through helping the concrete to resist higher tensile principal stresses and therefore allowing the beam to handle higher deflections. The fibers resistance to this separation is based on their high modulus. It is important for fibers used for reinforcing concrete members to have a high elongation capacity, as the fibers bonding quality and elongation capacity helps in resisting stresses separating the concrete in the critical region. Early studies performed on fiber-reinforced structural members have reported on the pivotal role of high-modulus fibers in resisting crack widening (Ashour, et. Al, 1992). Concrete crushing failure was more evident in SNFRC beams in comparison to RC and RCS beams, meaning that SNFRC beams were able to resist shear stresses at greater magnitudes. The compression zone, aggregate interlock and dowel action of longitudinal steel reinforcement helps in resisting forces after the main diagonal crack occurs in RC beams. While the diagonal cracks widen and tension increases in concrete, leading to an increased dowel force which results in cracks (horizontal) along the length of the longitudinal steel reinforcement. On the other hand, SNFRC beams showed stable and subtle shear crack propagation and crack widening, as previously seen in research studies performed on macro-synthetic fibers (Altoubat, et. Al, 2007).

4.1.2 Strain Measurements

4.1.2.1 Principal Strains in Concrete

The following procedure is used to calculate the maximum principal strain (ε_p), minimum principal strain (ε_Q) and shear strain (γ) using data obtained from rosette gauges on surface on concrete beams

$$\frac{\varepsilon_p + \varepsilon_Q}{2} + \frac{\varepsilon_p - \varepsilon_Q}{2} \cdot \cos(2 \cdot \theta) = \varepsilon_1$$

$$\frac{\varepsilon_p + \varepsilon_Q}{2} + \frac{\varepsilon_p - \varepsilon_Q}{2} \cdot \cos(2 \cdot (\theta + 45 \text{ deg})) = \varepsilon_2$$

$$\frac{\varepsilon_p + \varepsilon_Q}{2} + \frac{\varepsilon_p - \varepsilon_Q}{2} \cdot \cos(2 \cdot (\theta + 90 \text{ deg})) = \varepsilon_3$$

$$\gamma = |\varepsilon_p - \varepsilon_Q|$$

For instance, for RC BM#1, calculation for location of F5 is calculated by:

$$\varepsilon_1 = 41.34 \mu\varepsilon, \varepsilon_2 = 131.12 \mu\varepsilon, \varepsilon_3 = 98.93 \mu\varepsilon$$

$$\begin{bmatrix} \varepsilon_p \\ \varepsilon_Q \\ \theta \end{bmatrix} := \mathbf{find}(\varepsilon_p, \varepsilon_Q, \theta) = \begin{bmatrix} 137.6 \\ 2.7 \\ 2.1 \end{bmatrix}$$

$$\theta = 2.1 \text{ radian} = 122.36 \text{ degree}$$

$$\theta_{p,\max} = -122.36 \text{ degree}$$

$$\theta_{p,\min} = 57.64 \text{ degree}$$

$$\theta_{p,\gamma} = -32.36 \text{ degree}$$

$$\gamma = |\varepsilon_p| - |\varepsilon_Q| = 134.88 \mu\varepsilon$$

$$y_{dir1} := \frac{\varepsilon_p - \varepsilon_Q}{2} \cdot \sin(2 \cdot \theta) = -13.5$$

$$y_{dir2} := \frac{\varepsilon_p - \varepsilon_Q}{2} \cdot \sin(2 \cdot (\theta + 45 \text{ deg})) = -36.78$$

$$y_{dir3} := \frac{\epsilon_p - \epsilon_Q}{2} \cdot \sin(2 \cdot (\theta + 90 \text{ deg})) = 13.5$$

The Mohr-circle of the stacked rosette strain gauges is shown in Figure 46 for the three orientations of the strains.

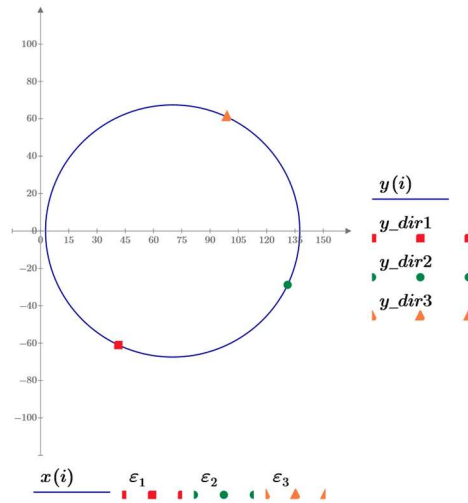


Figure 46 Mohr-circle for rosette concrete strain gauge in RC BM#1 on gridline F5
 Appendix B includes tabulated values of principal strains and tensile cracking strains of large-scale concrete beams.

4.2 Tensile Cylinder Specimens

Table 9 Tensile strength of cylinder specimens

TENSILE STRENGTH OF CYLINDERS			
Cylinder #	Cylinder Type	Tensile Strength (psi)	Avg. Tensile Strength (psi)
1	Plain Conc.	525.0	527.4
2		534.3	
3		522.9	
1	SNFRC 0.5%	562.5	582.0
2		601.0	
3		582.5	
1	SNFRC 0.75%	715.4	691.0
2		629.9	
3		727.8	

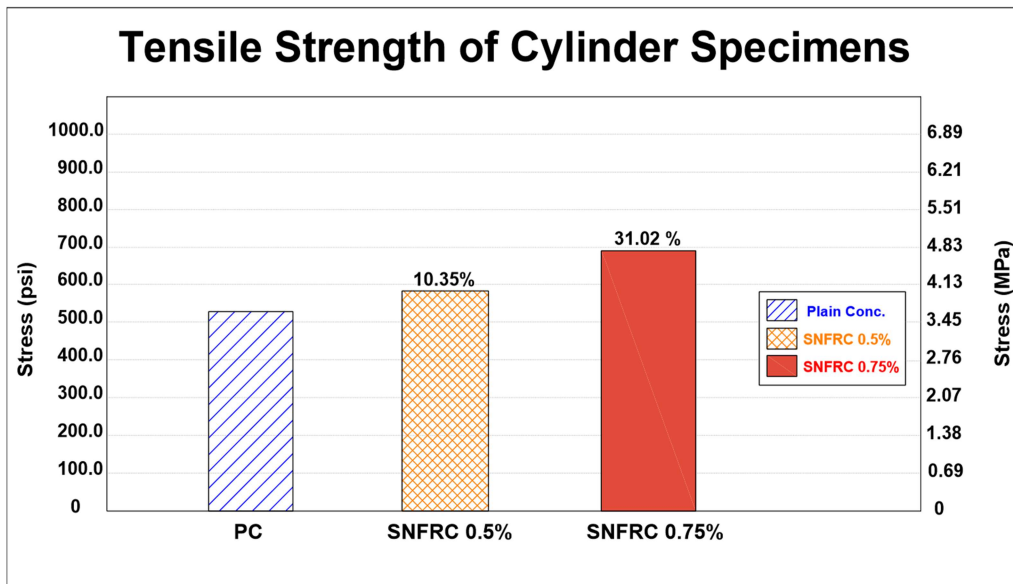


Figure 47 Average tensile strength of cylinders

4.3 Compressive Cylinder Specimens

Table 10 Compressive strength of cylinder specimens

COMPRESSIVE STRENGTH OF CYLINDERS			
Cylinder #	Cylinder Type	Comp. Strength (ksi)	Avg. Comp. Strength (ksi)
1	Plain Conc.	4.88	4.94
2		5.01	
3		4.85	
4		4.92	
1	SNFRC 0.5%	5.56	5.38
2		5.16	
3		5.42	
1	SNFRC 0.75%	5.59	5.53
2		5.65	
3		5.35	

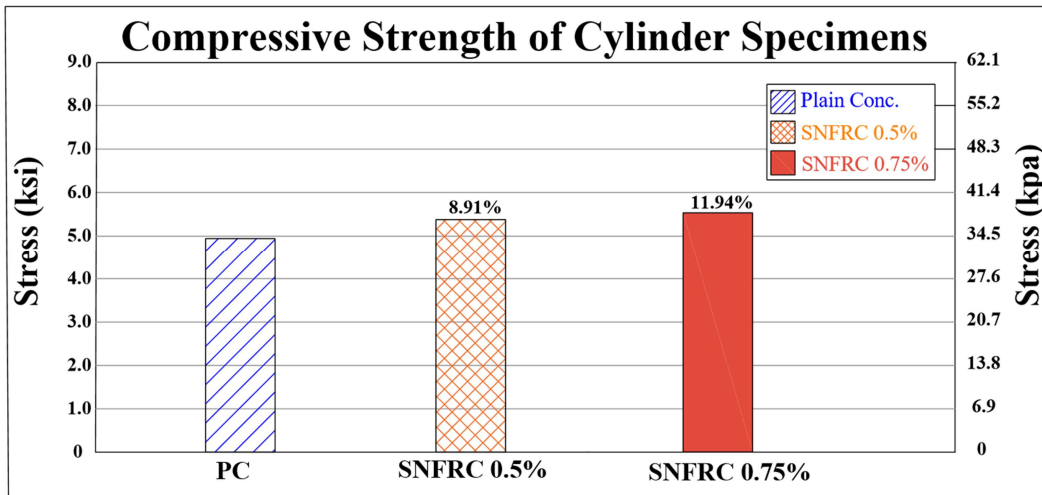


Figure 48 Average compressive strength for cylinders

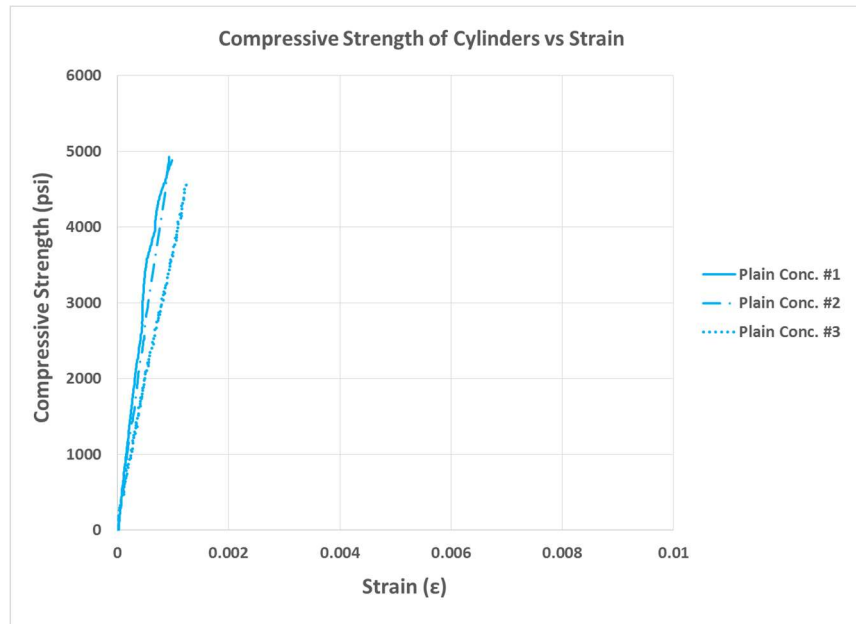


Figure 49 Compressive stress-strain curves for Plain-Concrete cylinders

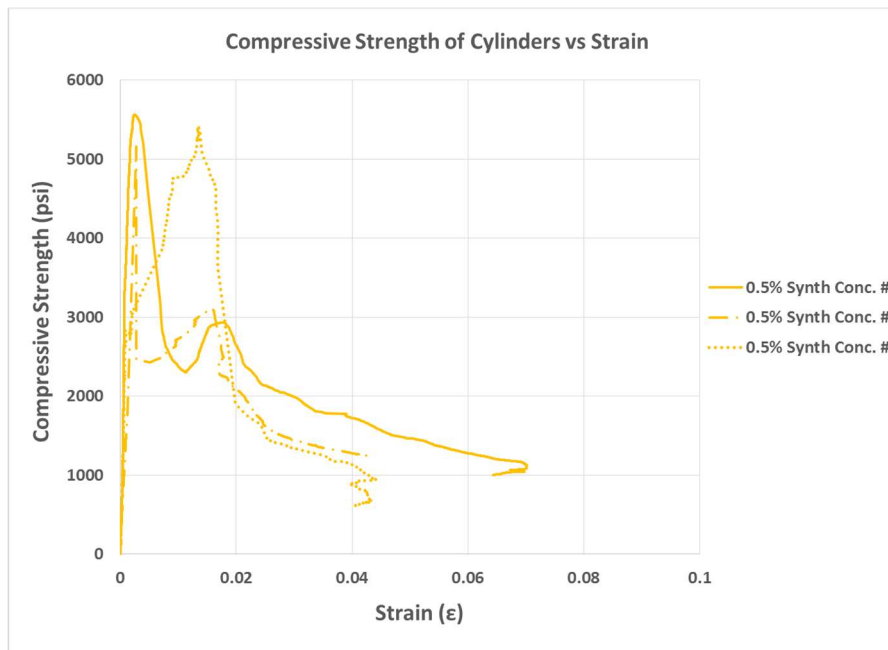


Figure 50 Compressive stress-strain curves for SNFRC 0.5% cylinders

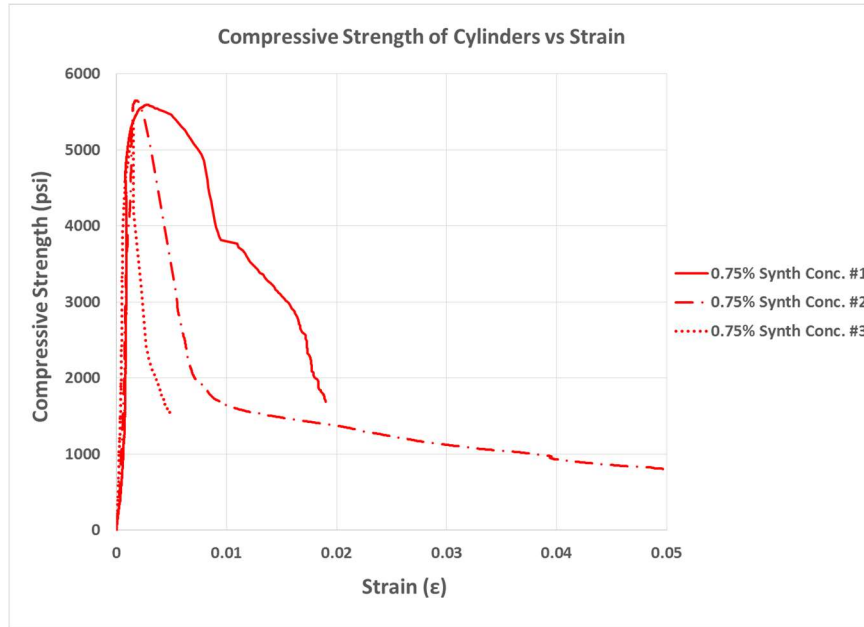


Figure 51 Compressive stress-strain curves for SNFRC 0.75% cylinders

4.4 Flexural Beam Specimens

Table 11 Flexural strength of small-scale beam specimens

FLEXURAL STRENGTH OF BEAMS			
Beam #	Beam Type	Tensile Strength (psi)	Avg. Tensile Strength (psi)
1	Plain Conc.	765.01	752.0
2		750.30	
3		740.70	
1	SNFRC 0.5%	810.90	812.2
2		795.12	
3		830.53	
1	SNFRC 0.75%	936.70	940.8
2		944.22	
3		941.50	

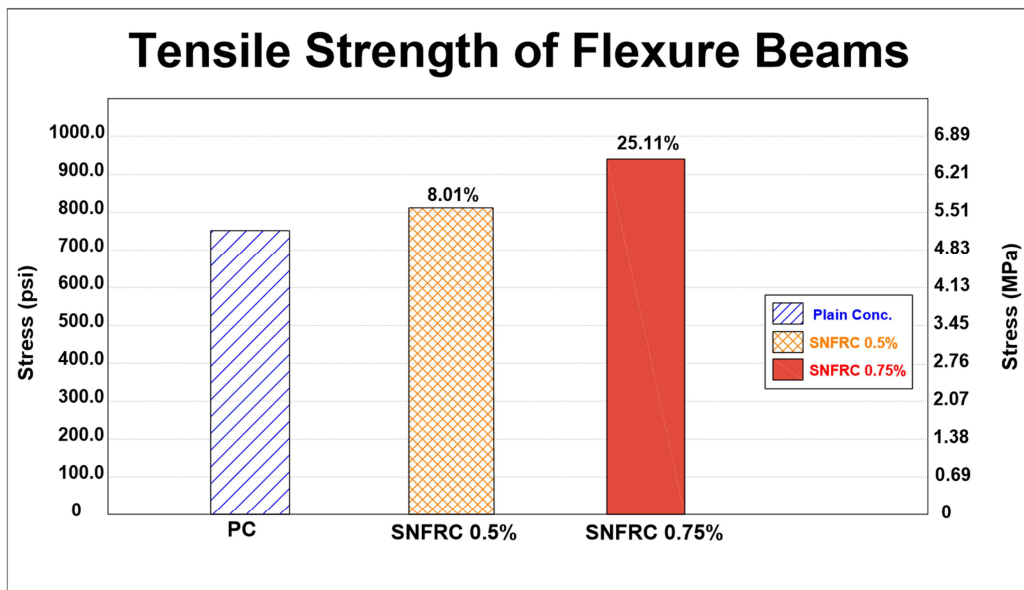


Figure 52 Average tensile strength for flexural beams

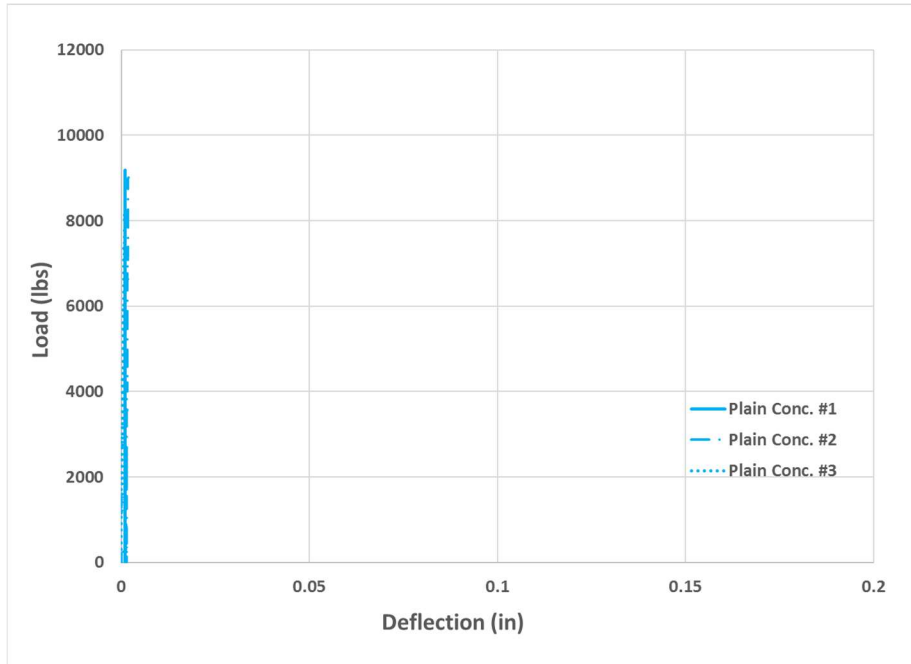


Figure 53 Load-deflection curves for Plain Concrete beams

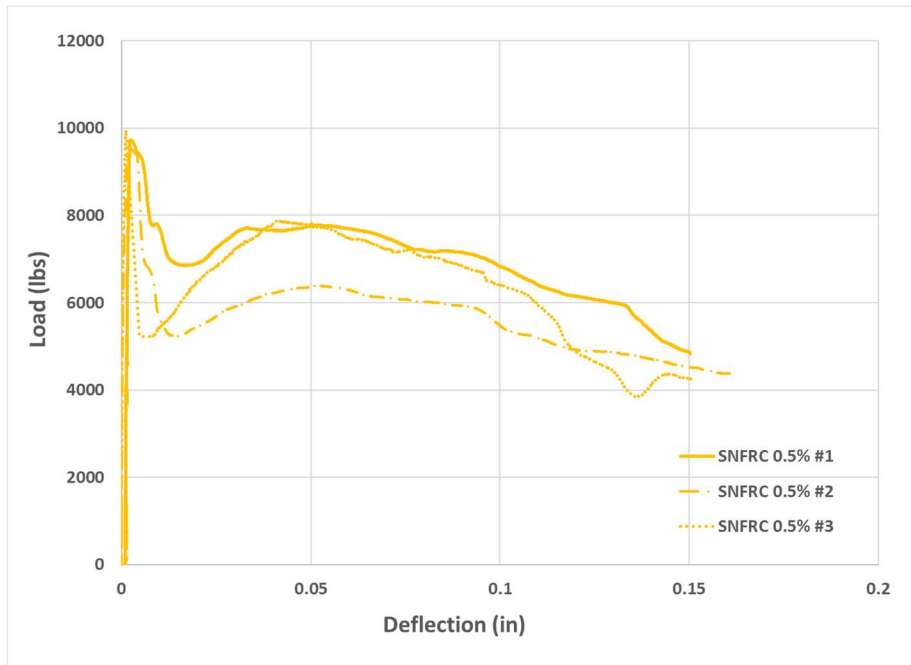


Figure 54 Load-deflection curves for SNFRC 0.5% beams

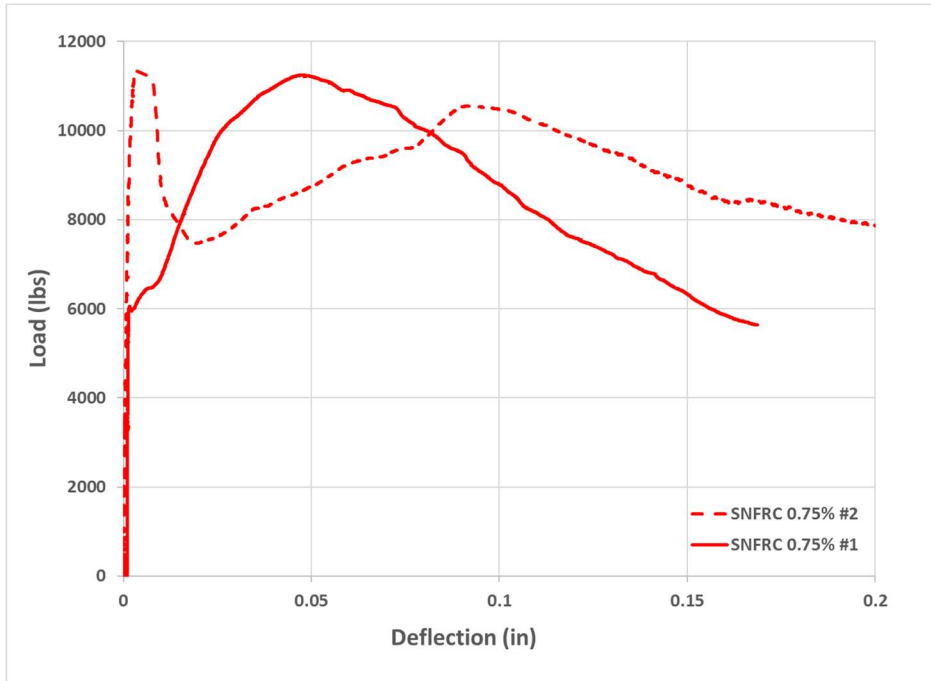


Figure 55 Load-deflection curves for SNFRC 0.75% beams

Table 12 Energy dissipation values for small-scale beams

	Energy Dissipation							
	Plain Concrete			SNFRC 0.5%			SNFRC 0.75%	
	BM #1	BM #2	BM #3	BM #1	BM #2	BM #3	BM #1	BM #2
Energy Dissipation (lb-in)	5	9	6	1010	910	985	1370	1850
Average (lb-in)	7			969			1610	

5 SUMMARY AND CONCLUSIONS

In summary, the shear strength performance and failure mechanism of 8 large-scale beams with and/or without transverse reinforcement is studied and discussed in this research study. Large-scale beams with various fiber volumes were produced and tested at Civil Engineering Laboratory Building (CELB) at the University of Texas at Arlington. This includes longitudinally reinforced concrete beams (RC), reinforced concrete beams with minimum transverse reinforcement (RCS), 0.5% volume macro-synthetic polypropylene fiber reinforced concrete beams (SNFRC 0.5%), and 0.75% macro-synthetic polypropylene fiber-reinforced concrete beams (SNFRC 0.75%). Large-scale beams are tested using a 400-kip compression testing machine using a simply supported setup. The resulting load-deflection curves, load-strain curves for each specimen are obtained and discussed. The results showed improved overall performance of large-scale beams reinforced using synthetic fibers. Furthermore, a total of 19 cylindrical specimens, 4-inch diameter and 8-inch height, were tested after 28 days curing using a 500-kip compression testing machine per ASTM C39 and ASTM C496 standards. The resulting stress-strain curves obtained from these tests demonstrate improved compression capacity of polypropylene synthetic fiber reinforced concrete cylinders. Likewise, the splitting-tensile tests not only showed improved tensile capacity but also considerable improvement in failure mechanism of synthetic fiber-reinforced cylinders relative to plain concrete specimens. In addition, a total of 9 beam specimens, 6-in by 6-in. by 20-in. were produced and tested per ASTM C1609. The results showed improved flexural crack resistance and higher tensile load capacity of synthetic fiber reinforced concrete beams. This study reports on the increased shear strength performance of large-scale beams due to the application of 0.5% and 0.75% macro-synthetic polypropylene fibers into the concrete matrix.

In conclusion, the results obtained through experimental testing of polypropylene fiber-reinforced concrete specimens showed relative improvement in shear strength, tensile strength and compressive strength. Testing of large-scale specimens showed that beams with minimum transverse reinforcement (RCS) have 31% higher shear capacity in comparison to beams with no transverse reinforcement (RC). However, reinforcing the mix with 0.5% volume fraction of fibers increased the shear capacity of specimens by nearly 17%. Furthermore, reinforcing the concrete matrix with 0.75% volume fraction of fibers increased the shear capacity of a beam without any stirrups up to nearly 29%. In addition, failure mechanism, crack resistance behavior and crack propagation of specimens significantly changed when fibers were used. SNFRC beams showed great ductility after the main failure crack. The fibers helped the concrete resist widening of the cracks as induced load increased during failure. SNFRC beams did not show brittle explosive failure.

Cylinders tested in tension showed similar improvement in tensile capacity of concrete. On average, 0.5% fiber-reinforced concrete cylinders showed 10% higher tensile strength in comparison to plain concrete specimens while 0.75% fiber-reinforced concrete cylinders showed 31% higher tensile strength. It is noteworthy to mention that although plain concrete cylinders were extremely brittle in tension, fiber-reinforced cylinders showed ductile behavior. Likewise, 0.5% fiber-reinforced cylinders subjected to compression testing showed nearly 9% higher compressive strength versus plain concrete specimens. Whereas 0.75% fiber-reinforced cylinders showed nearly 12% higher compressive strength relative to plain concrete cylinders. Therefore, fiber-reinforced cylinders could withstand higher strains and higher compressive forces.

Fiber-reinforced small-scale beams specimens tested per ASTM 1609 standards demonstrated higher tensile capacity, improved ductility and significantly higher energy

absorption capacity. 0.5% fiber-reinforced concrete small-scale beams showed nearly 9% higher tensile strength and absorbed 969 lb-in of energy versus plain concrete beams that demonstrated extreme brittle behavior and negligible flexural toughness. Furthermore, 0.75% fiber-reinforced small-scale concrete beams showed more than 25% improvement in tensile capacity in comparison to plain concrete specimens. In addition, increasing the fiber content by 0.25% resulted in a 66% higher energy absorption capacity in 0.75% fiber-reinforced concrete beams. It is also noteworthy to mention that fiber-reinforced small scale specimens showed considerably higher ductility, resisting up to 0.2 inch of net deflection.

Appendix A
Crack Patterns and Propagation

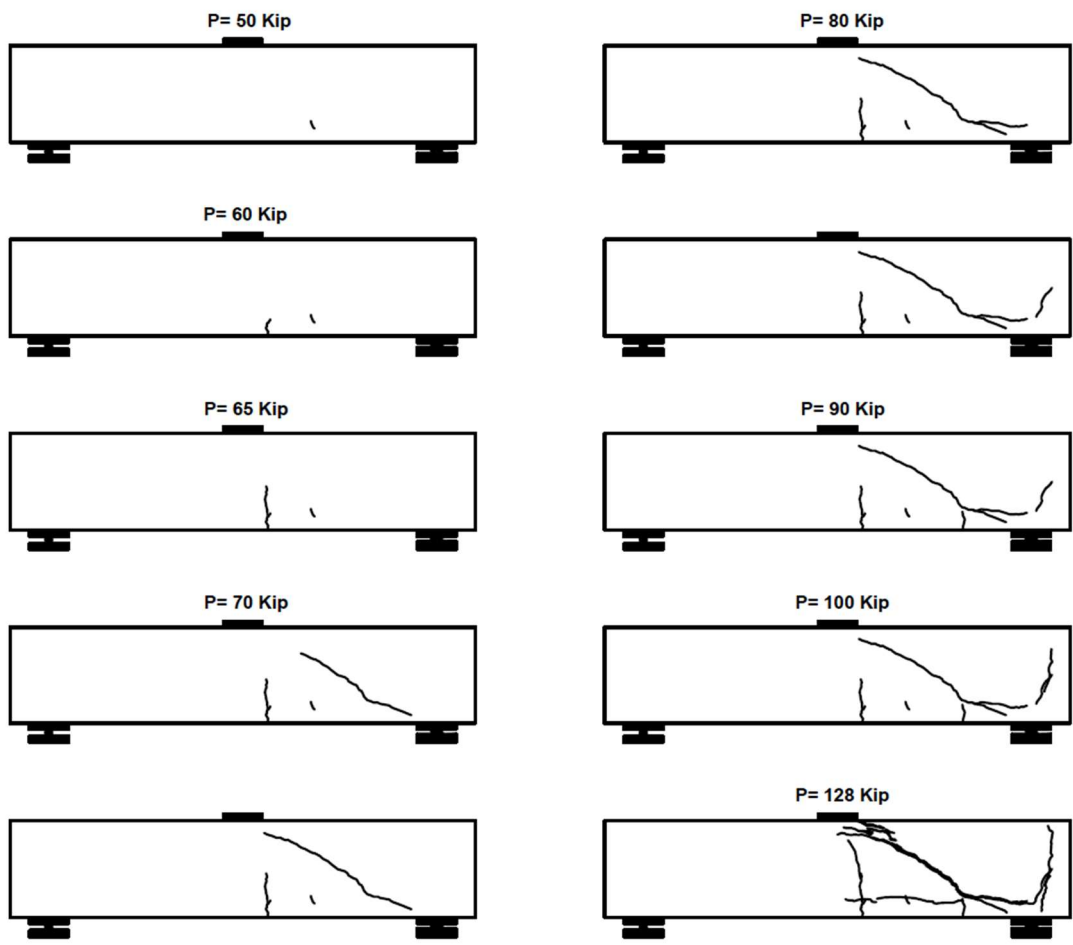


Figure A1 Crack pattern for RC BM #1

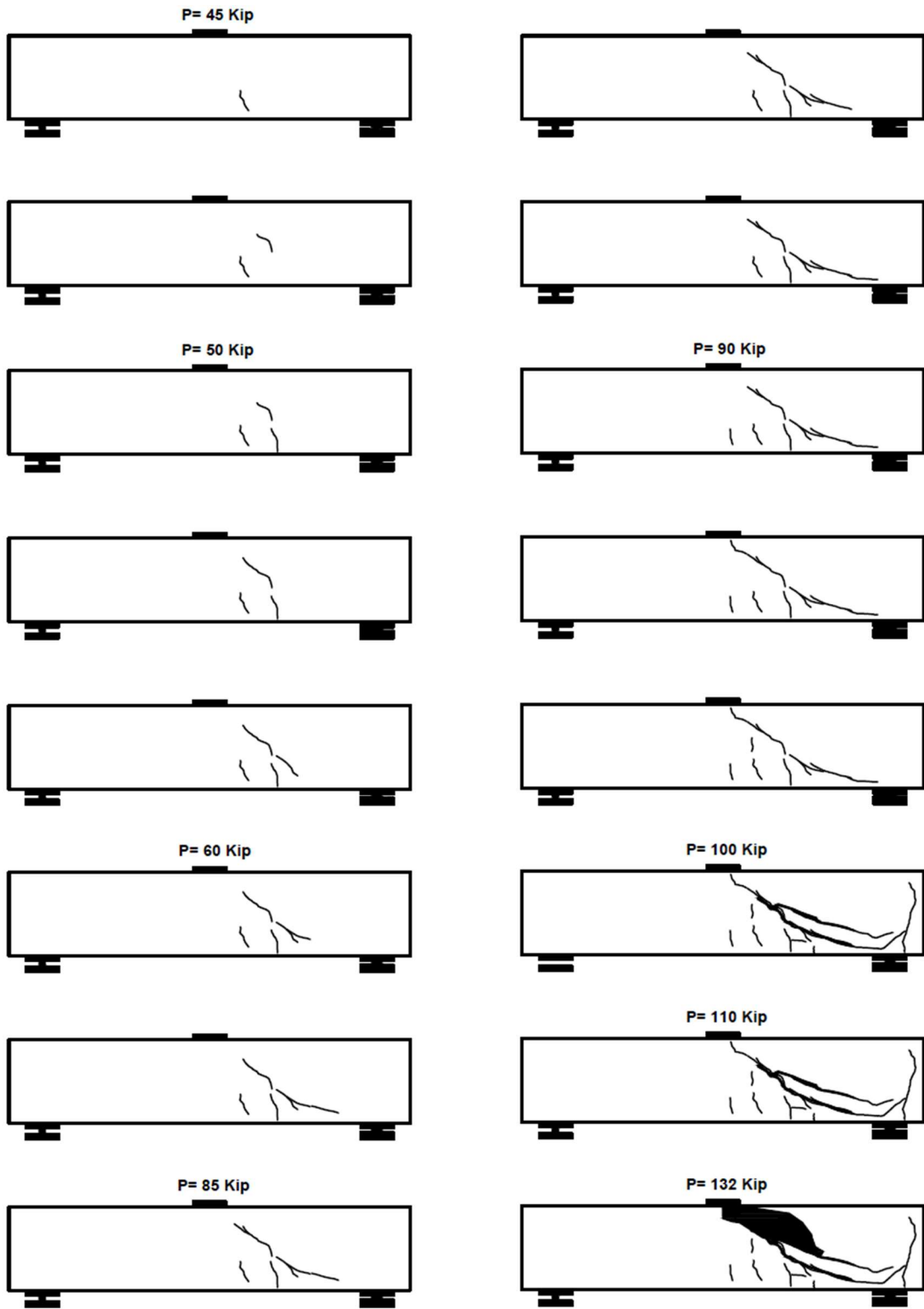


Figure A2 Crack pattern for RC BM #2

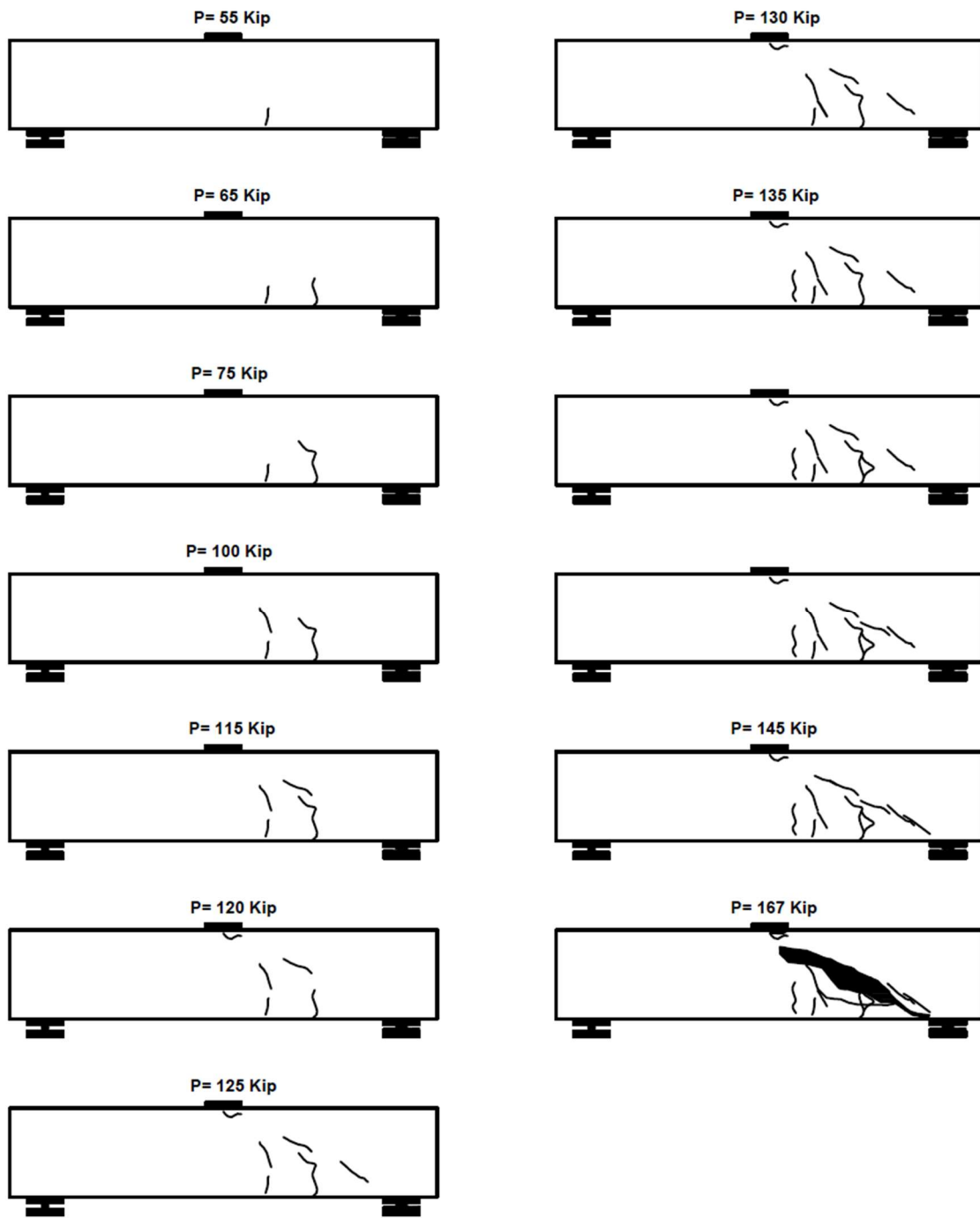


Figure A3 Crack pattern for RCS BM #3

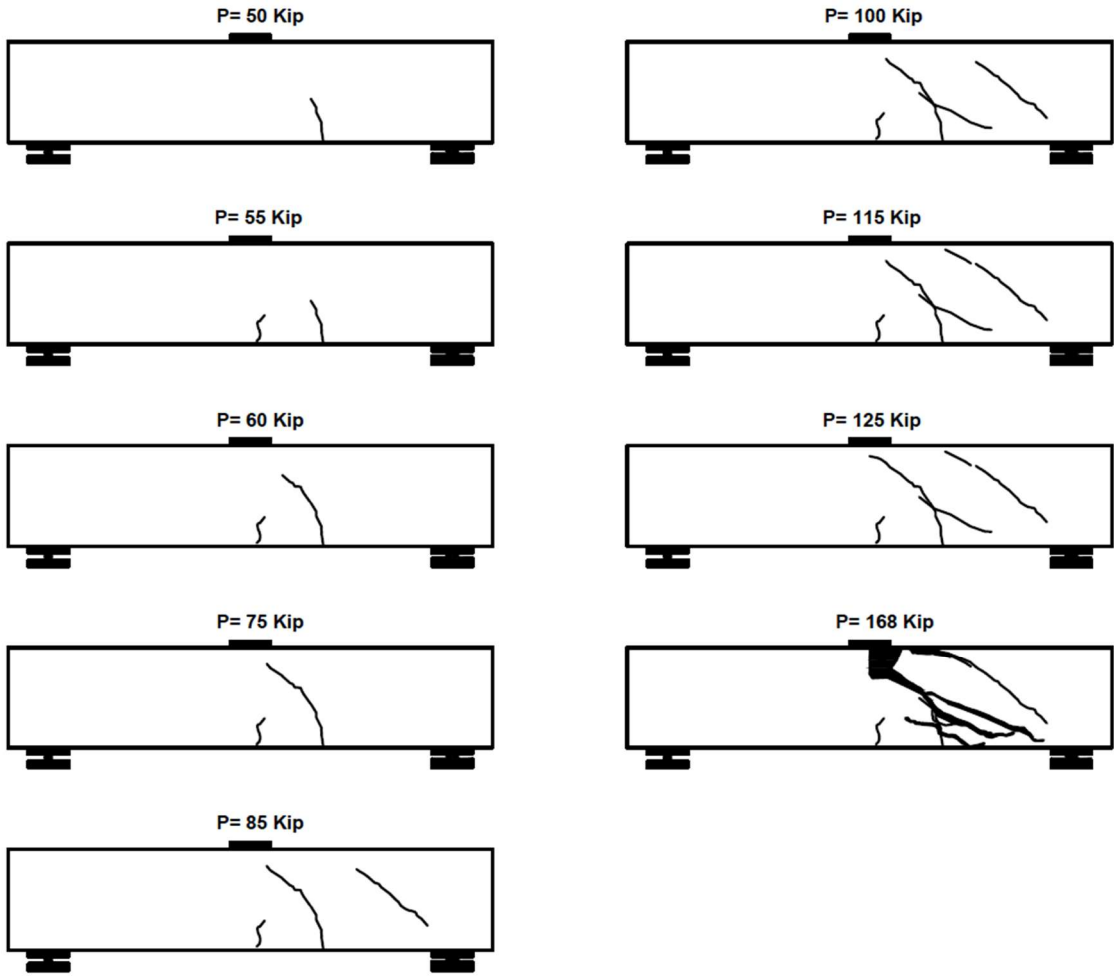


Figure A4 Crack pattern for RCS BM #4

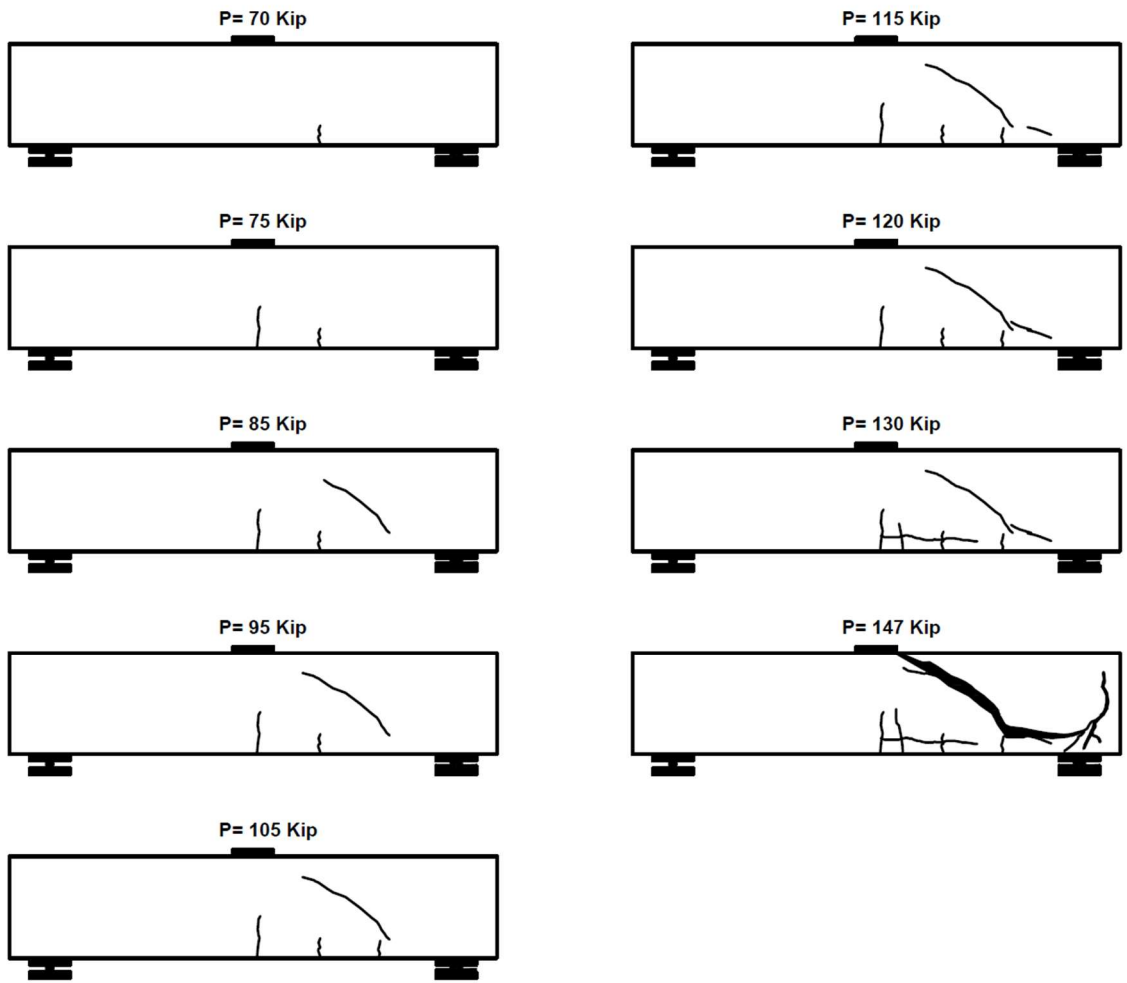


Figure A5 Crack pattern for SNFRC 0.5% BM #5

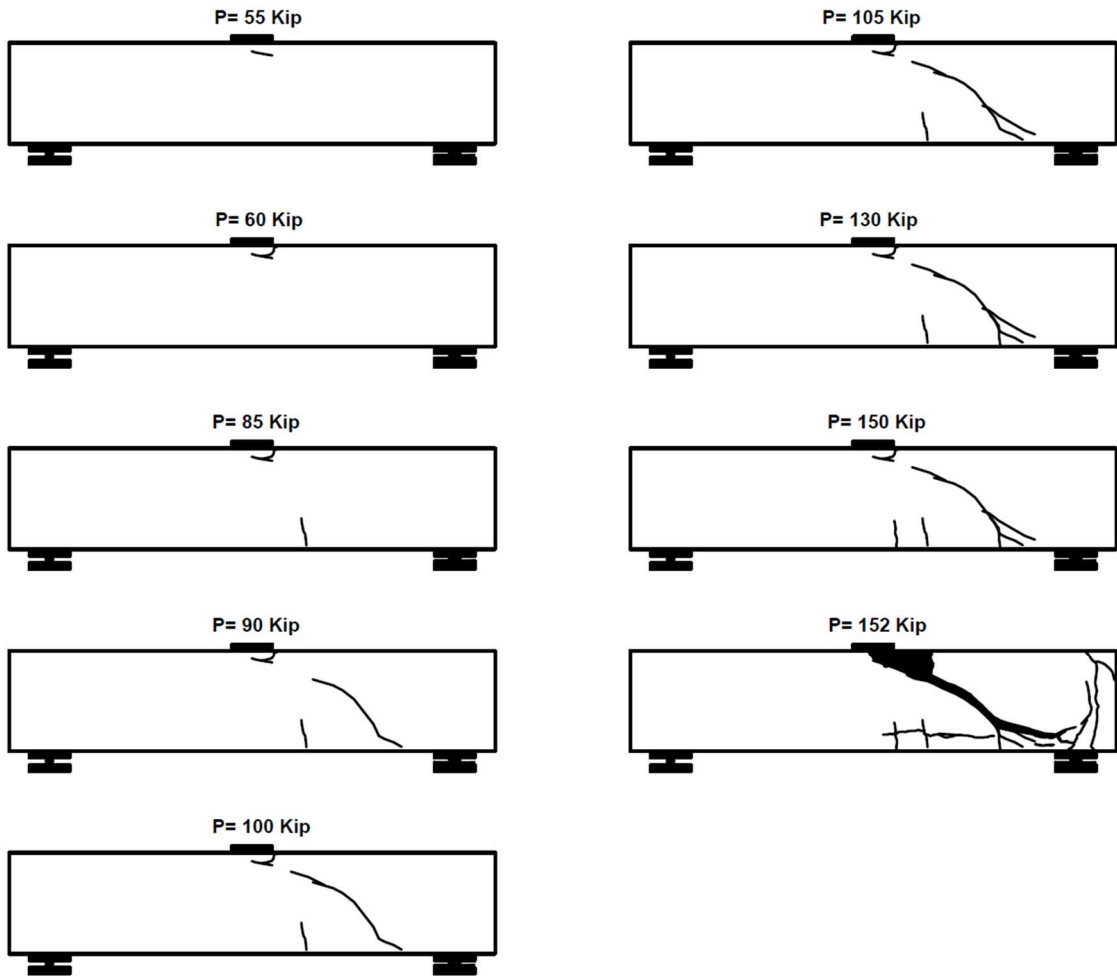


Figure A6 Crack pattern for SNFRC 0.5% BM #6

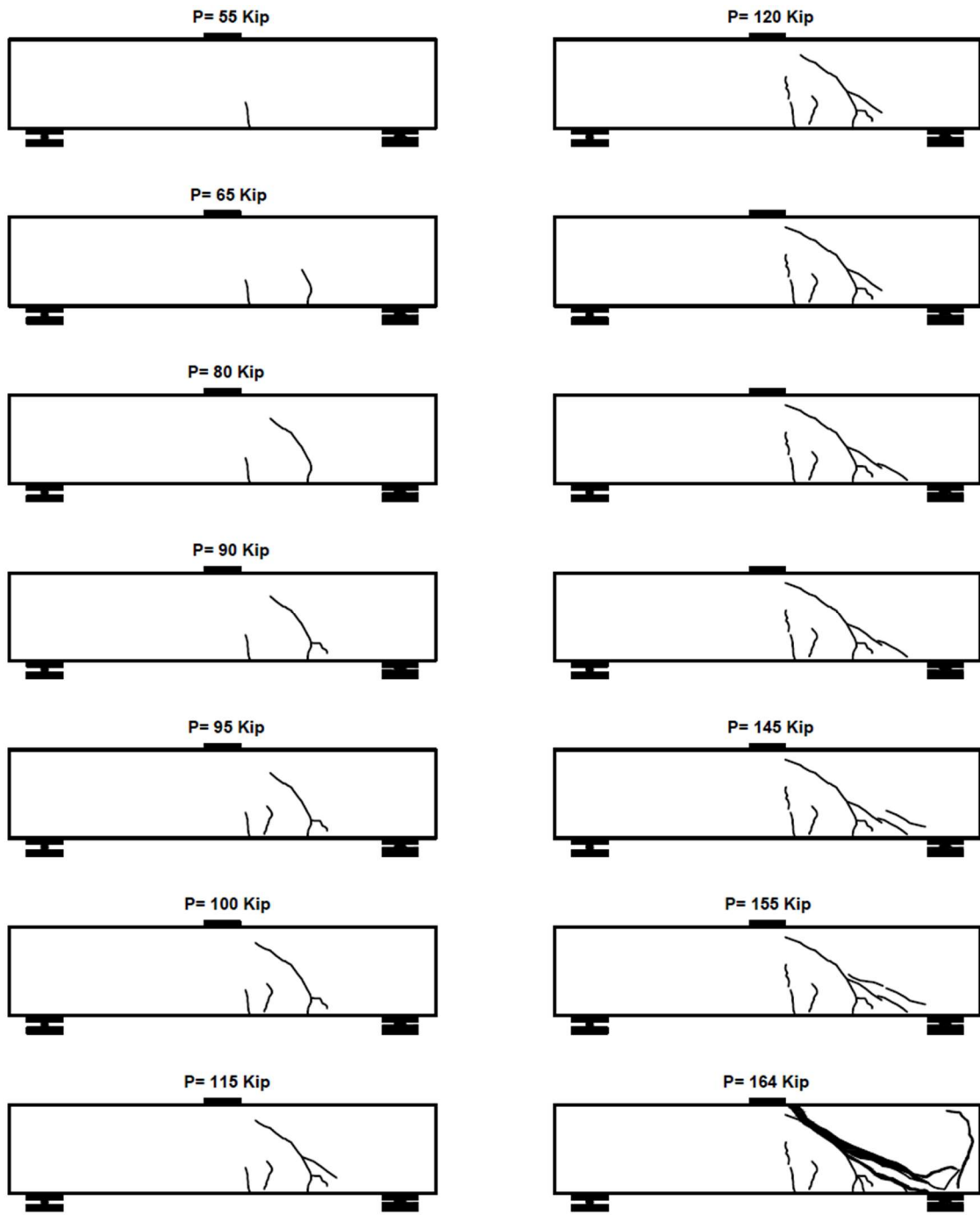


Figure A7 Crack pattern for SNFRC 0.75% BM #7

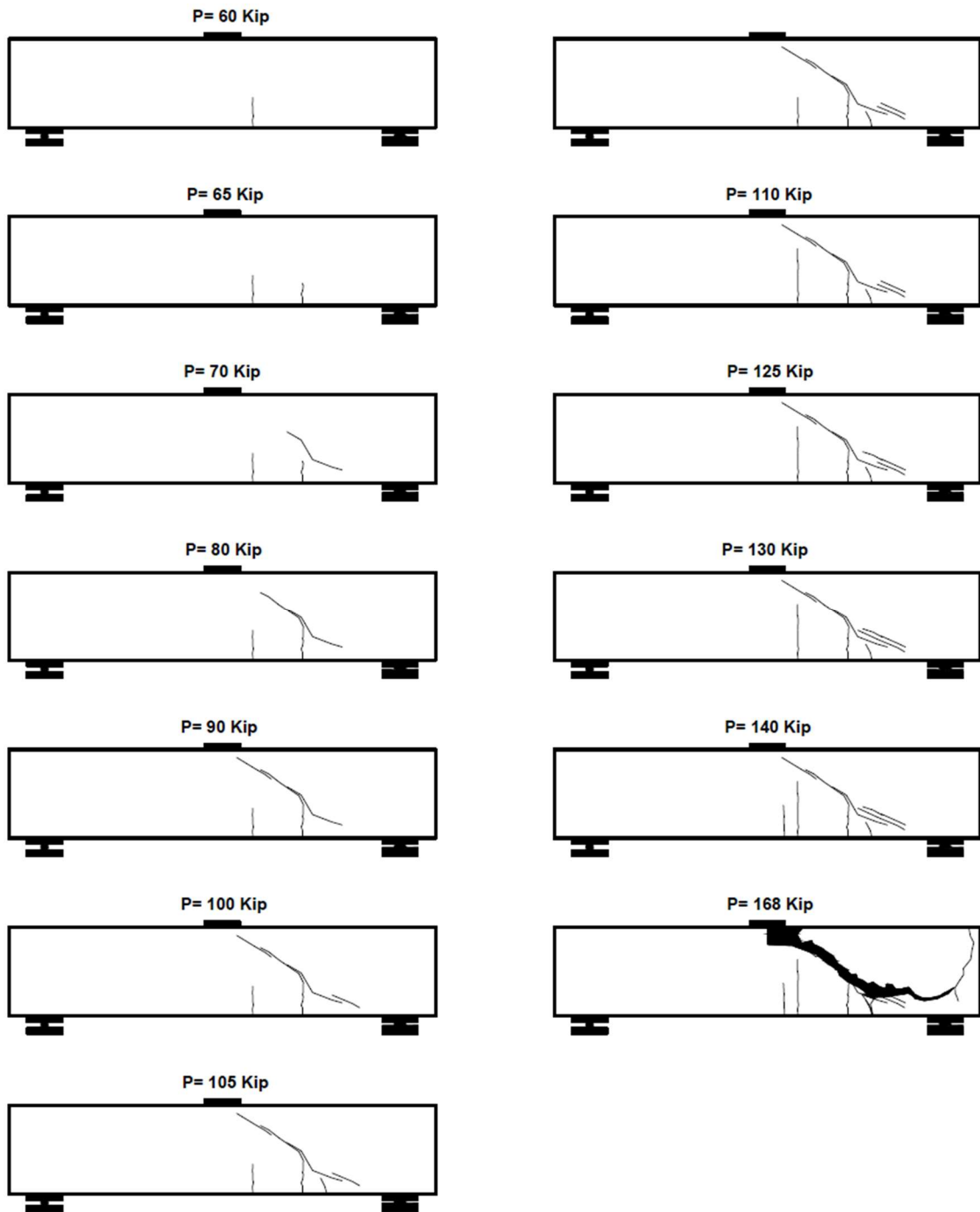


Figure A8 Crack pattern for SNFRC 0.75% BM #8

Appendix B
Principal Strain Values

Table B-1 Principal Strain values for BM #1 and BM #2

BM #	Beam Type	Location of Conc. SGs	ϵ_1	ϵ_2	ϵ_3	ϵ_p	ϵ_Q	γ	θ (deg)
1	RC ($V_f=0$)	F5	4.1	23	18.5	25.1	-2.5	27.6	119.3
1	RC ($V_f=0$)	H4	-20.9	4.2	15.8	17	-22.1	39.1	100.1
1	RC ($V_f=0$)	J3	-23.2	-2.3	20.9	20.9	-23.3	44.2	88.5
1	RC ($V_f=0$)	L2	-192.1	-272.6	-76.4	15.6	-284	299.6	56.3
2	RC ($V_f=0$)	F5	-3.7	33.5	7.9	34	-30	64	129.7
2	RC ($V_f=0$)	H4	-31	-35.6	-18.4	-12.1	-37.3	25.2	60
2	RC ($V_f=0$)	J3	-8.4	-59.1	5.1	56.2	-59.5	115.7	48.3
2	RC ($V_f=0$)	L2	-40.9	-131.7	-189	-39	-191	152	6.4

Table B-2 Principal Strain Values for BM #3 and BM #4

BM #	Beam Type	Location of Conc. SGs	ϵ_1	ϵ_2	ϵ_3	ϵ_p	ϵ_Q	γ	θ (deg)
3	RCS ($V_f=0$)	F5	-21.3	-4.1	-1.3	1	-23.7	24.7	107.9
3	RCS ($V_f=0$)	H4	-103.7	20.7	157.1	157.2	-103.8	261	88.7
3	RCS ($V_f=0$)	J3	-39.7	-22	-49	-21.5	-67.2	45.7	140.9
3	RCS ($V_f=0$)	L2	-142	-232	-70.3	24.7	-237	261.7	52.9
4	RCS ($V_f=0$)	F5	-27.6	33.4	40.8	50.1	-36.8	86.9	109
4	RCS ($V_f=0$)	H4	-72.4	-20.3	39.6	39.7	-72.5	112.2	88
4	RCS ($V_f=0$)	J3	-82.8	-54.3	-62.6	-51.7	-93.7	42	120.6
4	RCS ($V_f=0$)	L2	-276.7	-181.2	49.3	62.8	-290.1	352.9	78.7

Table B-3 Principal Strain Values for BM #5 and BM #6

BM #	Beam Type	Location of Conc. SGs	ϵ_1	ϵ_2	ϵ_3	ϵ_p	ϵ_Q	γ	Θ (deg)
5	SNFRC 0.5%	F5	6.2	-37.5	-52.8	9.5	-56	65.5	12.8
5	SNFRC 0.5%	H4	-8.7	-1.7	-24	0.1	-32.9	33	-31.2
5	SNFRC 0.5%	J3	-62.4	-3.4	-12.2	4.9	-79.5	84.4	116.7
5	SNFRC 0.5%	L2	-18.3	-115.9	-60.2	40.2	-118.7	158.9	37.4
6	SNFRC 0.5%	F5	-9.4	12	16.7	19.2	-11.8	31	106.4
6	SNFRC 0.5%	H4	-19	7.9	15.3	17.9	-21.6	39.5	104.8
6	SNFRC 0.5%	J3	-37.2	-27.7	9.4	13.2	-41	54.2	74.6
6	SNFRC 0.5%	L2	-108.9	-94.3	14.8	30.8	-124.9	155.7	71.3

Table B-4 Principal Strain Values for BM #7 and BM #8

BM #	Beam Type	Location of Conc. SGs	ϵ_1	ϵ_2	ϵ_3	ϵ_p	ϵ_Q	γ	Θ (deg)
7	SNFRC 0.75%	F5	0.9	35.2	14.3	36	-20.8	56.8	128.2
7	SNFRC 0.75%	H4	10.6	-51.2	-94.1	11.4	-94.9	106.3	5.1
7	SNFRC 0.75%	J3	-18.9	-6.8	-26.7	-6.3	-39.3	33	141.9
7	SNFRC 0.75%	L2	-45.3	-86.5	-47.5	-6.3	-86.5	80.2	44.2
8	SNFRC 0.75%	F5	46.8	103.8	12.7	105.8	-46.2	152	141.5
8	SNFRC 0.75%	H4	7.5	-23.2	-25.1	13	-30.5	43.5	20.7
8	SNFRC 0.75%	J3	-14.2	-40.6	-55.4	-56.2	-13.4	42.8	97.8
8	SNFRC 0.75%	L2	-109.5	-180.1	-39.9	36.3	-185.7	222	54.1

Appendix C
Principal Strain Orientations

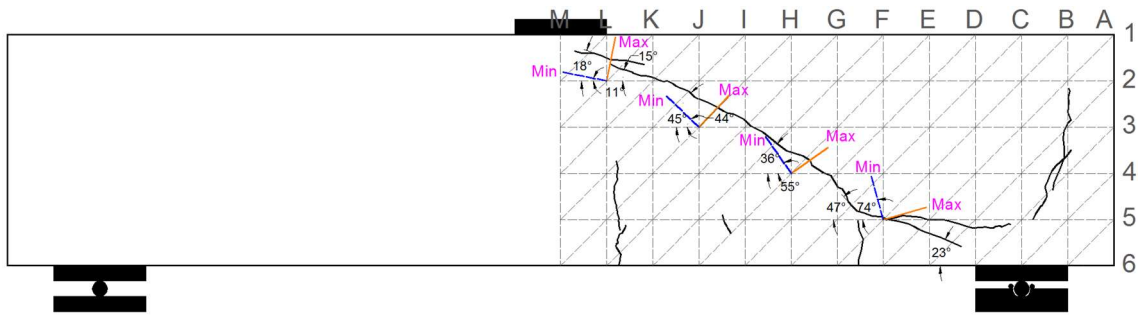


Figure C1 Principal strain orientations for RC BM #1

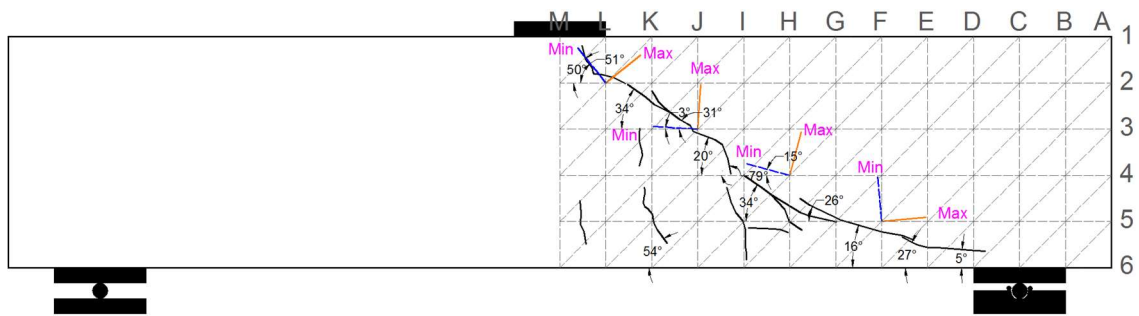


Figure C2 Principal strain orientations for RC BM #2

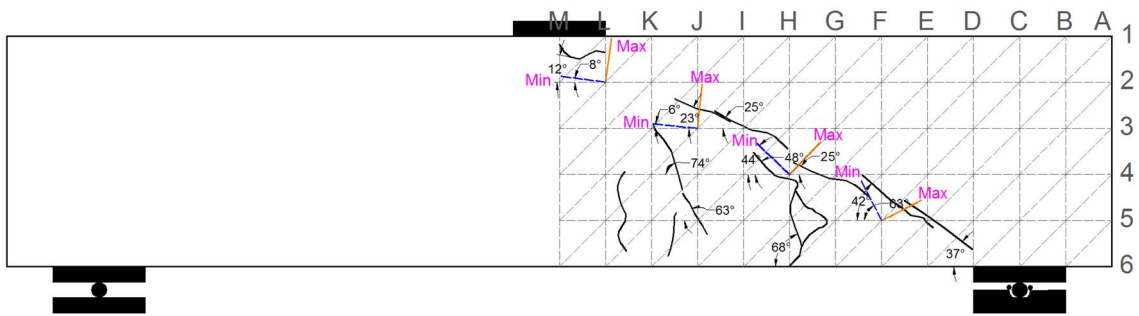


Figure C3 Principal strain orientations for RCS BM #3

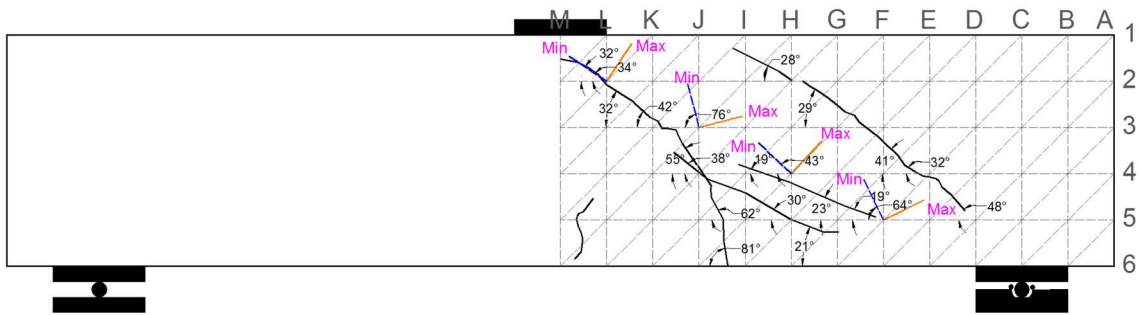


Figure C4 Principal strain orientations for RCS BM #4

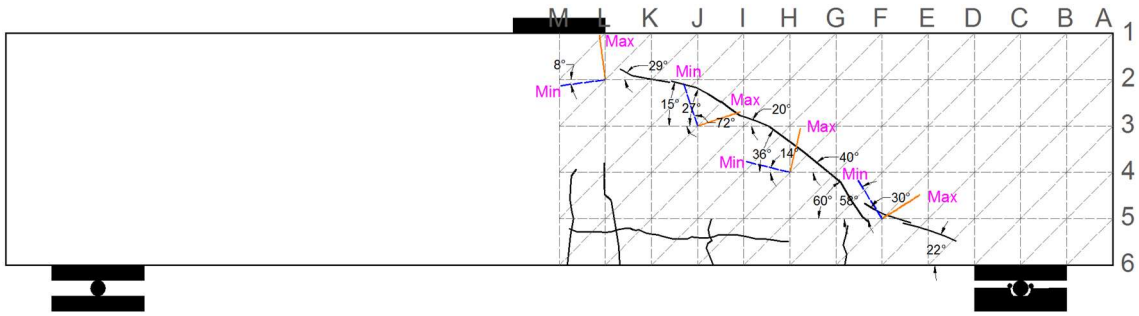


Figure C5 Principal strain orientations for SNFRC 0.5% BM #5

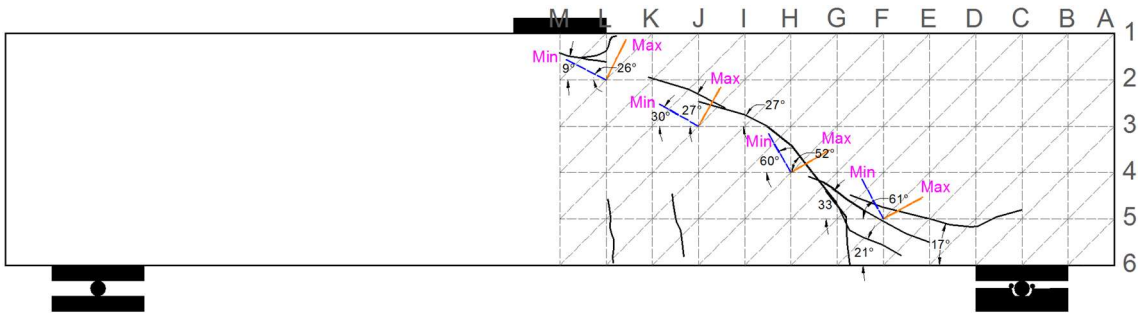


Figure C6 Principal strain orientations for SNFRC 0.5% BM #6

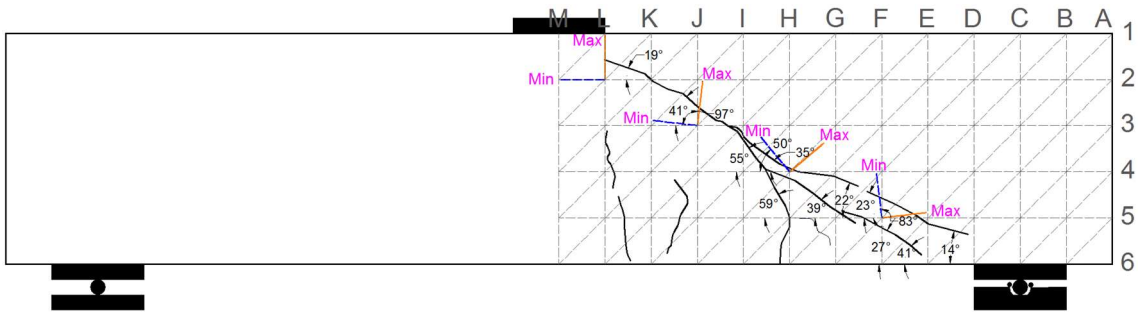


Figure C7 Principal strain orientations for SNFRC 0.75% BM #7

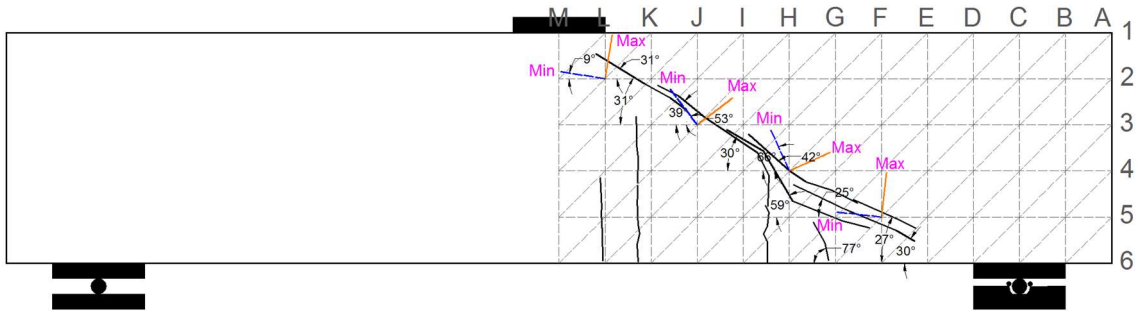


Figure C8 Principal strain orientations for SNFRC 0.75% BM #8

Appendix D
Failure Crack Patterns

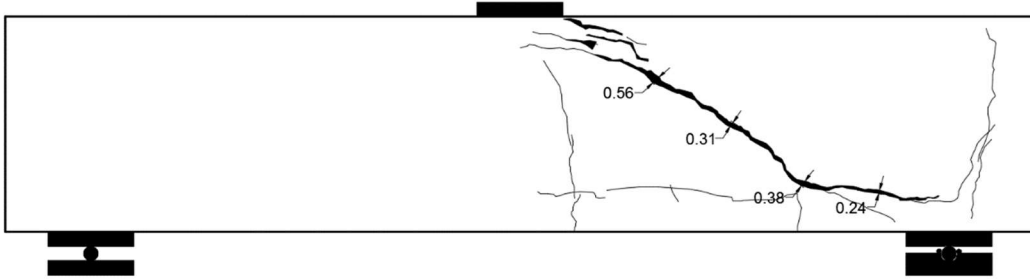


Figure D1 Crack pattern at failure for RC beam #1

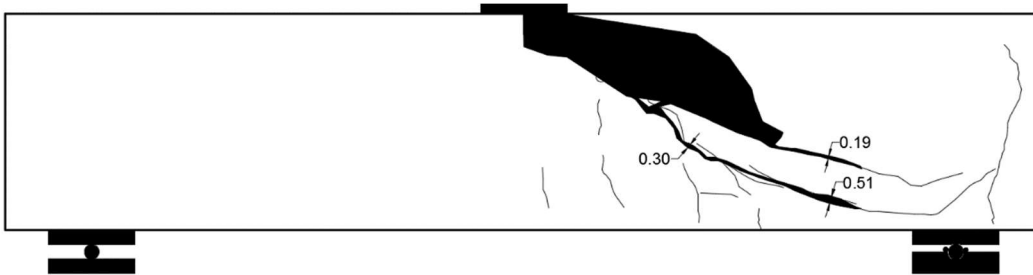


Figure D2 Crack pattern at failure for RC beam #2

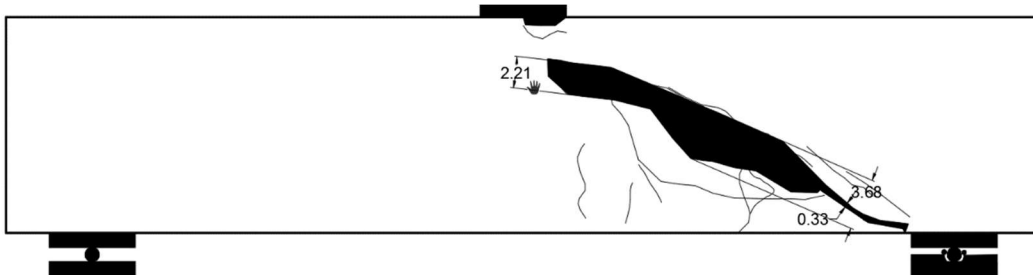


Figure D3 Crack pattern at failure for RCS beam #3

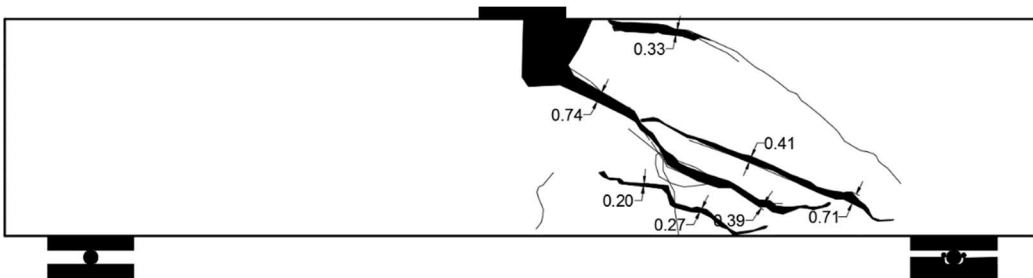


Figure D4 Crack pattern at failure for RCS beam #4



Figure D5 Crack pattern at failure for SNFRC 0.5% beam #5

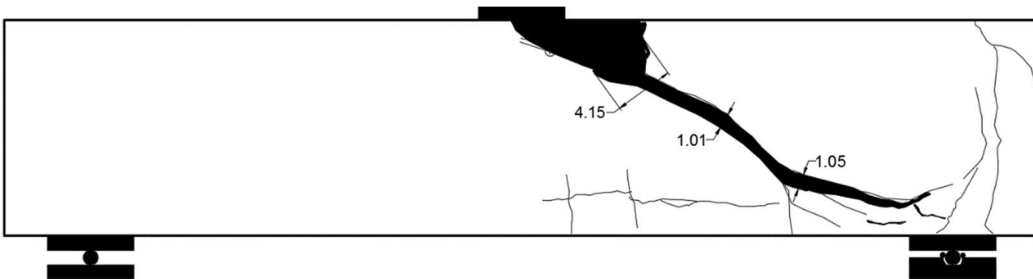


Figure D6 Crack pattern at failure for SNFRC 0.5% beam #6



Figure D7 Crack pattern at failure for SNFRC 0.75% beam #7

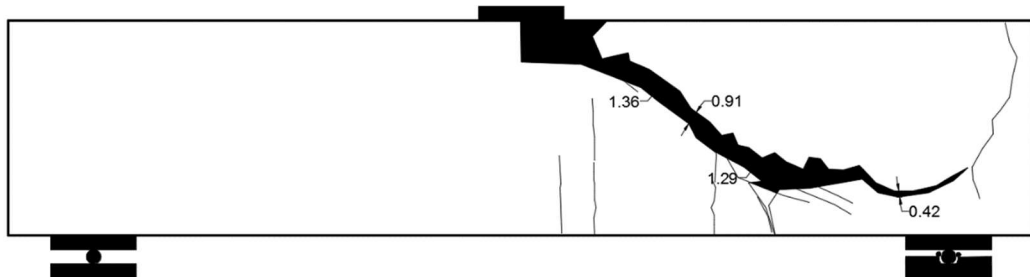


Figure D8 Crack pattern at failure for SNFRC 0.75% beam #8

Appendix E

Load-Deflection curves for large-scale specimens

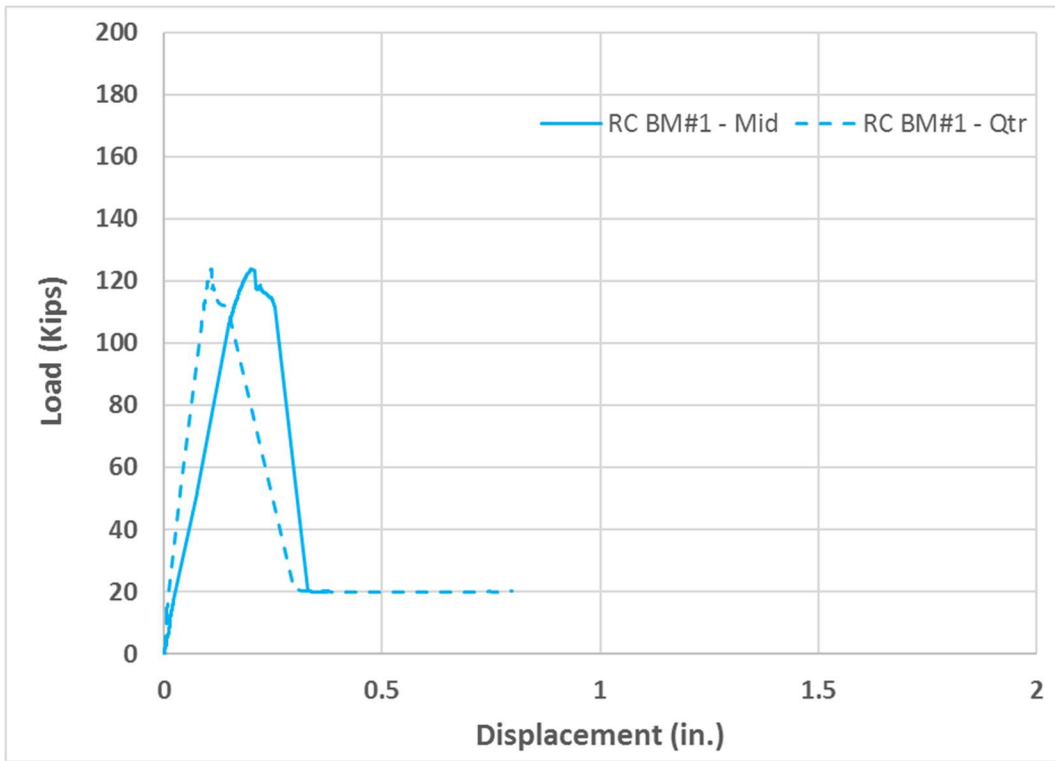


Figure E1 Load-deflection response for RC BM #1

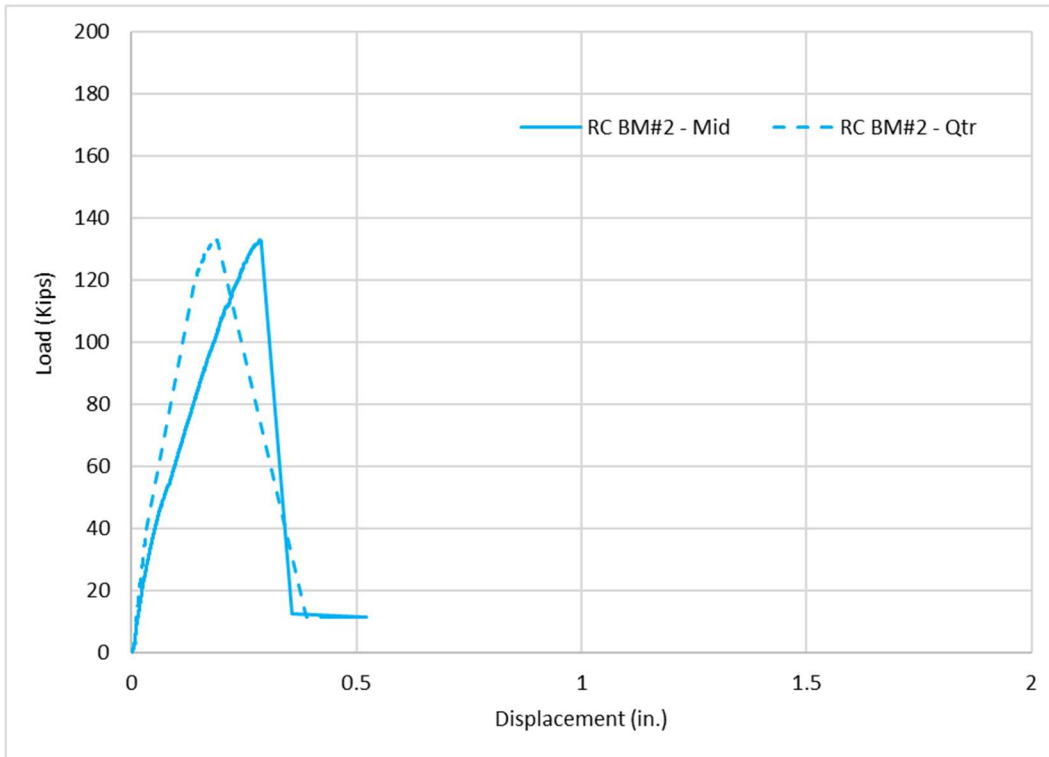


Figure E2 Load-deflection response for RC BM #2

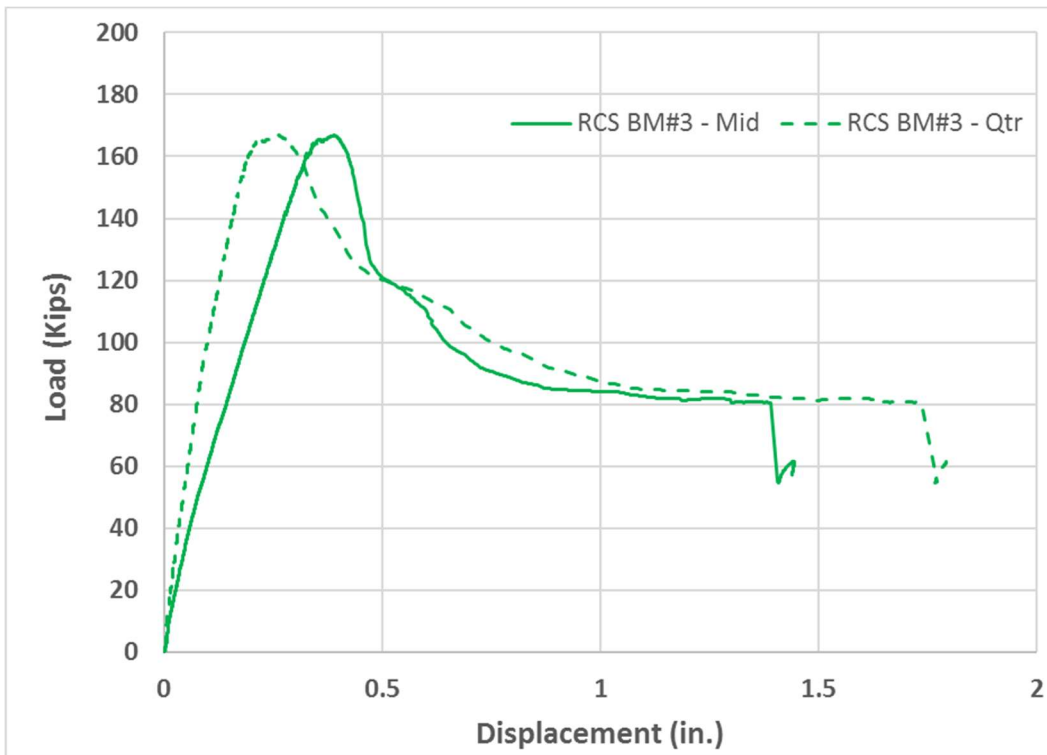


Figure E3 Load-deflection response for RCS BM #3

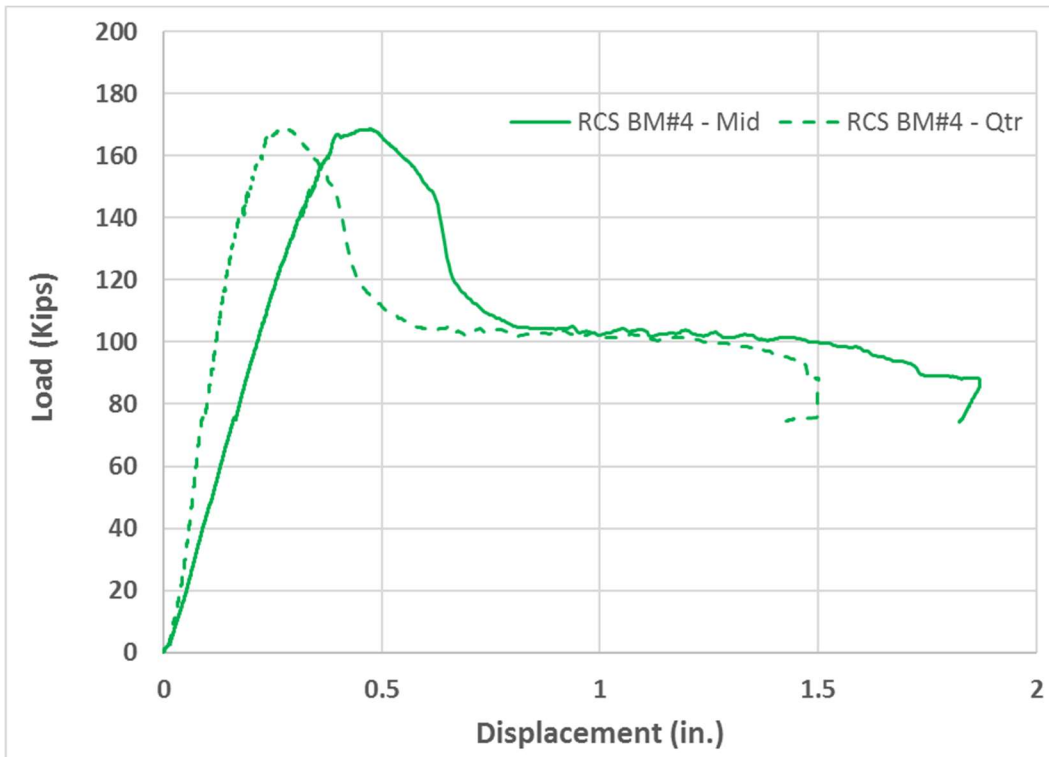


Figure E4 Load-deflection response for RCS BM #4

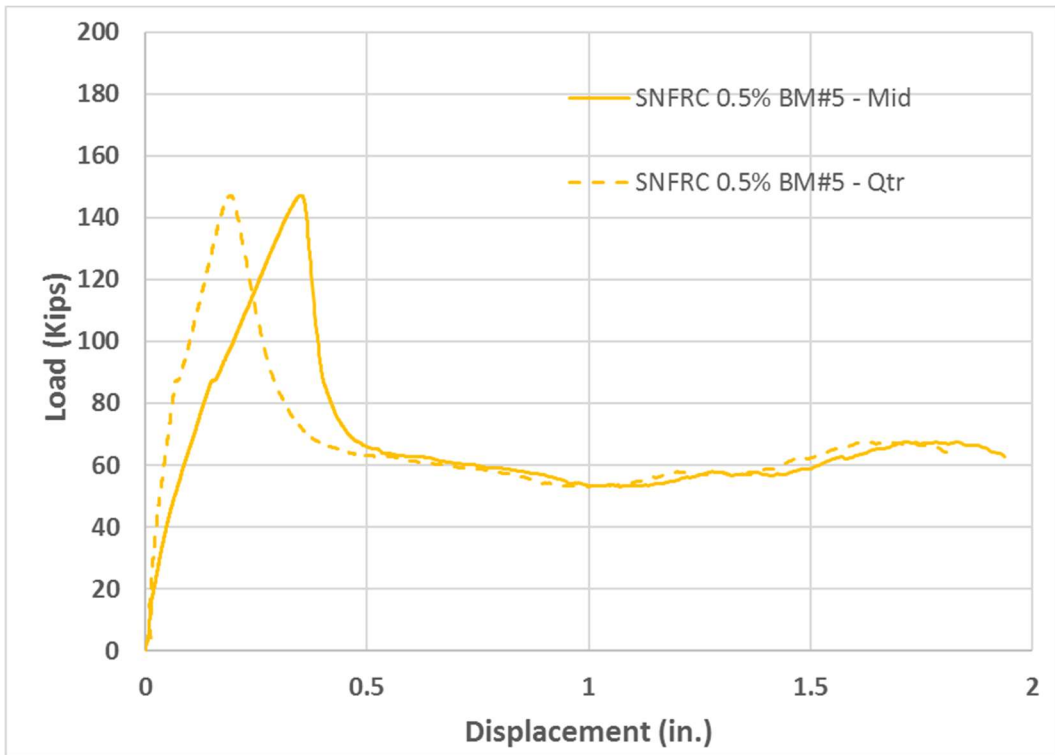


Figure E5 Load-deflection response for SNFRC 0.5% BM #5

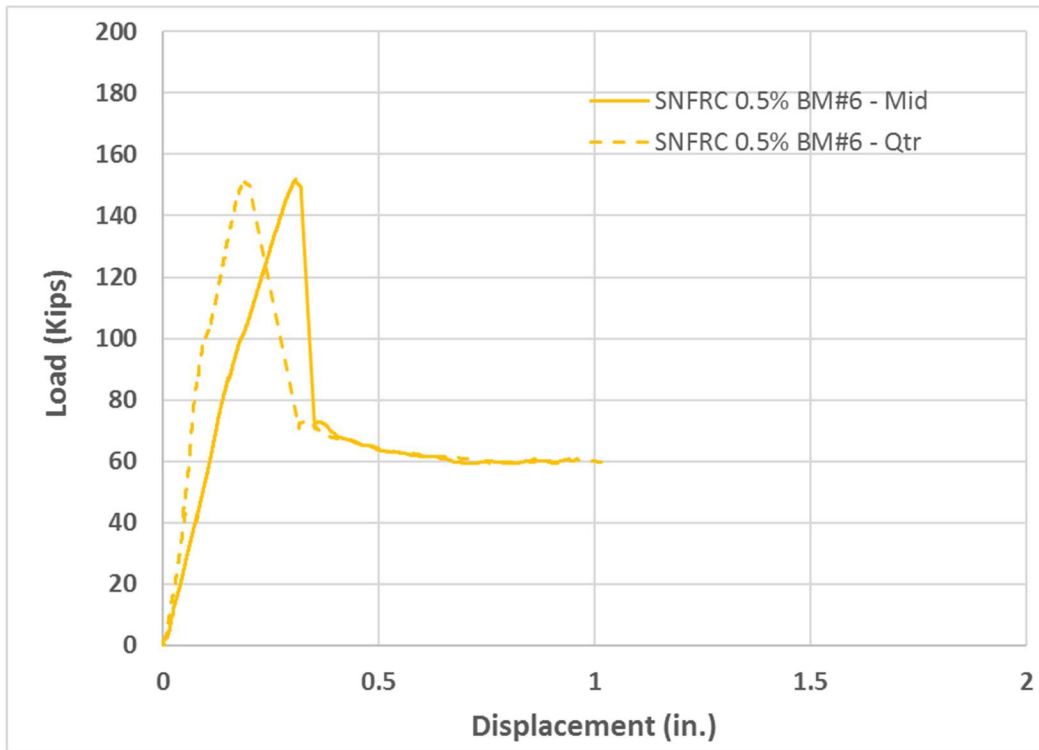


Figure E6 Load-deflection response for SNFRC 0.5% BM #6

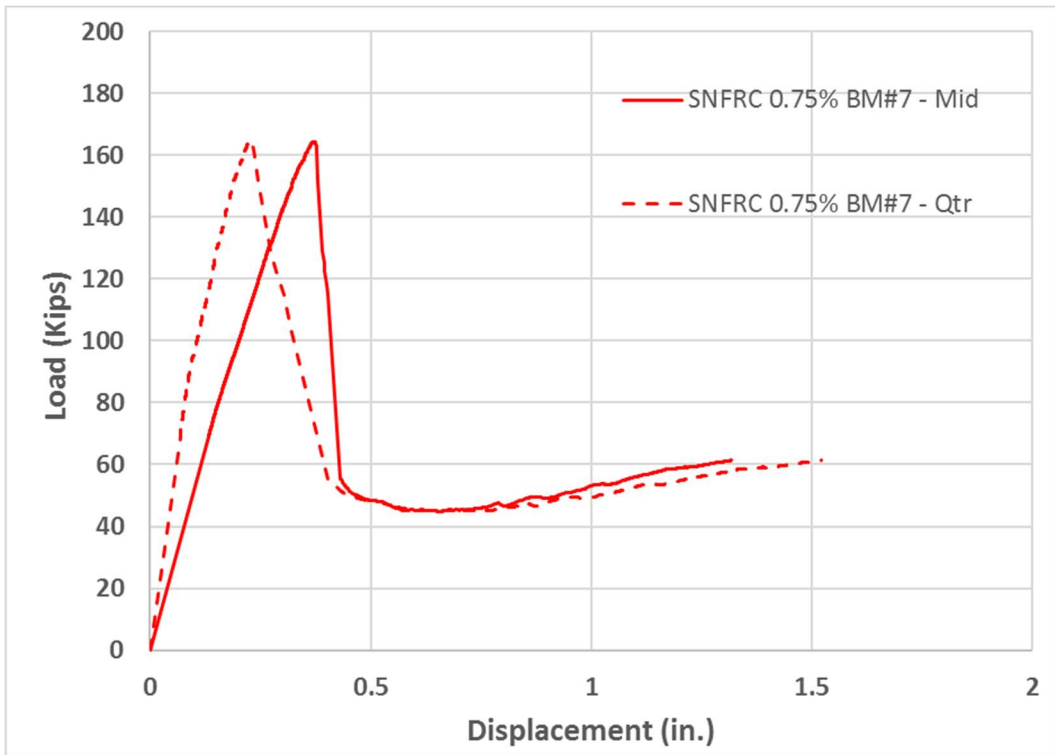


Figure E7 Load-deflection response for SNFRC 0.75% BM #7

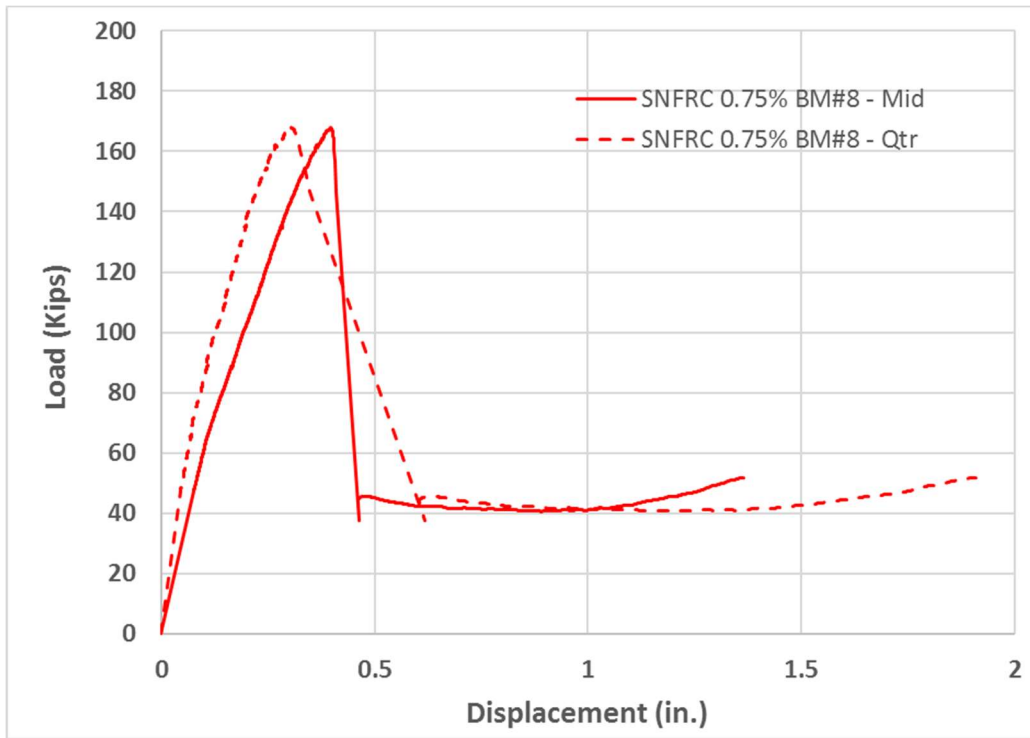


Figure E8 Load-deflection response for SNFRC 0.75% BM #8

Appendix F
Steel Strain-Gauges

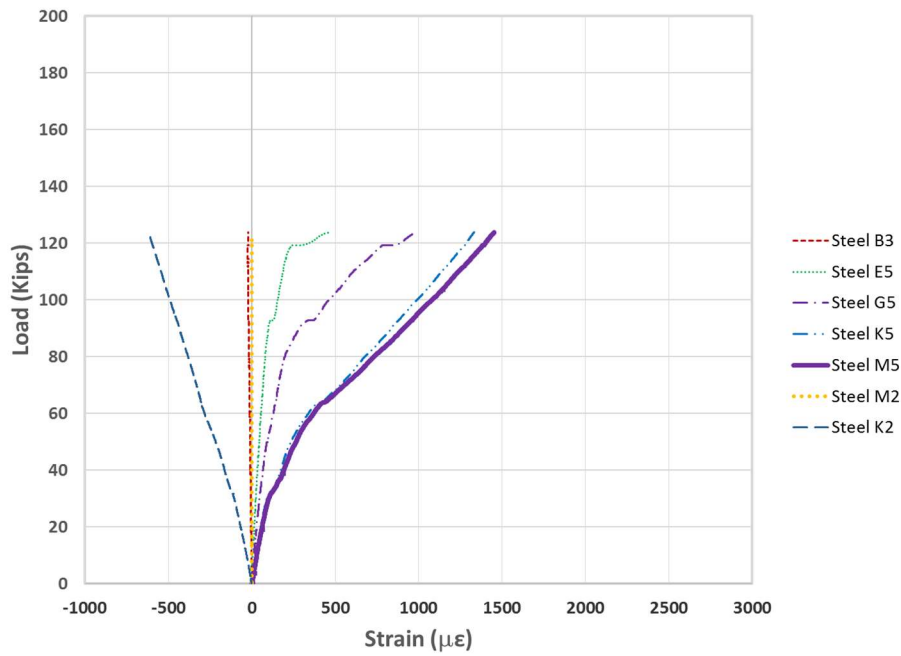


Figure F1 Load-strain response for RC BM #1

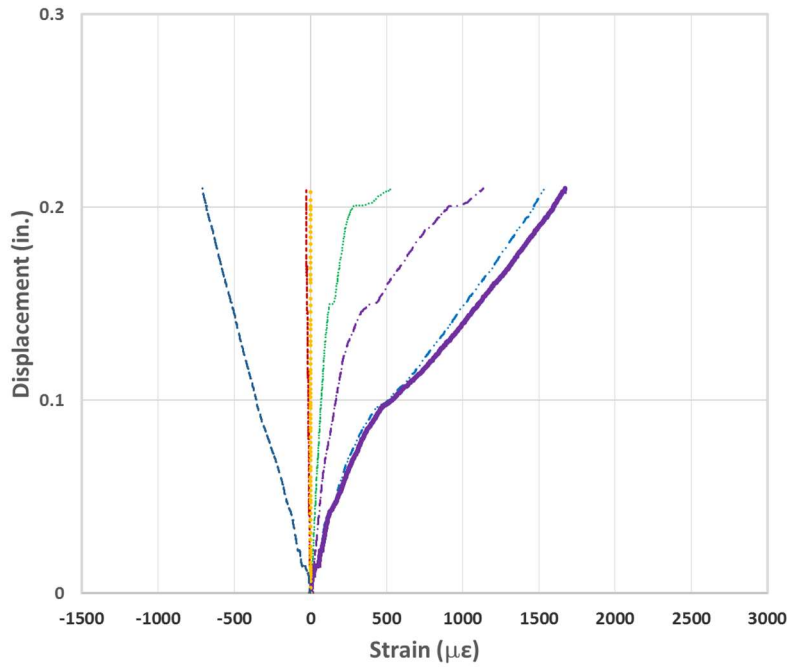


Figure F2 Displacement-strain response for RC BM #1

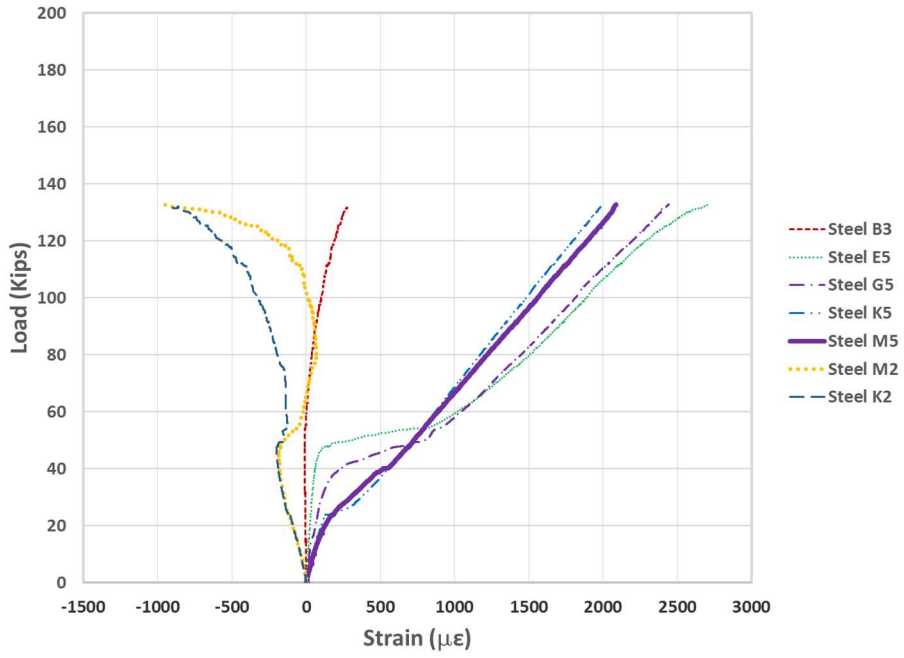


Figure F3 Load-strain response for RC BM #2

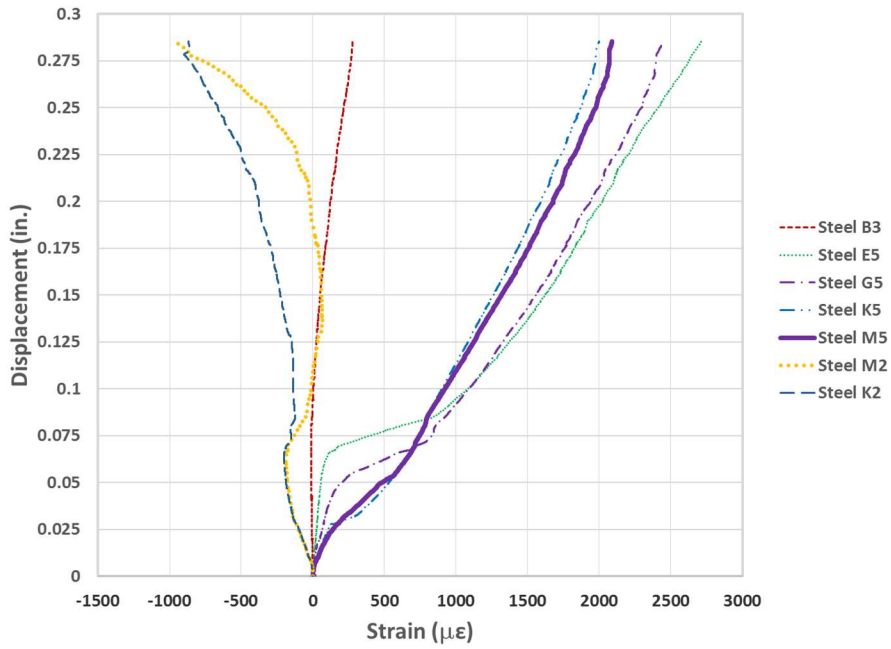


Figure F4 Displacement-strain response for RC BM #2

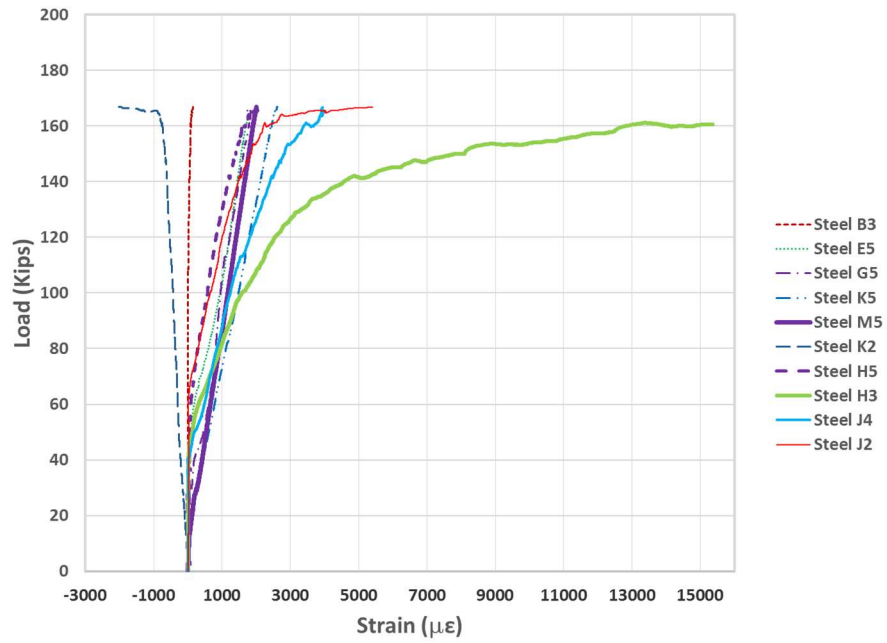


Figure F5 Load-strain response for RCS BM #3

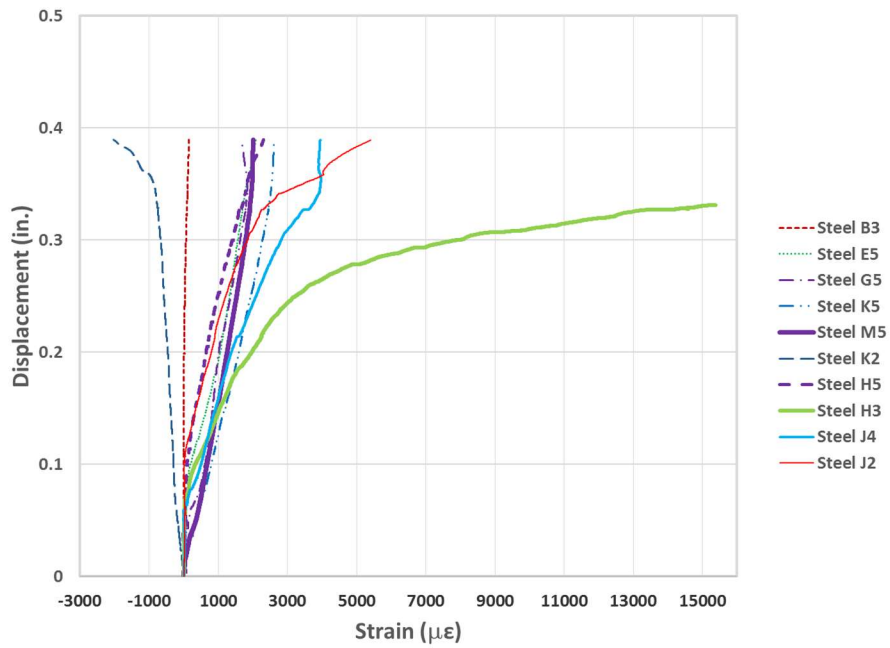


Figure F6 Displacement-strain response for RCS BM #3

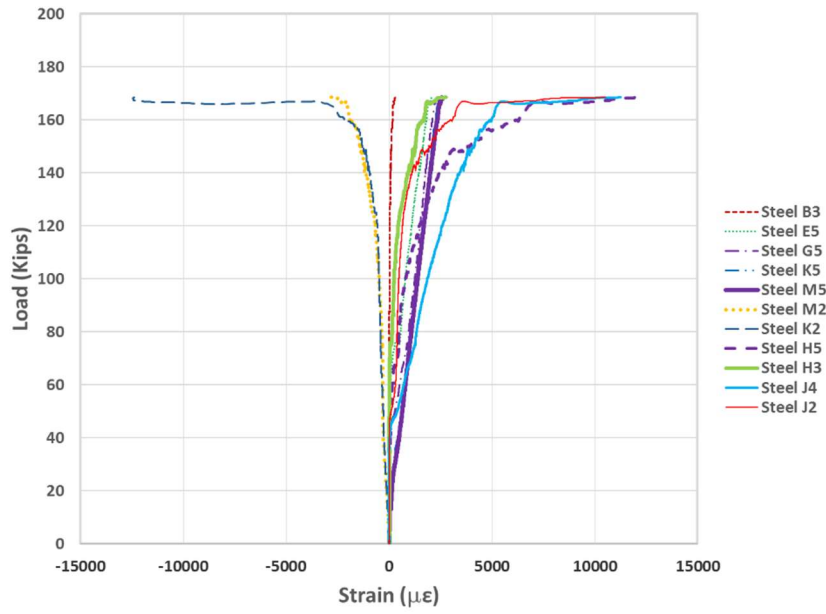


Figure F7 Load-strain response for RCS BM #4

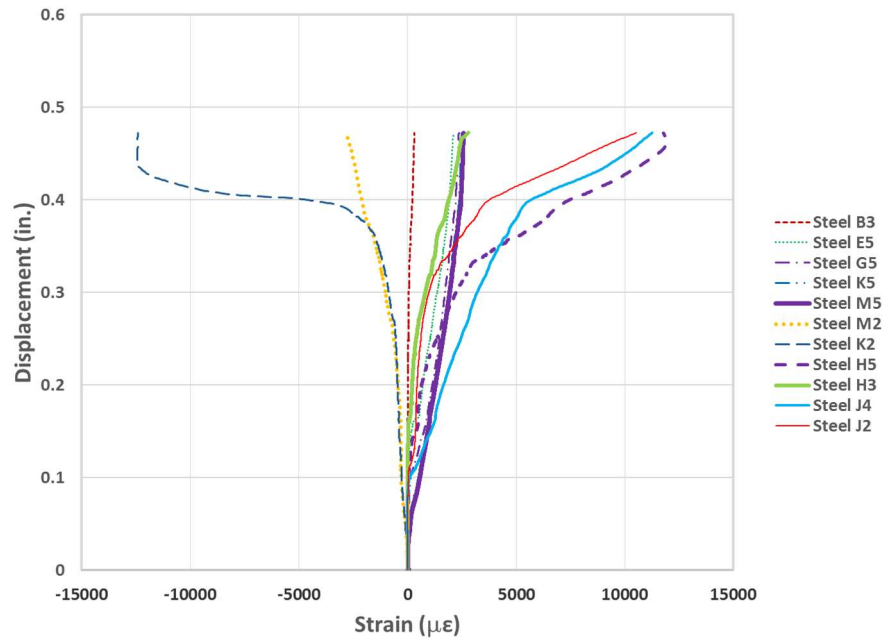


Figure F8 Displacement-strain response for RCS BM #4

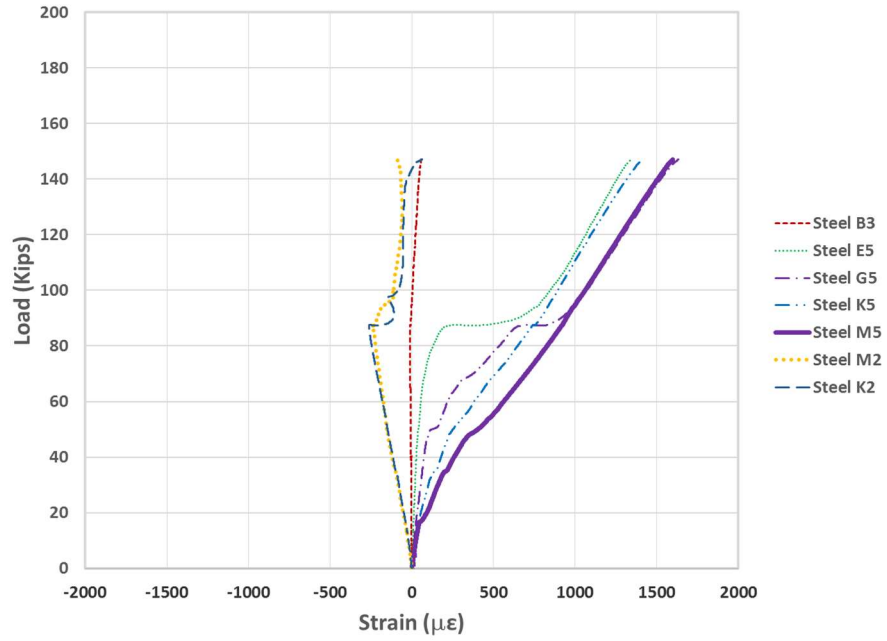


Figure F9 Load-strain response for SNFRC 0.5% BM #5

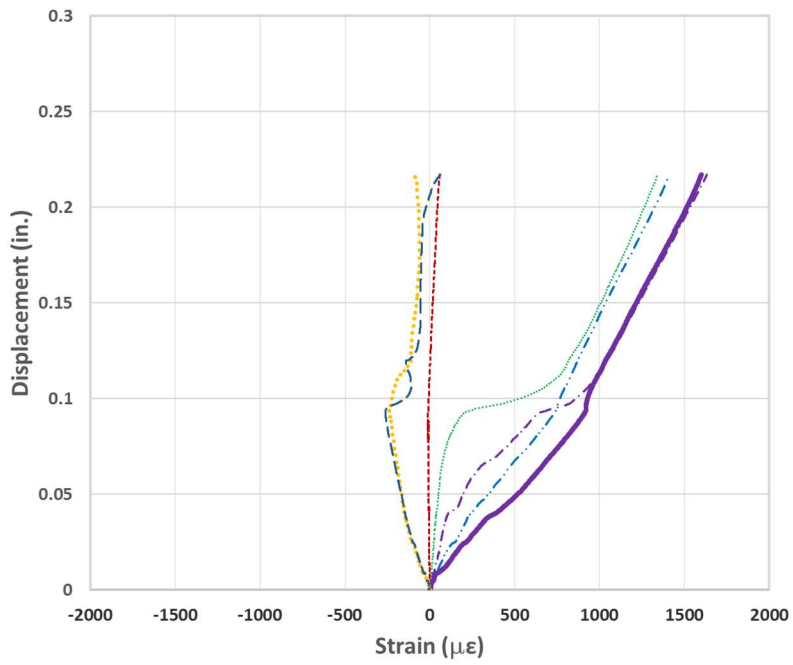


Figure F10 Displacement-strain response for SNFRC 0.5% BM #5

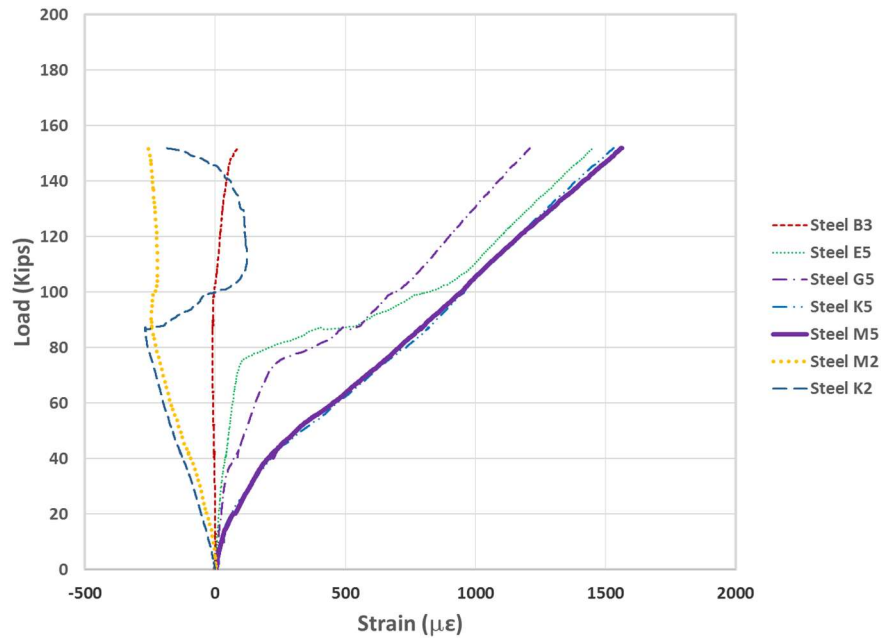


Figure F11 Load-strain response for SNFRC 0.5% BM #6

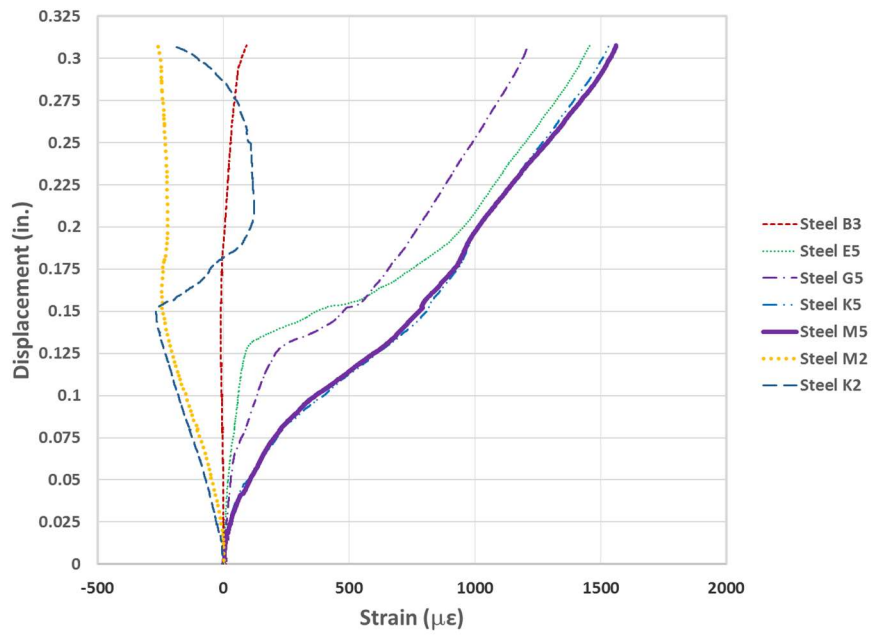


Figure F12 Displacement-strain response for SNFRC 0.5% BM #6

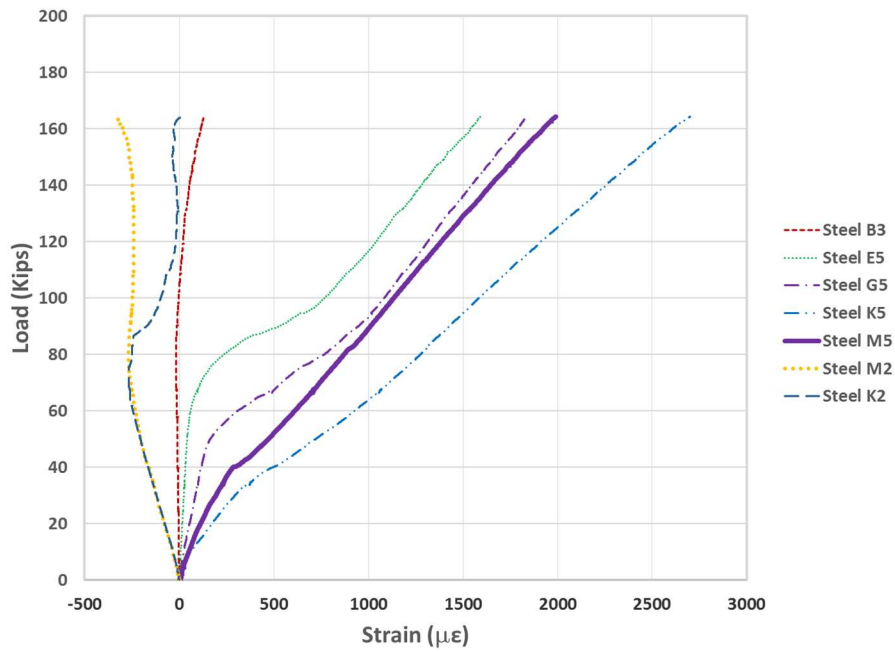


Figure F13 Load-strain response for SNFRC 0.75% BM #7

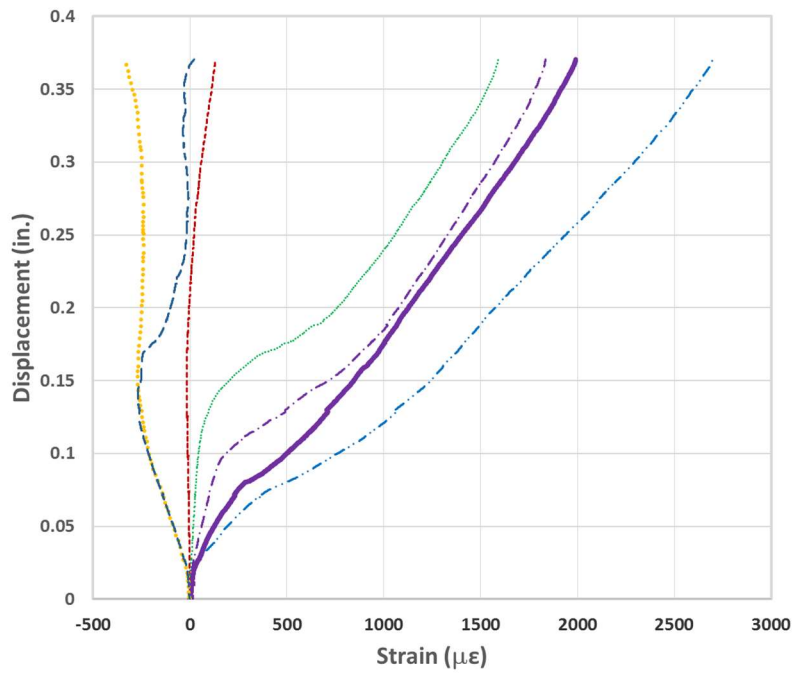


Figure F14 Displacement-strain response for SNFRC 0.75% BM #7

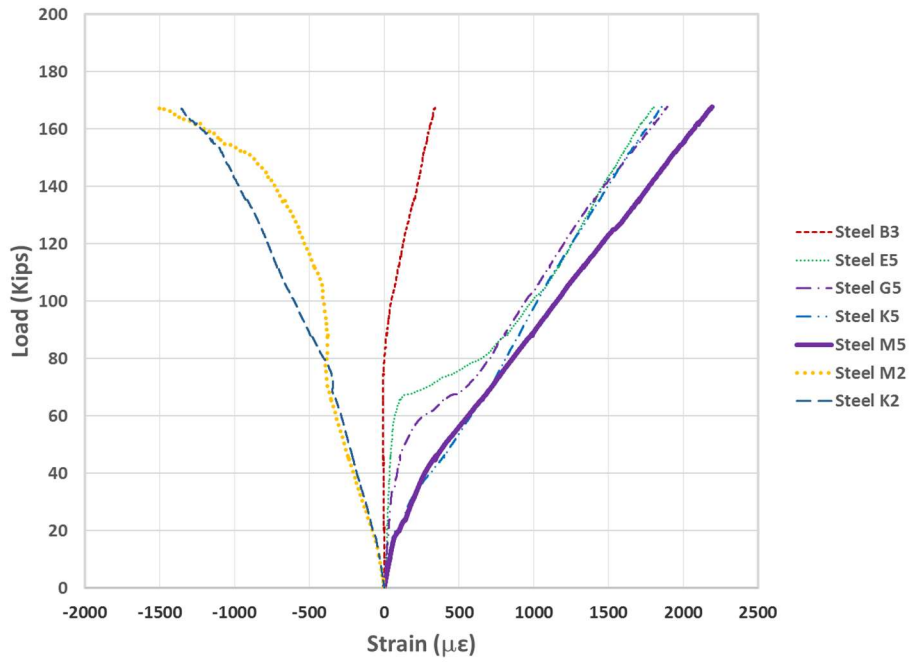


Figure F15 Load-strain response for SNFRC 0.75% BM #8

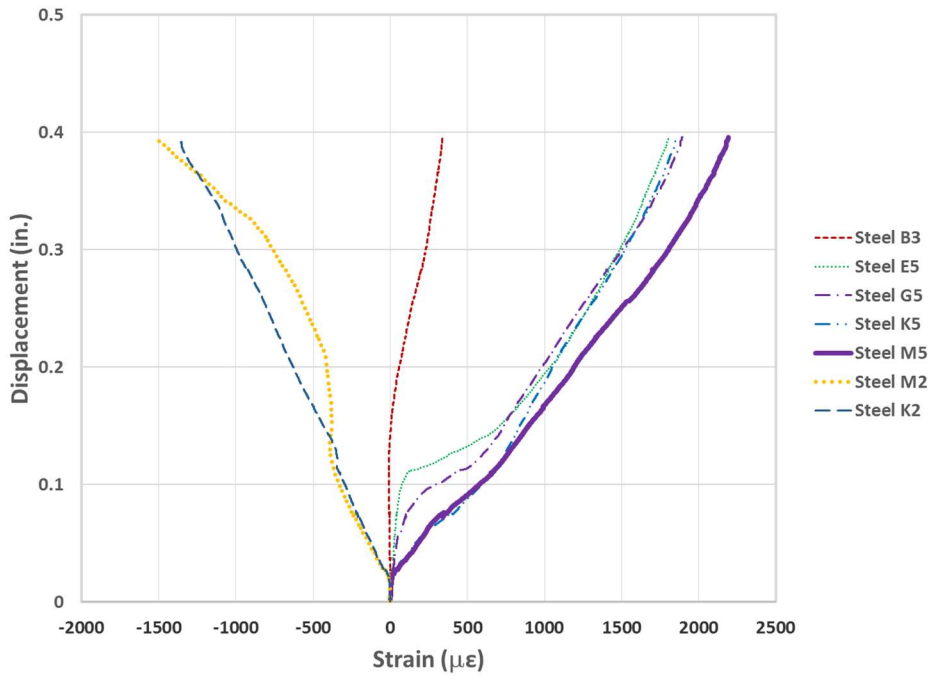


Figure F16 Displacement-strain response for SNFRC 0.75% BM #8

Appendix G
Concrete Strain-Gauges

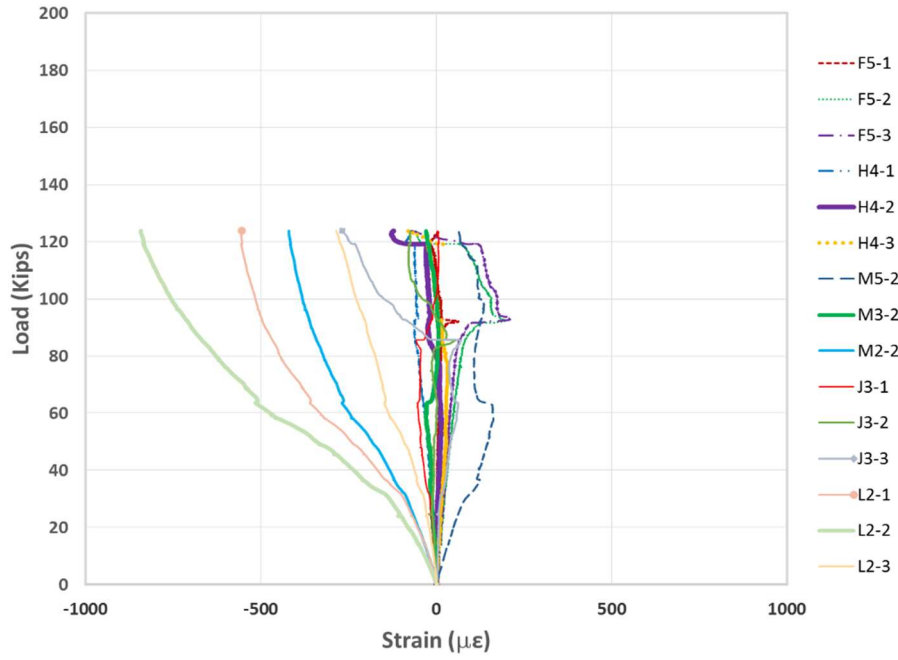


Figure G1 Load-strain response for RC BM#1

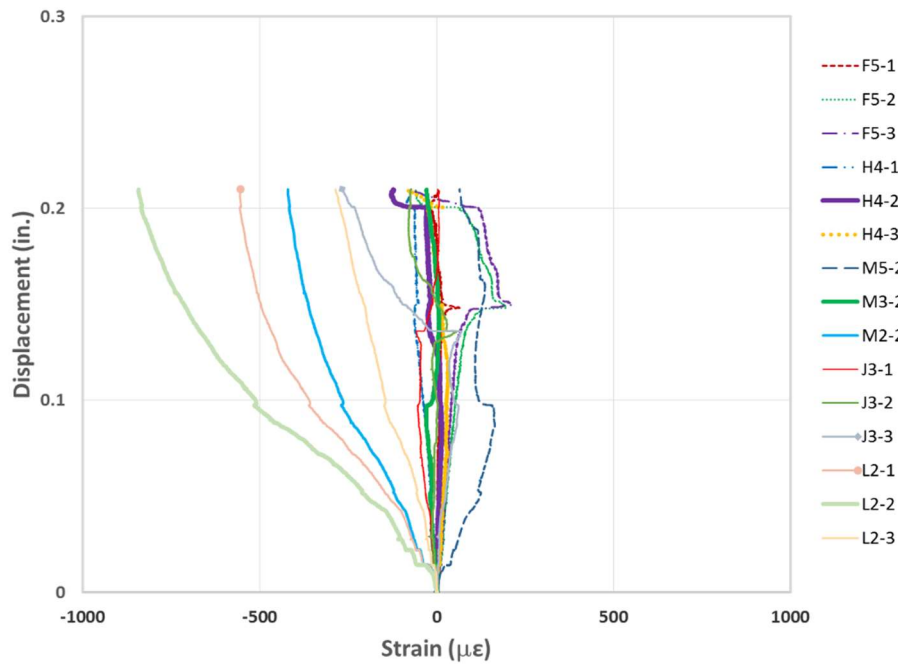


Figure G2 Displacement-strain response for RC BM#1

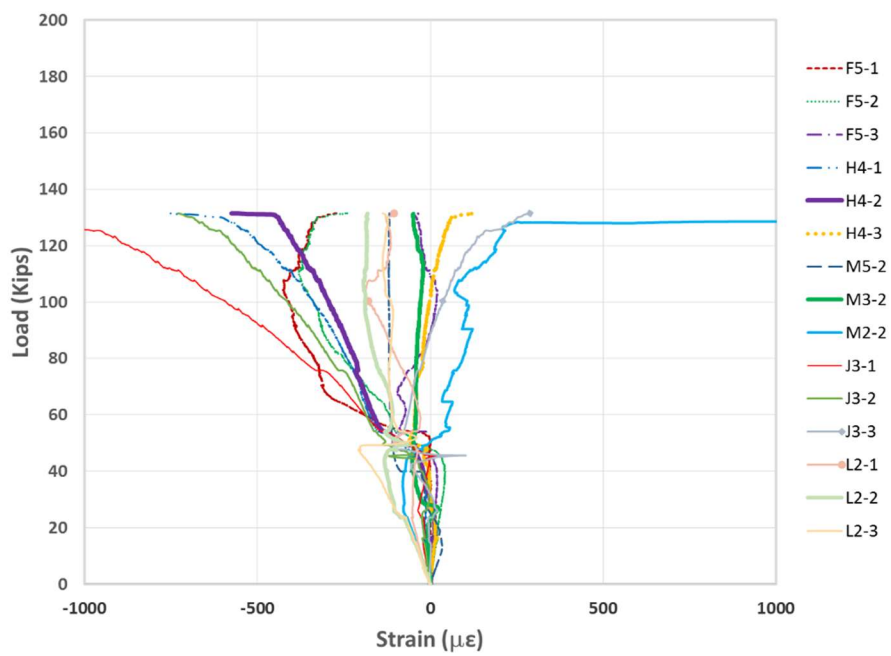


Figure G3 Load-strain response for RC BM#2

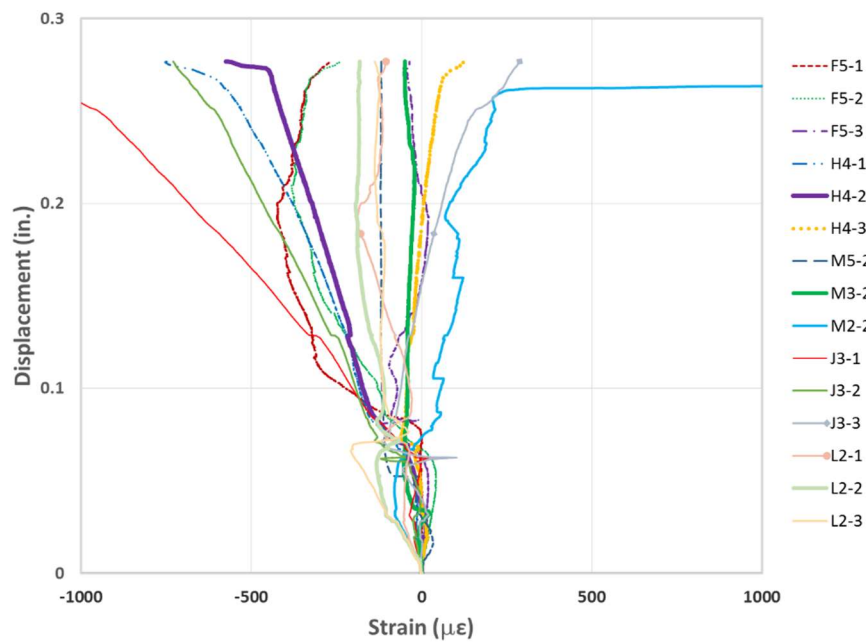


Figure G4 Displacement-strain response for RC BM#2

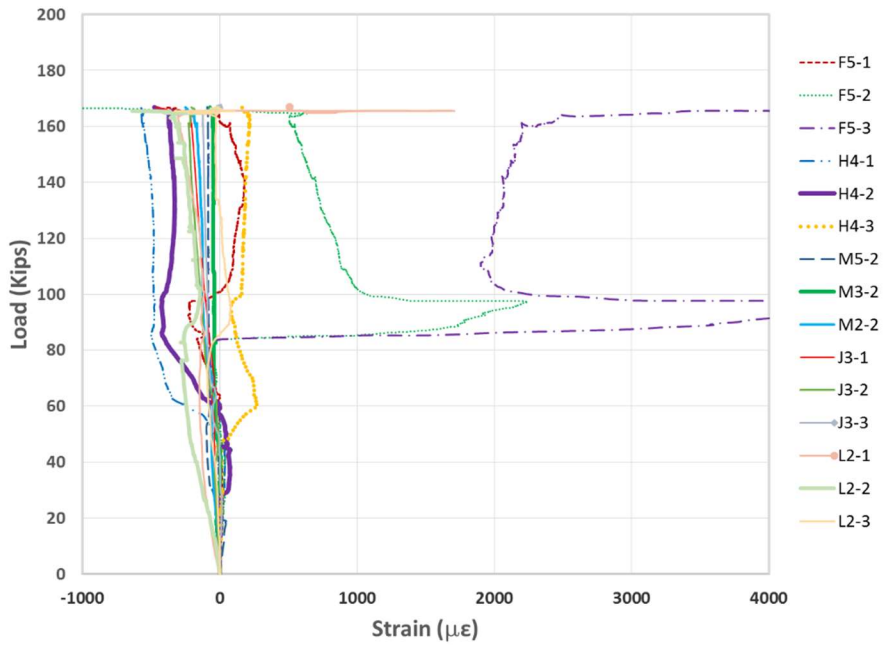


Figure G5 Load-strain response for RCS BM#3

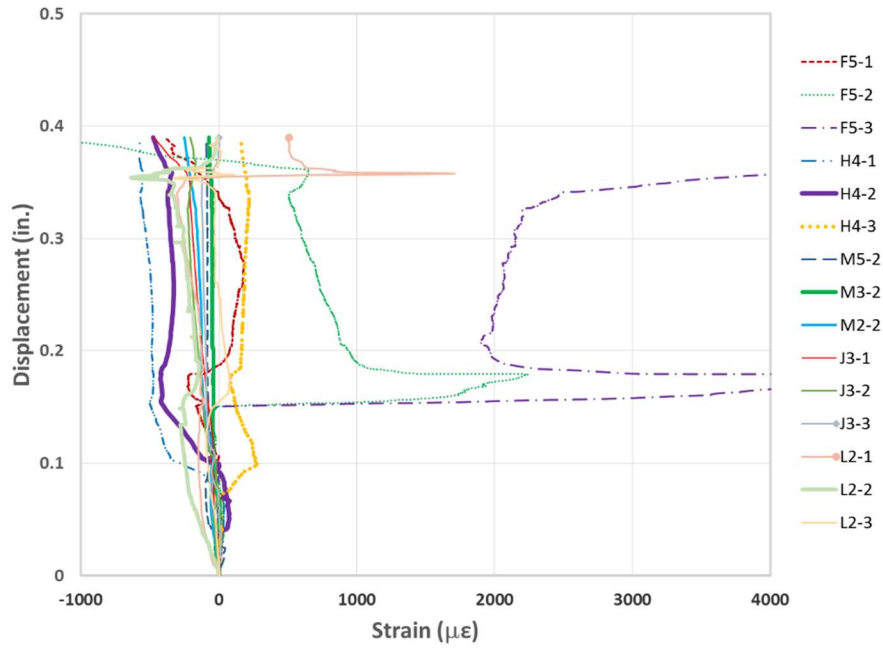


Figure G6 Displacement-strain response for RCS BM#3

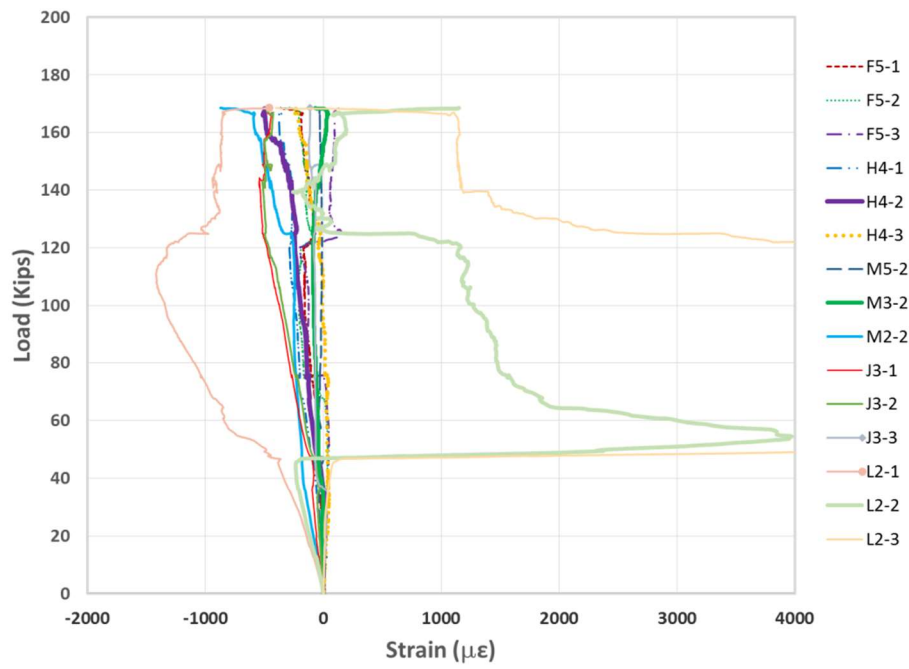


Figure G7 Load-strain response for RCS BM#4

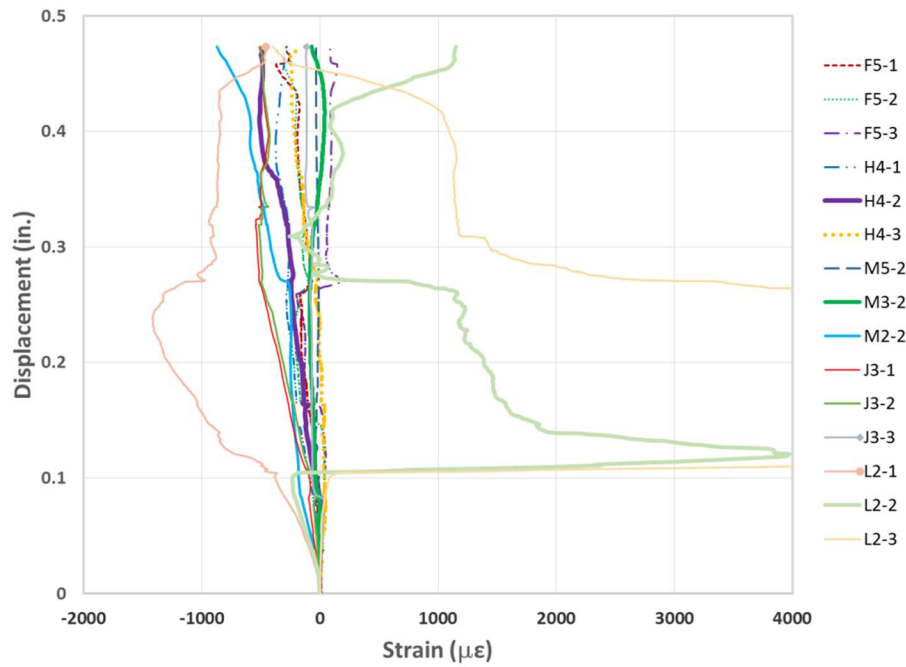


Figure G8 Displacement-strain response for RCS BM#4

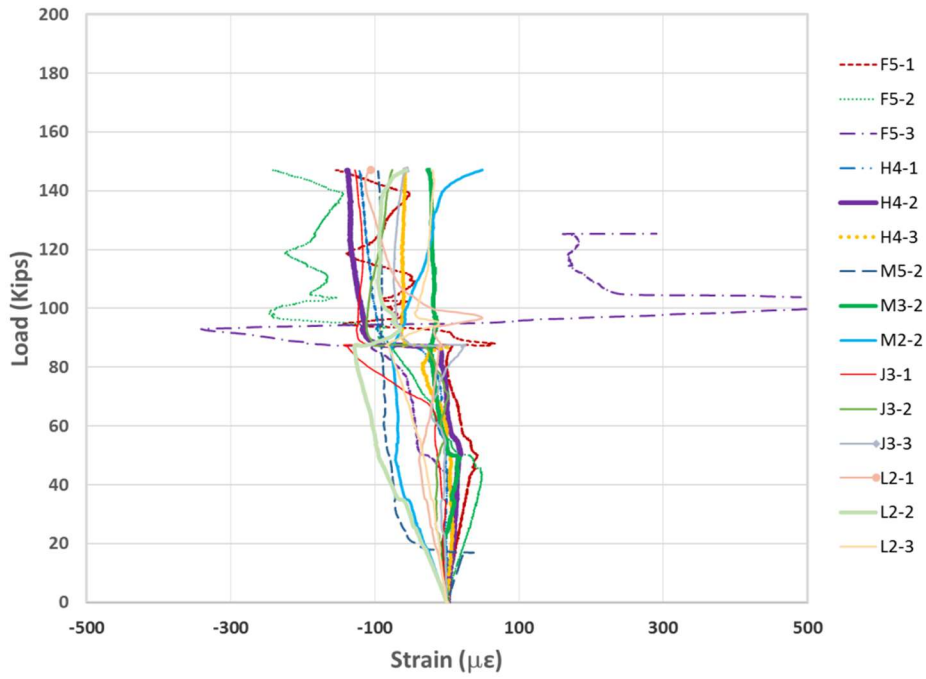


Figure G9 Load-strain response for SNFRC 0.5% BM#5

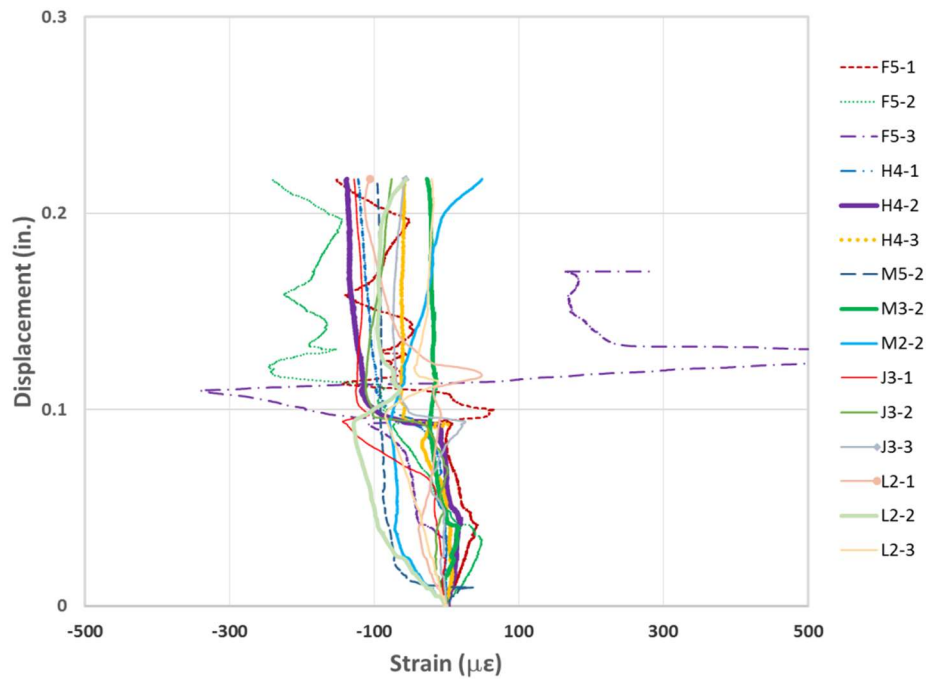


Figure G10 Displacement-strain response for SNFRC 0.5% BM#5

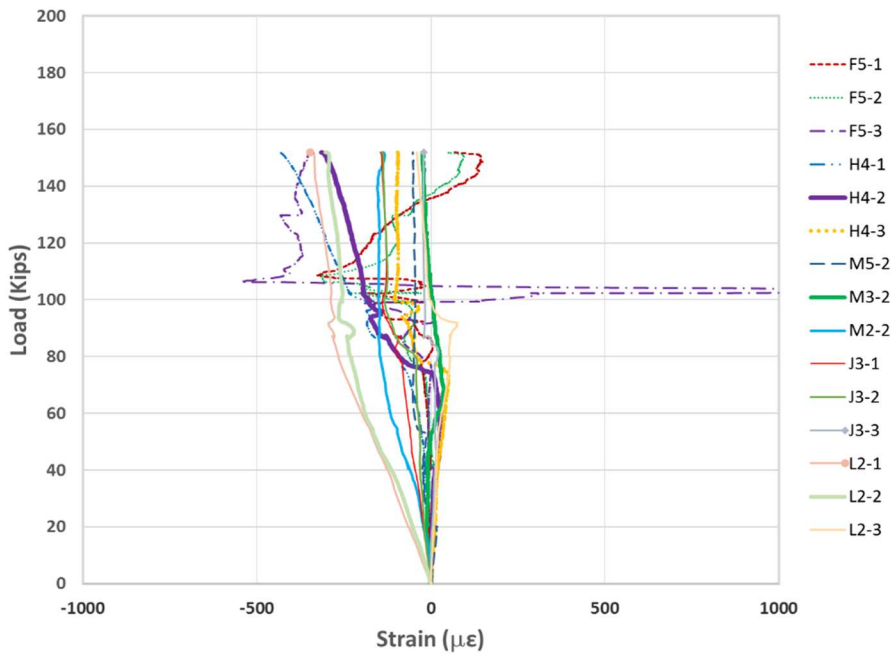


Figure G11 Load-strain response for SNFRC 0.5% BM#6

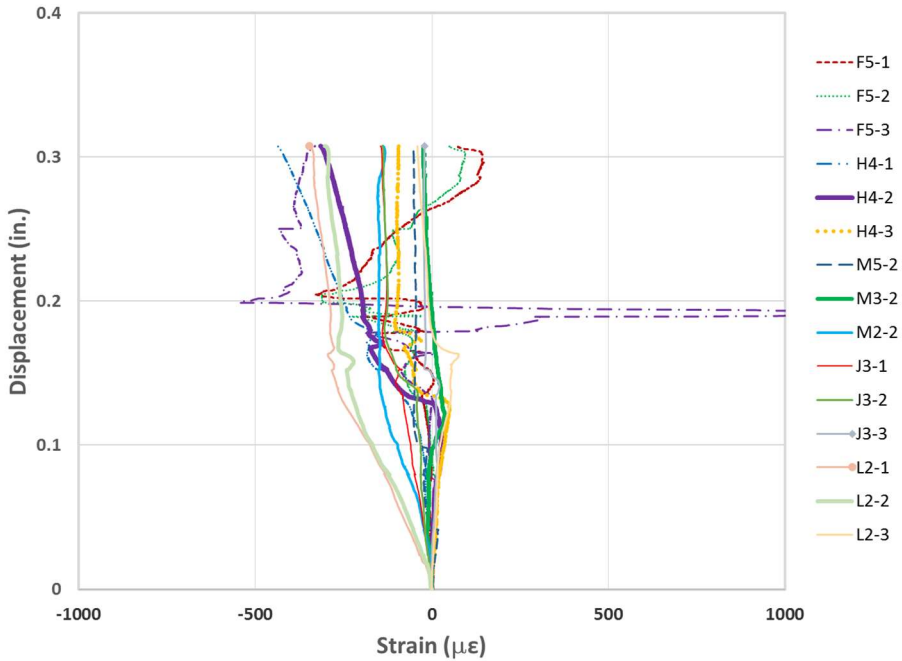


Figure G12 Displacement-strain response for SNFRC 0.5% BM#6

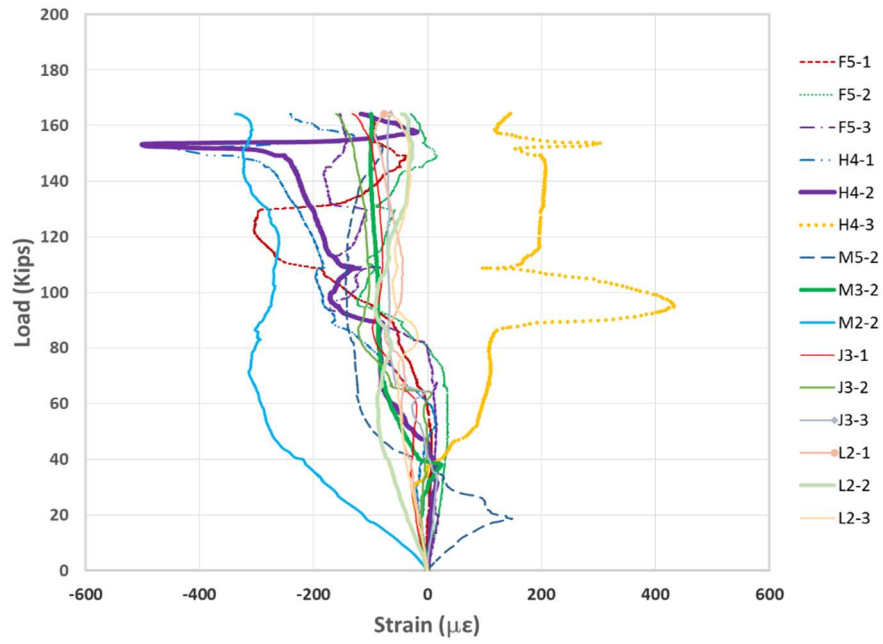


Figure G13 Load-strain response for SNFRC 0.75% BM#7

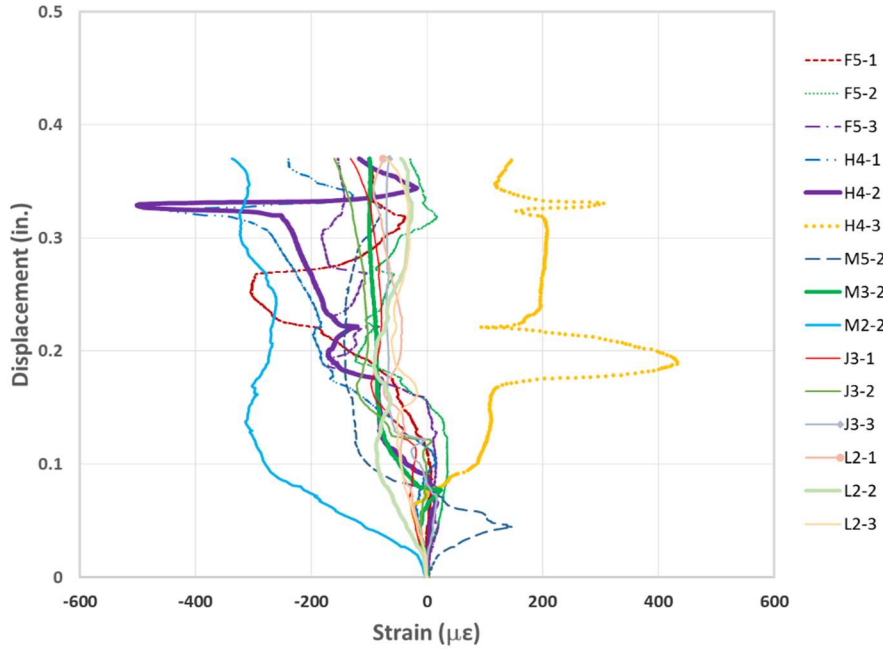


Figure G14 Displacement-strain response for SNFRC 0.75% BM#7

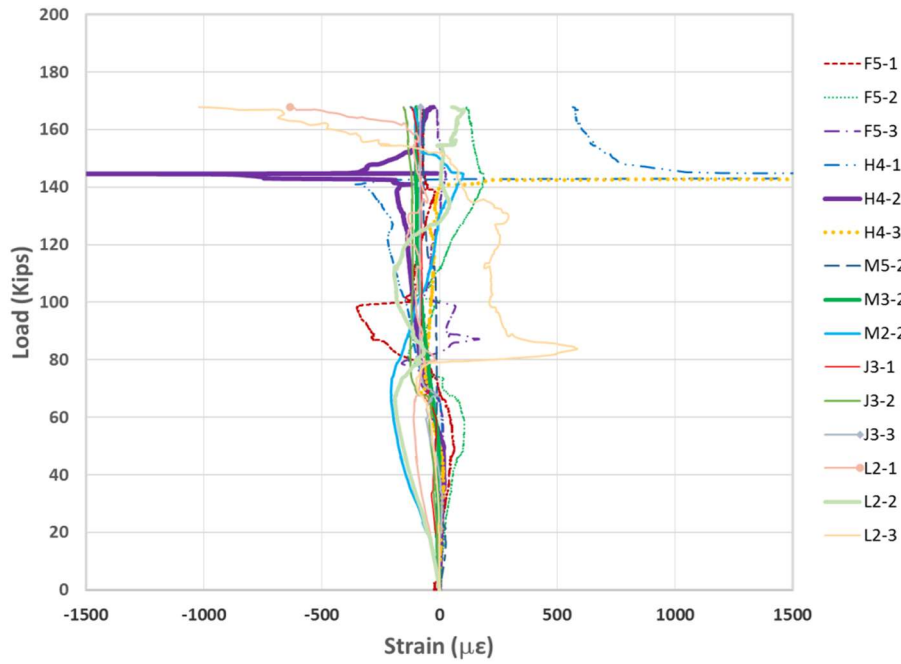


Figure G15 Load-strain response for SNFRC 0.75% BM#8

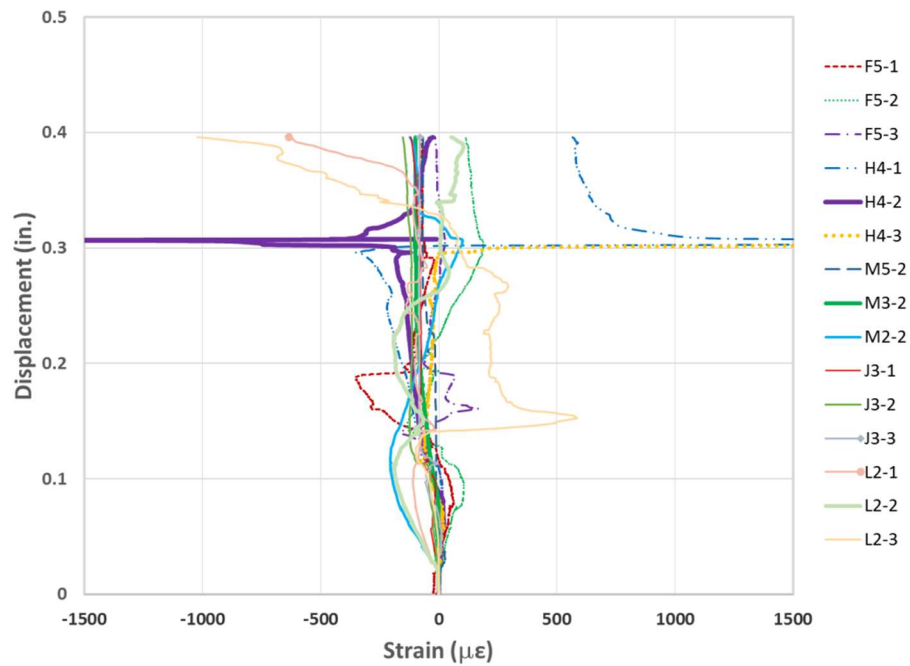


Figure G16 Displacement-strain response for SNFRC 0.5% BM#8

Appendix H
Design of Large-Scale Beams

SHEAR AND MOMENT CAPACITY OF REINFORCED CONCRETE BEAMS

$$b := 10 \text{ in}$$

$$h := 15 \text{ in}$$

$$d := 12.6 \text{ in}$$

$$\beta := 0.8$$

$$f'_c := 5 \text{ ksi}$$

$$f_y := 60 \text{ ksi}$$

$$f_{yt} := 60 \text{ ksi}$$

$$a := 2.5 \text{ ft}$$

$$\frac{a}{d} = 2.38$$

No. 3 double-leg stirrups

$$A_s := 3 \cdot 1.0 \text{ in}^2 = 3 \text{ in}^2$$

$$A'_s := 2 \cdot 0.2 \text{ in}^2 = 0.4 \text{ in}^2$$

Note: Minimum Beam Width (in.) for 3 No. 9 bars per layer based on clear cover of 1.5in. and No3 double leg stirrup is 10in.

$$A_{smin} := \frac{200 \text{ psi}}{f_y} \cdot b \cdot d = 0.42 \text{ in}^2$$

$$\rho := \frac{A_s}{b \cdot d} = 0.02$$

$$A_{smin} < A_s \quad O.K.$$

$$a := \frac{A_s \cdot f_y}{0.85 f'_c \cdot b} = 4.24 \text{ in}$$

$$c := \frac{a}{\beta} = 5.29 \text{ in}$$

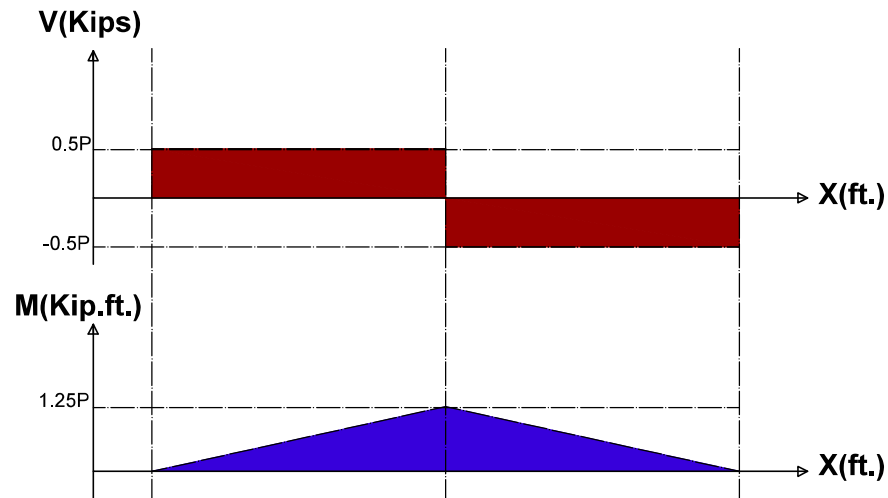
$$\epsilon_s := 0.003 \cdot \frac{d - c}{c} = 4.14 \cdot 10^{-3}$$

$$\epsilon_y < \epsilon_s < 0.005 \quad \epsilon_s - \frac{60}{29000}$$

$$\phi := 0.65 + .25 \cdot \frac{0.005 - \frac{60}{29000}}{0.005 - \frac{60}{29000}} = 0.83$$

$$M_n := A_s \cdot f_y \cdot (d - 0.5 a) = 157.24 \text{ ft} \cdot \text{kip}$$

$$\phi \cdot M_n = 129.98 \text{ ft} \cdot \text{kip}$$



$$P_{moment} := \frac{\phi \cdot Mn}{1.25 \text{ ft}} = 103.98 \text{ kip}$$

$$V_c := 2 \cdot \sqrt{\frac{f'_c}{\text{psi}}} \cdot b \cdot d \cdot \text{psi} = 17.82 \text{ kip}$$

$$\phi := 0.75$$

$$A_v := 2 \cdot 0.11 \text{ in}^2 = 0.22 \text{ in}^2$$

$$s := 3 \text{ in}$$

$$A_{vmin} := 0.75 \cdot \sqrt{\frac{f'_c}{\text{psi}}} \cdot \frac{b \cdot s}{f_{yt}} \cdot \text{psi} = 0.03 \text{ in}^2$$

$$S_{max} := \frac{A_v \cdot f_{yt}}{50 \text{ psi } b} = 26.4 \text{ in}$$

$$V_{smax} := 8 \cdot \sqrt{\frac{f'_c}{\text{psi}}} \cdot b \cdot d \cdot \text{psi} = 71.28 \text{ kip}$$

$$V_s := \frac{A_v \cdot f_{yt} \cdot d}{s} = 55.44 \text{ kip} \quad V_s < V_{smax} \text{ O.K.}$$

$$P_{shear_left} := 2 \cdot 0.75 \cdot (V_s + V_c) = 109.89 \text{ kip}$$

$$P_{shear_right} := 2 \cdot 0.75 \cdot (0 + V_c) = 26.73 \text{ kip}$$

$$s := 6 \text{ in}$$

$$V_s := \frac{A_v \cdot f_{yt} \cdot d}{s} = 27.72 \text{ kip}$$

$$P_{shear_right_min} := 2 \cdot 0.75 \cdot (V_s + V_c) = 68.31 \text{ kip}$$

Appendix I
Project Planning

Table I1 Schedule and work break down structure of experimental phase for research study

WBS	Task Description	Duration (Days)	M1	M2	M3	M4	M5	M6	M7	M8	M9	M10	M11	M12
1	Experimental Program	228												
1.1	Trial Phase: Large-Scale beams	42												
1.1.1	Casting	7	█											
1.1.2	Curing	28	█	█										
1.1.3	Testing	7		█										
1.2	Large-Scale Beams, flexural beams and cylinders	63												
1.2.1	Building formworks	24		█										
1.2.2	Casting	7			█									
1.2.3	Curing	28			█	█								
1.2.4	Strain Gauge Installation	4				█								
1.3	Testing	33												
1.3.1	Large-Scale Beams	10				█								
1.3.2	Small-Scale Beams	9					█							
1.3.3	Compressive Strength Test of Cylinders	8						█						
1.3.4	Tensile Strength Test of Cylinders	6							█					
2	Analysis of Results	90							█	█	█			

REFERENCES

1. ACI Committee, American Concrete Institute, & International Organization for Standardization. (2008). Building code requirements for structural concrete (ACI 318-08) and commentary. American Concrete Institute.
2. ACI Committee, American Concrete Institute, & International Organization for Standardization. (2014). Building code requirements for structural concrete (ACI 318-14) and commentary. American Concrete Institute.
3. Altoubat, S. A., Yazdanbakhsh, A., & Rieder, K. A. (2007). Effect of synthetic macro-fibers on shear behavior of concrete beams. *Special Publication*, 248, 41-52.
4. Altoubat, S., Yazdanbakhsh, A., & Rieder, K. A. (2009). Shear behavior of macro-synthetic fiber-reinforced concrete beams without stirrups. *ACI Materials Journal*, 106(4), 381-389.
5. Ashour, S. A., Hasanain, G. S., & Wafa, F. F. (1992). Shear behavior of high-strength fiber reinforced concrete beams. *Structural Journal*, 89(2), 176-184.
6. ASTM, C. (2001). 39, Standard test method for compressive strength of cylindrical concrete specimens. *ASTM International*.
7. ASTM, C. (2005). 1609: Standard Test Method for Flexural Performance of Fiber-Reinforced Concrete (Using Beam With Third-Point Loading). *ASTM International*, 100.
8. Balaguru, P. N., & Shah, S. P. (1992). *Fiber-reinforced cement composites*.
9. Cho, S. H., & Kim, Y. I. (2003). Effects of steel fibers on short beams loaded in shear. *Structural Journal*, 100(6), 765-774.

10. Cifuentes, H., García, F., Maeso, O., & Medina, F. (2013). Influence of the properties of polypropylene fibres on the fracture behaviour of low-, normal-and high-strength FRC. *Construction and Building Materials*, 45, 130-137.
11. C143, A. S. T. M. (2003). Standard Test Method for Slump of Hydraulic-Cement Concrete. *Annual Book of ASTM Standards*, Conshohocken, PA, USA.
12. Daniel, J. I., Gopalaratnam, V. S., Galinat, M. A., Ahmad, S. H., Hoff, G. C., Schupack, M., ... & Johnston, C. D. (2002). Report on Fiber Reinforced Concrete.
13. Di Maida, P., Radi, E., Sciancalepore, C., & Bondioli, F. (2015). Pullout behavior of polypropylene macro-synthetic fibers treated with nano-silica. *Construction and Building Materials*, 82, 39-44.
14. Fenwick, R. C., & Pauley, T. (1968). Mechanism of shear resistance of concrete beams. *Journal of the Structural Division*, 94(10), 2325-2350.
15. Furlan, S., & de Hanai, J. B. (1997). Shear behaviour of fiber reinforced concrete beams. *Cement and Concrete Composites*, 19(4), 359-366.
16. Greenough, T., & Nehdi, M. (2008). Shear behavior of fiber-reinforced self-consolidating concrete slender beams. *ACI materials Journal*, 105(5), 468-477.
17. Hoff, G. C. (1987). Durability of fiber reinforced concrete in a severe marine environment. *Special Publication*, 100, 997-1042.
18. Hwang, J. H., Lee, D. H., Ju, H., Kim, K. S., Seo, S. Y., & Kang, J. W. (2013). Shear behavior models of steel fiber reinforced concrete beams modifying softened truss model approaches. *Materials*, 6(10), 4847-4867.
19. Kang, T. H., Kim, W., Kwak, Y. K., & Hong, S. G. (2011). Shear testing of steel fiber-reinforced lightweight concrete beams without web reinforcement. *ACI Structural Journal*, 108(5), 553.

20. KraaiP, P. (1998). ACI-544, measurement of properties of fiber reinforced concrete. *Materials Journal*, 85(1), 45-65.
21. Kwak, Y. K., Eberhard, M. O., Kim, W. S., & Kim, J. (2002). Shear strength of steel fiber-reinforced concrete beams without stirrups. *ACI Structural Journal*, 99(4), 530-538.
22. Li, V. C., Ward, R., & Hamza, A. M. (1992). Steel and synthetic fibers as shear reinforcement. *ACI Materials Journal*, 89(5), 499-508.
23. Majdzadeh, F., Soleimani, S. M., & Banthia, N. (2006). Shear strength of reinforced concrete beams with a fiber concrete matrix. *Canadian Journal of Civil Engineering*, 33(6), 726-734.
24. Micro-Measurements, V. (2008). Strain gage rosettes: Selection, application and data reduction. *Technical note TN*, 515, 151-161.
25. Micro-Measurements, V. (2009). Surface preparation for strain gage bonding. *Online document*.
26. Naaman, A. E. (1985). Fiber Reinforcement for Concrete. *Concrete International: Design and Construction*, 7(3), 21-25.
27. NACE International White Paper, "NACE International White Paper Corrosion Control Plan for Bridges". National Association of Corrosion Engineers, 2012.
28. Narayanan, R., & Darvish, I. (1987). Use of steel fibers as shear reinforcement.
29. Noghabai, K. (2000). Beams of fibrous concrete in shear and bending: experiment and model. *Journal of structural engineering*, 126(2), 243-251.
30. Roesler, J. R., Lange, D. A., Altoubat, S. A., Rieder, K. A., & Ulreich, G. R. (2004). Fracture of plain and fiber-reinforced concrete slabs under monotonic loading. *Journal of Materials in Civil Engineering*, 16(5), 452-460.

31. Romualdi, J. P., and Batson, G. B. (1963). Mechanics of Crack Arrest in Concrete. *J. Eng. Mech. Div., ASCE*, 89(EM3), 147-168.
32. Sahoo, D. R., Solanki, A., & Kumar, A. (2014). Influence of steel and polypropylene fibers on flexural behavior of RC beams. *Journal of Materials in Civil Engineering*, 27(8), 04014232.
33. Standard, A. S. T. M. (1984). Standard test method for splitting tensile strength of cylindrical concrete specimens. In *Annual Book of ASTM Standards 04.02*. American Society for Testing and Materials Philadelphia.
34. Wight, J. K., & MacGregor, J. G. (2012). Reinforced concrete: mechanics and design. Upper Saddle River, NJ: Pearson Prentice Hall.
35. Wight, J. K. (2016). Reinforced concrete: mechanics and design. Hoboken, NJ: Pearson.

BIOGRAPHICAL INFORMATION

Ehsan was born in Iran in August of 1991. He grew up in Dubai, UAE where he graduated with honors from Mawakeb High school. He received his Bachelor's of Science in Civil Engineering degree from the American University of Sharjah (AUS) in 2014. He worked as a structural engineer on construction of a 48-story high-rise residential structure in UAE. He then joined the Center for Structural Engineering Research (CSER) as a graduate research assistant in Fall 2015 pursuing a Master of Science degree under the supervision of Dr. Abolmaali. In September 2016, Ehsan joined the building's design department at JQ Engineering, participating in design of numerous reputable projects in Texas and neighboring states.